Bioanalytical Methods for Investigating Bacterial Adhesion and the Antibacterial Action of Nitric Oxide

by
Susan M. Deupree

A dissertation submitted to the faculty of the University of North Carolina at Chapel Hill in partial fulfillment of the requirements for the degree of Doctor of Philosophy in the Department of Chemistry (Biological Chemistry).

Chapel Hill
2009

Approved by:

Professor Mark Schoenfisch

Professor Michael Falvo

Professor Susan Lord

Professor Sergei Sheiko

Professor Linda Spremulli

Abstract

Susan M. Deupree: Bioanalytical Methods for Investigating Bacterial Adhesion and the Antibacterial Action of Nitric Oxide

(Under the direction of Professor Mark Schoenfisch.)

Infection is a continuing problem in both hospital and community settings, further compounded by swift adaptation and rising emergence of more virulent and antibacterial-resistant pathogens. The complex mechanisms underlying the process of infection must be understood in order to develop preventative technologies. Simultaneously, effective solutions must be devised to counter infections as they arise. My dissertation research has contributed to both aspects by working to understand the process of adhesion as well as the development of novel therapeutic strategies.

To investigate bacterial adhesion at a fundamental level, a quantitative method was developed for measuring the shear force required to detach individual adhered bacteria using atomic force microscopy (AFM) that featured both improved accuracy and higher-throughput data acquisition. This technique was employed to characterize the adhesion strength kinetics of *Pseudomonas aeruginosa* and *Staphylococcus aureus*. Both the magnitudes of detachment force and rates of increase in adhesion strength were greater for *P. aeruginosa* than for *S. aureus*. Furthermore, adhered cells demonstrated a range of adhesion forces that broadened with time, indicating that change in adhesion strength does not proceed uniformly.

Morphological analyses were conducted to study the antimicrobial properties of nitric oxide (NO) against two Gram-negative pathogens. The effects of NO as a function of concentration, exposure time, and delivery format were studied using two materials with differing NO-release properties. Analysis of cell topography revealed that higher doses of NO correlated with increasing membrane roughness. Treatment with amoxicillin, an antibiotic that compromises the integrity of the cell wall, led to morphologies resembling those resulting from NO treatment. Our observations indicated cell wall deterioration is a consequence of NO-exposure for both species studied.

The combination of NO and silver sulfadiazine (AgSD) was evaluated for bactericidal efficacy using a modified broth microdilution technique and a checkerboard-type assay. The combination of NO and AgSD proved synergistic against most pathogens, particularly the Gram-positive species. A highly synergistic effect was produced against *S. aureus* and *E. faecalis*, including a vancomycin-resistant strain. The synergistic activity of AgSD and NO against a broad range of pathogens advocates future investigation of this therapeutic combination for use as a topical anti-infective.

TABLE of CONTENTS

List of Tables

List of Figures

List of Abbreviations and Symbols

θ	angle related to AFM probe geometry
Φ	angle of cantilever tilt
~	approximately
β	beta
Δ	change
°	degree(s)
>	greater than
<	less than
≤	less than or equal
µg	microgram(s)
µL	microliter(s)
µm	micrometer(s)
µM	micromolar
µmol	micromole(s)
-	negative
19^{th}	nineteenth
%	percent
$^{+}$	positive
±	statistical margin of error
AFM	atomic force microscope/microscopy
Ag	silver
Ag^{+}	silver ion
Ag^{0}	metallic silver
$AgNO_3$	silver nitrate
AgSD	silver sulfadiazine
AHAP3	*N*-(6-aminohexyl)aminopropyltrimethoxysilane
Ar	argon gas
ATCC	American Type Culture Collection
atm	atmosphere
ATP	adenosine triphosphate

BTMOS	isobutyltrimethoxysilane
C	Centigrade
Ca^{2+}	calcium ion
CF	cystic fibrosis
CFC	closed fluid cell
cfu	colony forming unit(s)
cm	centimeter(s)
cos	cosine
d	day(s)
DAPI	4',6-diamidino-2-phenylindole
dim.	dimension(s)
DMSO	dimethylsulfoxide
DNA	deoxyribonucleic acid
E. coli	*Escherichia coli*
E. faecalis	*Enterococcus faecalis*
e.g.	for example
EPS	exopolysaccharide
Eq.	equation
et al.	and others
F_{app}	applied force
F_{lat}	lateral component of an applied force
F_z	force in z-direction
FBC_{120}	fractional bactericidal concentration at 120 minutes
FDA	Food and Drug Administration
FIC	fractional inhibitory concentration
Fig.	figure
g	acceleration equal to standard gravity
g	gram(s)
GFP	green fluorescent protein
gNO	gaseous nitric oxide
h	hour(s)

HIV	human immunodeficiency virus
Hz	hertz
I	Roman numeral “one”
I_c	ionic concentration
II	Roman numeral “two”
i.e.	in essence
in	inch(es)
k	spring constant
K^+	potassium ion
kDa	kilodalton
kHz	kilohertz
log	logarithm
LPS	lipopolysaccharide
m	meter(s)
M	molar
MΩ	megaohm(s)
MBC	minimum bactericidal concentration
MBC_{120}	minimum bactericidal concentration at 120 minutes
MBEC	minimum biofilm eradication concentration
MDR	multi-drug resistant
MIC	minimum inhibitory concentration
min	minute(s)
mg	milligram(s)
Mg^{2+}	magnesium ion
mL	milliliter(s)
mm	millimeter(s)
MRSA	methacillin-resistant *Staphylococcus aureus*
MSSA	methacillin-susceptible *Staphylococcus aureus*
n	number of samples
N	newton(s)
N_2	molecular nitrogen

N_2O_3	dinitrogen trioxide
nm	nanometer(s)
nmol	nanomole(s)
nN	nanonewton(s)
NO	nitric oxide
NO^+	nitrosonium ion
NO_2	nitrogen dioxide
NO_2^+	nitronium ion
NOA	nitric oxide analyzer
NONO-ate	*N*-diazeniumdiolate
NOS	nitric oxide synthase
O_2	molecular oxygen
O_2^-	superoxide
OD_{600}	optical density at 600 nm wavelength
OH^-	hydroxide ion
OM	optical microscopy
$ONOO^-$	peroxynitrite
p	para
P. aeruginosa	*Pseudomonas aeruginosa*
PABA	para-aminobenzoic acid
PBS	phosphate buffered saline
PDMS	polydimethylsiloxane
pH	-log of proton concentration
pK_a	-log of acid dissociation constant
pmol	picomole(s)
ppb	parts per billion
PPFC	parallel plate flow cell
ppm	parts per million
PROLI/NO	diazeniumdiolate-modified proline
PU	polyurethane
PVC	polyvinylchloride

QCM	quartz crystal microbalance
rms	root-mean-square
RNOS	reactive nitrogen oxide species
RNS	reactive nitrogen species
RSNO	*S*-nitrosothiol
RSPF	radial stagnation point flow
S	sulfur
s	second(s)
S^{-1}	inverse optical lever sensitivity
S. aureus	*Staphylococcus aureus*
SD	sulfadiazine
SEM	scanning electron microscope/microscopy
Si_3N_4	silicon nitride
SNAP	*S*-nitroso-*N*-acetylpenicillamine
SPR	surface plasmon resonance
$t_{1/2}$	half-life
TEM	transmission electron microscope/microscopy
TSA	tryptic soy agar
TSB	tryptic soy broth
UV	ultraviolet
V	volt(s)
v:v	ratio of volumes
vs.	versus
VREF	vancomycin-resistant *Enterococcus faecalis*
VSEF	vancomycin-susceptible *Enterococcus faecalis*
x	by
XDR	extensively drug resistant

Chapter 1:

Introduction to the problem and process of bacterial infection and the development of antibacterial agents used to remediate infection

1.1 Bacterial adhesion and infection

1.1.1 Bacteria as human pathogens. There are approximately 10 times more bacteria living in a human body than there are human cells of which that body is composed.[1] Populations of bacteria colonize the skin, the mouth, and the digestive and genitourinary tract of humans.[2] Most resident bacteria are harmless, existing in symbiotic relationships with their hosts that are either commensal (neither beneficial nor harmful to the host) or mutualistic (beneficial to both parties). In fact, the colonization of the human body by innocuous bacteria actually protects against disease by occupying the preferred niches of more harmful species, thereby providing a passively beneficial function to the host through competitive exclusion.[1,2] However, a small fraction of bacteria are pathogenic (infectious disease-causing), including many species that constitute the natural flora of the host.[2]

The first level of defense against pathogenic bacteria is provided by physical and mechanical barriers such as the skin, the mucosa lining the hollow organs, cilia, and flushing mechanisms.[3] Once the exterior barriers have been breached, the host immune system responds through stimulation of the inflammatory response and recruitment of phagocytes (i.e., monocytes, macrophages, and neutrophils) that engulf and destroy the microorganisms. Ideally, the skin and the immune system work in tandem to protect against invasion of

foreign pathogens, although certain events that compromise these defense systems, such as removal of the skin barrier (e.g., burns, wounds), introduction of foreign materials (e.g., implantation of medical devices), or a weakened immune systems (e.g., human immunodeficiency virus (HIV) or cystic fibrosis (CF) patients), leave the host more vulnerable to attack from harmful bacteria.

All clinically significant species of bacteria are chemoorganotrophs (heterotrophs), relying upon organic compounds with carbon backbones such as sugars, amino acids and proteins for nutrition.[4] Pathogenic bacteria cause infection by successfully colonizing animal tissue and utilizing the nutritive resources of the host in a relationship that is detrimental to the infected organism. Successful colonization of the host proceeds via four steps:[5]

1. adherences at the surface (biomaterial, tissue);
2. survival at the surface and/or penetration into the tissue;
3. multiplication within the host; and
4. undermining, evading, or eliminating the host defense response.

Infection by a pathogenic species does not always lead to disease expression, and the degree of pathogenicity of a microbe is termed its virulence.[2] Pathogenic bacteria possess characteristics, termed virulence determinants, which support their ability to survive within and cause disease to the host.[6] Virulence determinants may function by promoting attachment and colonization, evading the host immune defense, or damaging tissue. Virulence determinants often impart qualities that aid bacterial survival and proliferation within a very particular environment, such as in the lungs or on protein-coated material, and thus bacterial infections are characteristically localized to a specific area of the body.

1.1.2 The bacterial cell envelope. As the interface between the microbe and its surroundings, the cell envelope plays an integral role in determining both the bacterium's ability to colonize and infect its host as well as its susceptibility to various antimicrobial agents. Composed of the cell wall and one or two lipid membranes, the bacterial envelope provides shape and structure, governs transport of molecules into and out of the cell, protects against numerous environmental stressors, and determines (in part) the degree of pathogenicity toward a particular host environment.[5] Thus, knowledge of the structure and components of the cell wall is integral to understanding the fundamental process of infection as well as identifying potential treatment options.

Pathogenic bacteria are frequently classified according to similarities in the architecture of the cell envelope, a system that is particularly useful from a clinical standpoint. Two fundamental types of cell wall exist, which are often differentiated using the Gram stain procedure. Developed by Hans Christian Gram in 1884 prior to elucidation of cell wall structure,[4] immobilized bacteria are first stained with the positively charged dye crystal violet, now known to interact electrostatically with the negatively charged functional groups ubiquitous on the exterior of bacteria.[7,8] Following subsequent rinses with dilute iodine and ethanol solutions, some bacteria retain the initial violet stain (Gram positive) while others are decolorized by the ethanol (Gram negative), dependent upon chemical and physical properties of the envelope. A counter-stain, such as the red dye safranin, is frequently applied to visualize the otherwise colorless Gram-negative bacteria using a light microscope.[4]

The Gram-positive cell envelope is schematically illustrated in Figure 1.1A. It is a two-tiered structure composed of a cytoplasmic lipid bilayer surrounded by a thick peptidoglycan cell wall. Peptidoglycan is the fundamental skeletal feature of the bacterial cell wall

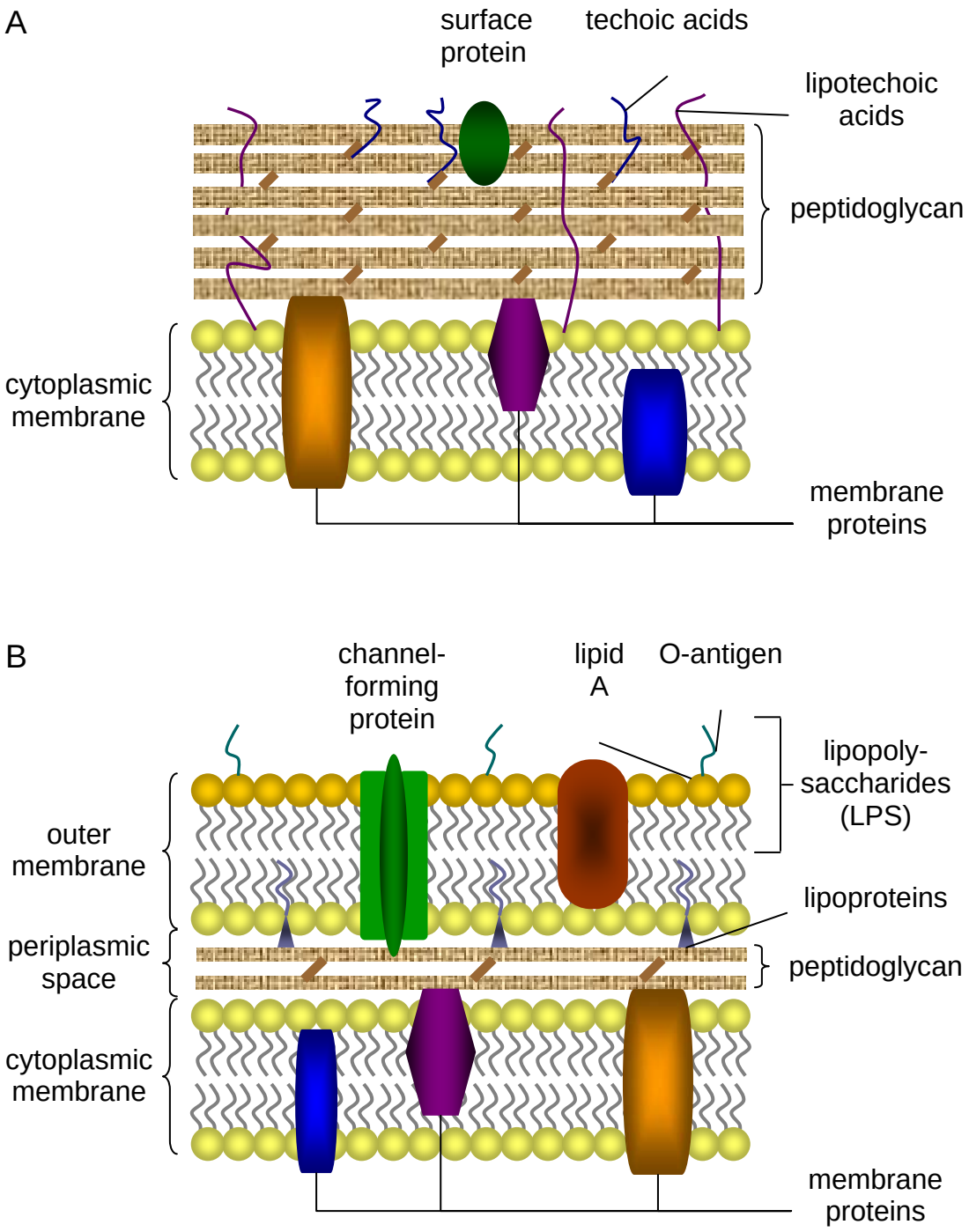

Figure 1.1 Schematic illustrations depicting cross-sections of the (A) Gram-positive and (B) Gram-negative cell wall.

comprised of long saccharide polymers crosslinked by peptide chains forming a two-dimensional, meshed network. Possessing many layers of peptidoglycan, Gram-positive bacteria efficiently retain the crystal violet dye and appear purple after Gram staining. The thick cell wall (constituting 40-60% of the entire cell mass) imparts a tremendous degree of rigidity and resistance to mechanical disruption, such that Gram-positive bacteria can withstand up to 50 atm of external pressure.[5] The peptidoglycan lattice has an estimated pore size of 2.2 nm and permits passage of hydrophilic molecules up to ~55 kDa (based on a globular protein structure).[5] Polysaccharides of mostly anionic character, including teichoic acids linked directly to peptidoglycan as well as lipoteichoic acids and lipoglycans tethered at the cytoplasmic membrane level (Fig. 1.1A), constitute 10-60% of the cell wall by mass, and the high negative charge density serves to bind essential metal cations (e.g., Mg^{2+}, Ca^{2+}, K^{+}).[5]

By contrast, Gram-negative species exhibit a three-tiered architecture, with a much thinner peptidoglycan stratum enclosed in the periplasmic space between a cytoplasmic membrane and a second, outer membrane (Fig. 1.1B). During the final ethanol rinse of the Gram-staining procedure, the outer membrane is dissolved and the peptidoglycan network is insufficiently thick to retain the crystal violet dye, decolorizing the cells. Gram-negative bacteria are much more flexible and prone to rupture (resisting only ~5 atm external pressure at the maximum) than their Gram-positive counterparts.[5]

The outer membrane of Gram-negative bacteria is of paramount importance, primarily as it functions as an extraordinarily efficient permeability barrier, with several classes of specific and non-specific channel-forming proteins required to facilitate entry of essential hydrophilic or charged molecules into the cell (Fig 1.1B). The exterior leaflet is composed of large quantities of lipopolysaccharides (LPS), possessing a hydrophobic segment (lipid A)

inserted into the lipid bilayer and a hydrophilic carbohydrate segment that extends out into the extracellular environment.[9] The hydrophilic portion is constructed of a core oligosaccharide, functionalized with numerous phosphate and carboxyl groups, capped by a much larger and more variable O-antigen polysaccharide.[5] Positioned just above the membrane, the layer of polysaccharides poses an additional barrier layer to hydrophobic compounds.[5] Bacteria deficient in O-antigen exhibit increased susceptibility to hydrophobic antibiotics.[10] While the structure of the Gram-negative cell envelope renders it particularly resistant to penetration by many molecular species, the anionic character of the core region attracts positively charged biocides such as aminoglycoside antibiotics or poly-cationic peptides like defensins.[5]

The sterically massive (up to 65 kDa)[9] and negatively charged LPS molecules make the outer membrane of Gram-negative bacteria inherently unstable,[11] although certain structural aspects provide a stabilizing effect. Specifically, the hydrophobic lipid A portion rich in fatty acid chains (~ 6) anchors this bulky molecule into the membrane, while the negatively charged functional groups in the core region are typically counterbalanced by divalent cations.[5] Under stress, vesicles of LPS, sometimes charged with excreted toxins, are shed in a process termed blebbing.[5] Notably, the lipid A portion of LPS represents an important virulence determinant as it is an endotoxin that can cause serious inflammation (e.g., fever, septic shock) only when released from the cell membrane during blebbing or lysis.[4,5]

Thus, while the Gram-positive cell wall possesses greater rigidity but remains relatively permeable to large, hydrophilic molecules, the Gram-negative cell wall exhibits opposing characteristics, namely being less resilient to physical stresses but capable of preventing the passive diffusion of most molecules across the cell envelope. Both Gram-negative and -

positive bacteria frequently produce a gel-like matrix of exopolysaccharides (EPS) called the capsule (if attached) or slime layer (if only loosely associated) which surrounds and encapsulates the cell, concentrating chemical nutrients and protecting against dessication.[4,5] This feature further elevates the overall virulence of the bacteria by preventing permeation of biocides, aiding the evasion of immune detection, and improving surface adhesion.[5] Gram-positive bacteria express a wide range of adhesins as cell-surface proteins that act as virulence determinants by promoting adhesion through specific and non-specific binding. One example are the M family proteins, which aid in evading phagocytosis and promote adhesion to host tissue through specific recognition of and binding to such proteins as albumin, fibrinogen, and fibronectin.[5] Adhesins are also present on fimbriae, filamentous appendages expressed almost exclusively by Gram-negative bacteria whose main function seem to be to support adhesion to host sugars via lectin interactions, characterized by very specific molecular recognition with regard to both the host and organ (tissue type).[5]

1.1.3 Bacterial adhesion to substrata. Bacteria that are planktonic (free) differ from their sessile (attached) form. While planktonic bacteria are believed to proliferate more quickly and exist to spread into new regions, sessile bacteria live in communities focused on perserverance.[12] It is evident that the exterior surface of bacteria is highly complex, and the process of bacterial adhesion to material surfaces has been previously reviewed in detail.[13-15] The number and relative contribution of independent interactions between the bacteria and the substrate are dependent upon multiple factors including species,[16,17] surface properties (e.g., hydrophobicity),[16,18-20] adsorption of proteins and other conditioning elements on the surface,[17,21-24] various experimental system parameters (e.g., temperature, exposure time and

conditions),[25,26] and the culture environment (e.g., growth phase, ionic strength, pH)[14,16,27,28] under which adhesion occurred.

The interactions involved in attachment and adhesion are frequently described in basic physicochemical terms. The time-dependent process of bacterial adhesion is often depicted as occurring in two distinct phases where a reversible, physicochemical association (Phase I) precedes irreversible adhesion through intimate molecular binding interactions (Phase II),[29-32] as shown in Figure 1.2. Phase I occurs quickly, where a combination of mechanical processes including Brownian motion, gravity, implementation of motility structures, and chemotaxis (locomotion in response to chemical signals) are first responsible for bringing the bacteria close enough to the surface for physical forces of attraction and repulsion to be felt. Attachment may then proceed via a combination of physicochemical interactions and long- and short-range reversible chemical interactions (i.e., electrostatic attractions/repulsions, hydrophobic interactions, and van der Waals forces) that occur along vectors perpendicular to the surface (Fig. 1.2A).[33] If the net attraction exceeds the repulsive forces, the bacteria become 'irreversibly' attached to the surface, and enter Phase II of adhesion.

During Phase II, macromolecules present on the exterior of the bacterium mediate attachment to the substratum via cellular and molecular interactions in a complex process that extends over a number of hours, signifying the transition from planktonic to sessile states (Fig. 1.2B). The two phases of adhesion differ distinctly. While Phase I involves interactions occurring away from and perpendicular to the surface eventually leading to a reversible association, Phase II is characterized by the reinforcement of attachment through numerous intimate binding interactions in order to establish a firm adherence of the cell to the underlying substrate. Surface proteins of *Staphylococcus* subspecies (SSP-1 and SSP-2)

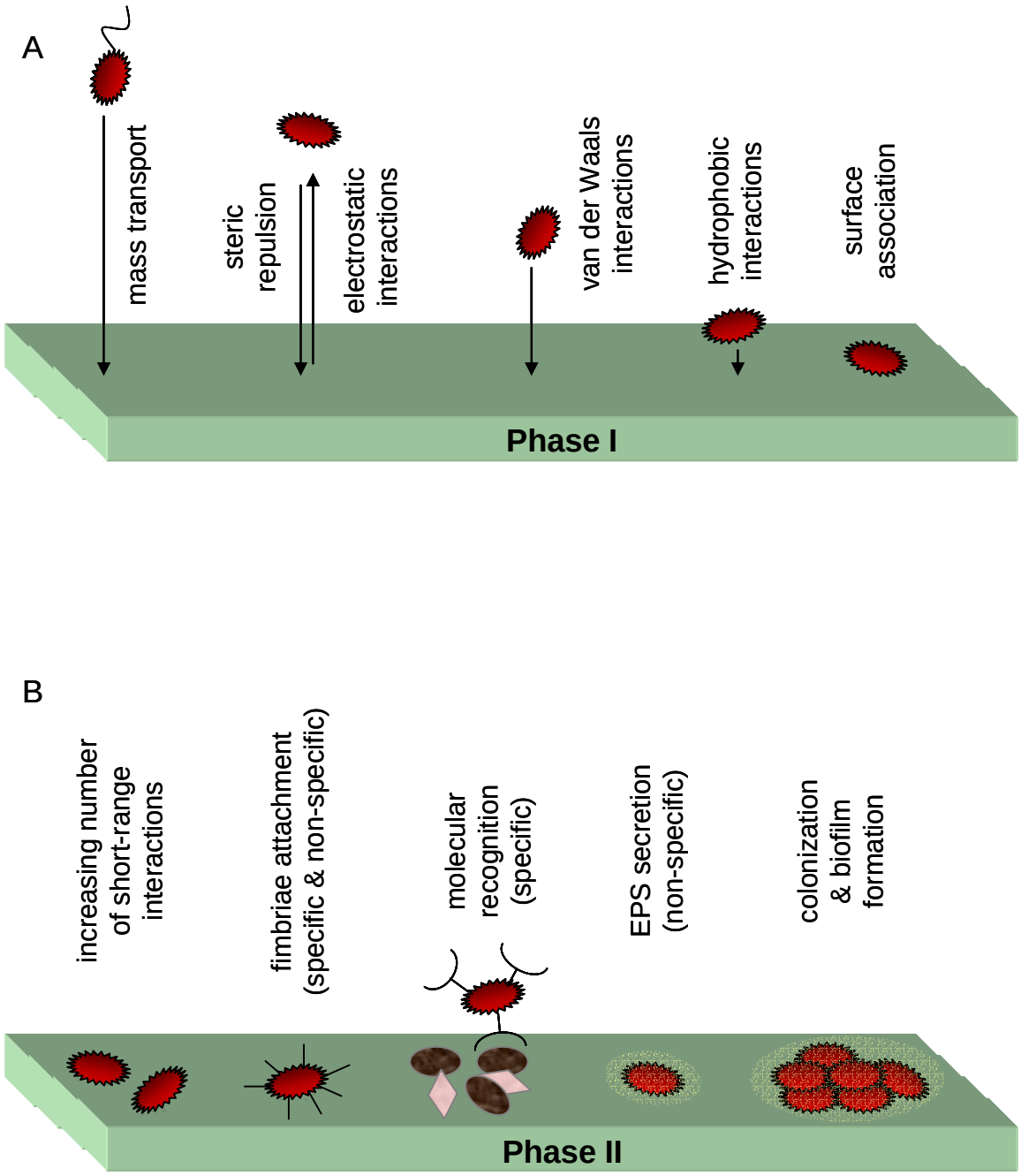

Figure 1.2 Schematic illustrating typical interactions involved in (A) Phase I and (B) Phase II of bacterial adhesion to a substratum.

have been shown to form pili-like structures to mediate attachment to bare plastic surfaces.[34] Motility structures may also prove to be important factors for adhesion, as *Pseudomonas aeruginosa* mutants deficient in flagella have been shown to attach poorly to polyvinylchloride (PVC).[35] During Phase II, bacteria attain irreversible adhesion to the surface and will not spontaneously dissociate.

In the absence of specific molecular recognition, this process is termed non-specific adhesion and may be useful for modeling a scenario where biomaterials become contaminated prior to implantation. Once implanted within the body, bare devices are instantaneously coated by a conditioning layer of proteins (e.g. fibrinogen, fibronectin), water, and organic molecules, which then mediates both non-specific and specific (receptor-mediated) interactions (Fig. 1.2B).[36] Specific interactions between biomacromolecules of the bacteria and host often play an important role in the adhesion process. Many pathogenic bacteria have evolved virulence factors that promote and enhance their ability to successfully colonize tissue or protein-coated materials. For example, alginate is an EPS excreted by *P. aeruginosa* almost exclusively within the lungs of CF patients and constitutes an important virulence determinant in this environment.[37,38] Furthermore, numerous proteins (e.g., lectins), phospholipids, and carbohydrates present on the surface of bacteria are all thought to act as adhesins in specific binding events.[5,39-41]

1.1.4 Biofilm formation and infection. Attachment of bacteria to a surface confers the dual advantages of permanent residence at a preferential site and subterfuge from host defenses.[42] Once bacteria have securely attached to a surface, they alter phenotypically by aggregating into microcolonies, composed of nearby sessile, daughter, and recruited planktonic cells. Costerton et al.[43] have compared these microcolonies to the tissue that

composes organs, suggesting they constitute the essential building blocks of biofilms. Confocal fluorescence microscopy has illuminated the surprising complexity of biofilm structure.[44] Biofilm communities form on either biotic or abiotic substrata,[12,45] and although counterintuitive, biofilms form preferentially in high-shear environments, where lateral forces aid in reorganization and strengthening of the underlying structure.[46] They excrete an EPS matrix, sometimes termed a glycocalyx, that binds them together as a structured consortium while trapping nutrients and allowing communication (via quorum sensing) and differentiation between cells. Existence in biofilms also confers resistance to immune system defenses as the bound community is too large to phagocytose.[47]

Failure of the immune system to control invading pathogens and prevent infection leads to an escalated inflammatory response. Ultimately, pathogenesis of infection may result in the self-destruction of the host, e.g., via extended fever, kidney failure due to massive deposition of immune complexes, or acute wasting disease caused by the overproduction of some cytokines such as tumor necrosis factor.[48] Thus, it is imperative to effectively treat infections as they arise. But as the development of antibiotic resistant infections becomes more common while the rate of discovery of novel antimicrobials has slowed almost to a halt, it is increasingly necessary to prevent infection from forming, therefore sidestepping the need for treatment. Much research in recent years has been devoted to understanding the fundamental process of bacterial adhesion to surfaces with the ultimate goal of developing surfaces that resist bacterial adhesion. Hence, there is a simultaneous need both to understand the process of infection in order to design the next generation of infection-resistant biomaterials and to devise novel and effective treatment options for present clinical application.

1.2 Techniques for studying bacterial adhesion

As the first step in bacterial colonization and infection, the adhesion of bacteria to a substrate is a necessary prerequisite to the development of infection. Therefore, complete elucidation of the fundamental process of bacterial adhesion is the primary hurdle to designing adhesion-resistant biomaterials that will prevent infection. As outlined in Section 1.1.3, the attachment of bacteria to a surface is a time-dependent process usually described in two phases. Two physical aspects of bacterial adhesion readily lend themselves to quantitative study: the affinity for association and the resistance to dissociation. Appraisal of the propensity for attachment relates information on the first stage of adhesion, while evaluating resistance to detachment provides insight into Phase II.

Numerous techniques have been used to study aspects of bacterial adhesion, and these have been previously reviewed.[49,50] Molecular biology and genetic screening allow the identification of specific genes and proteins that are essential to bacterial adhesion.[41,51] Additionally, techniques designed for the empirical observation of bacterial adhesion have been applied toward unraveling the complex interactions undergone during the adhesion process as well as evaluating substrata for potential biomedical uses. These employ more direct and non-invasive approaches that allow the study of adhesion under controlled circumstances and the determination of parameters such as the attachment rate and strength of adhesion.

The choice of bacteria and substrate for adhesion experiments depends on the type of problem being investigated. For example, if the aim of the experiment is to identify promising materials for improved hip implants that resist bacterial adhesion, *Staphylococcus aureus* would be a likely candidate as a common and particularly virulent pathogen in

orthopedic infections.[52,53] If, instead, the goal is to identify proteins that promote the binding of *S. aureus* to blood-contacting devices, then a representative biomaterial would be chosen and coated with relevant plasma proteins. Other experimental conditions that affect bacterial attachment include culture growth stage,[54,55] pH,[56,57] and ionic strength.[55-58]

1.2.1 Propensity for attachment. The proclivity of bacteria to interact and form associations with a surface is typically evaluated by determination of the rate of adhesion and the overall surface coverage of cells adhered to a substrate. Bacteria may be exposed to a surface under either static or flow conditions. Static experiments are the simplest to conduct and evaluate and involve incubating a segment of substrate within a suspension of bacteria for a specified length of time. The primary limitation to the static procedure is disruption of attached cells by an air-liquid interface upon removal for analysis.[59] Bacteria may also be exposed to a surface using dynamic (flow) systems. The ability to exchange liquid volumes by switching reservoirs of pumped fluid eliminates the need for introducing an air-water interface. Other advantages of using dynamic conditions include ease in obtaining kinetic attachment rates, continuous replenishment of bacteria at the surface, and simulation of shearing environments (e.g., circulatory systems). The two devices most commonly employed in dynamic studies are the parallel plate flow chamber (PPFC)[60] and radial stagnation point flow (RSPF) system,[55] depicted in Figure 1.3. For such experiments, the substrate may be placed within a chamber over which a bacterial suspension or rinse solution flows at a controlled rate. Differences in the direction of fluid movement inherent to each device have been shown to affect the overall number and rate of attachment of bacteria.[61] For example, the RSPF system exhibits a higher initial deposition rate, which has been attributed to the convection-controlled mass transport of bacteria to the substrate surface

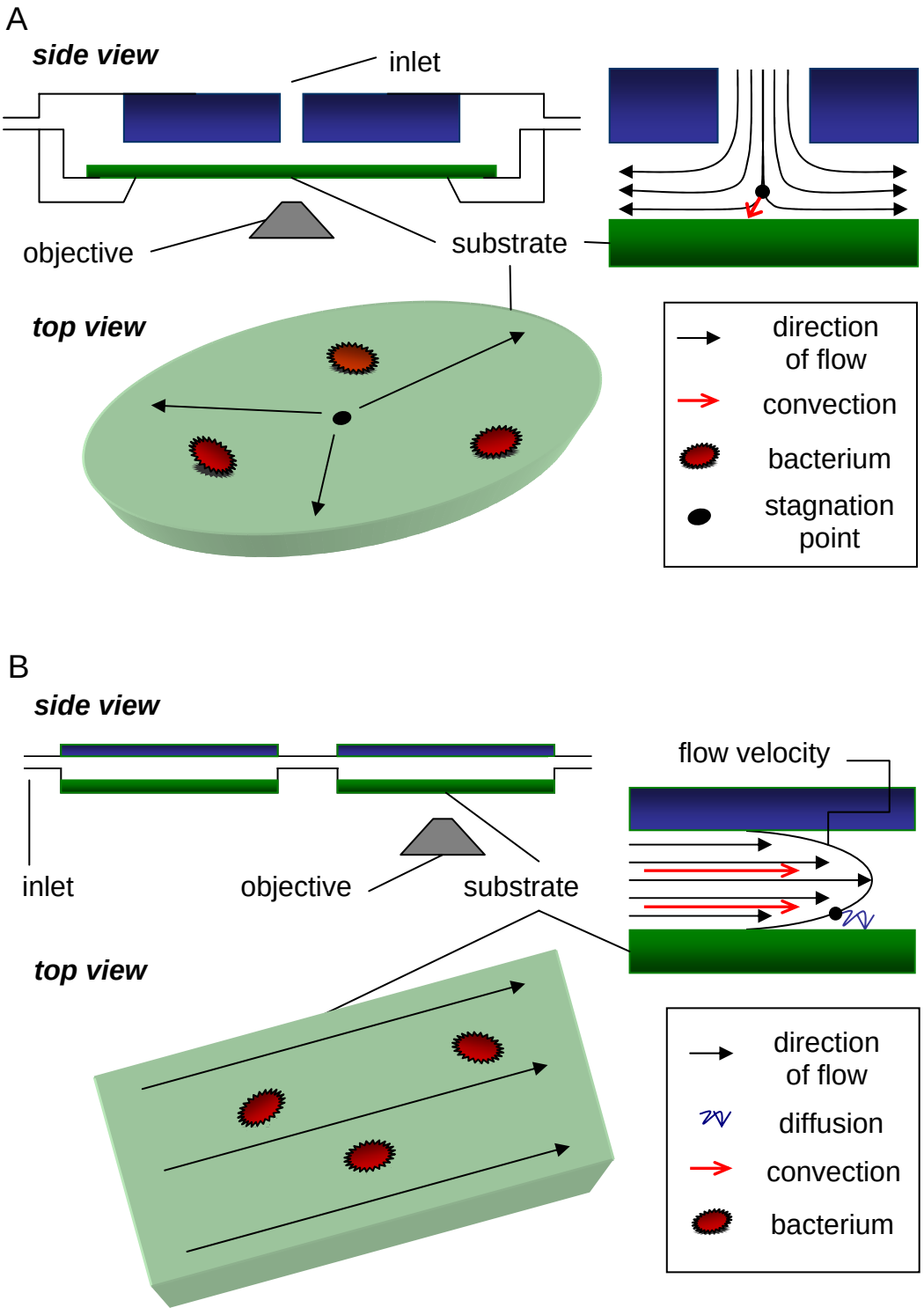

Figure 1.3 Schematic diagrams of (A) a radial stagnation point flow (RSPF) system and (B) a parallel plate flow chamber (PPFC).

(Fig. 1.3A) compared to the slower, diffusion-controlled transport mechanism characteristic of the PPFC (Fig. 1.3B).[61] Once surface-bound, bacteria can be detected by myriad techniques.

Microscopy is the most direct method for observing the propensity for attachment. The two parameters primarily determined via microscopy in bacterial adhesion studies are the adhesion rate (enumeration of individual cells as they adhere) and the overall percentage of the substrate surface area covered. In addition, patterns of adhesion (i.e., in clusters or individually) can be observed. As bacterial dimensions are on the micron scale, optical (light) microscopy (OM) is the most straightforward approach for visualizing adhered cells. A substantial advantage of OM is the ability to monitor the rate of bacterial adhesion in dynamic studies in real time through the coupling of a digital recording device. However, OM is only applicable to studies that use optically transparent systems (i.e., substrate, media, and apparatus), and the resolution limit often leads to difficulty discriminating between individual bacteria. Other methods, such as scanning electron microscopy (SEM), may be used to directly observe adhesion to opaque substrates while providing sufficient resolution to simultaneously distinguish cellular morphology. The sample preparation necessary for SEM, however, eliminates the possibility for in situ examination.

Fluorescence microscopy is a particularly powerful technique for studying bacterial adhesion that utilizes fluorochromes available in a variety of colors and labeling specificities. Blue fluorescent intercalating agents such as 4',6-diamidino-2-phenylindole (DAPI) and Hoechst stains readily transverse intact cell membranes and tightly bind to nucleic acids of both living and fixed bacteria.[62] Using fluorophore-conjugated biomolecules, molecular recognition may be harnessed to label and detect the presence of specific interactions. For

instance, whole cells can be marked and directly visualized using fluorescent antibodies. Fluorescence microscopy can also be used to detect and enumerate viable cells. Combination staining with SYTO 9 and propidium iodide can differentiate between healthy bacteria and those with compromised membranes. Similarly, metabolic activity may be monitored using fluorescence techniques or by detecting other biochemical markers, such as the production of ATP, and is assumed to indicate cell viability. Bacteria genetically modified to express fluorescent tags, such as green fluorescent protein (GFP), propagate the tag through cellular division. This technique allows specific detection of the genetically modified species and can be used to monitor growth (e.g., biofilm formation).[63] Some additional advantages conferred by fluorescence microscopy include rapid enumeration and the reduction of operator bias when combined with image analysis software.[50]

Viable bacteria may also be indirectly detected by sonication or homogenization of substrates with adhered bacteria followed by plating aliquots of the resulting solution on agar media. Each colony grown results from a single viable bacterium recovered from the substrate. While only viable cells may be detected by plating, dead bacteria are also of interest as they may possess virulence factors as well as provide specific receptors that promote binding and colonization of additional microbes.[64] Therefore, a complete technique for evaluating the propensity for attachment would enumerate both viable and dead cells. Such data may be obtained using fluorescent stains or a Coulter counter. Alternatively, radiolabeling bacteria has been implicated as a highly sensitive enumeration technique.[65] While viability cannot be determined as bacteria must be removed from a substrate and lysed prior to detection, this technique can be used to accurately determine the overall number of adhered cells. Less common techniques include QCM[66,67] and SPR,[68,69] which indirectly

detect bulk quantities of adhered bacteria and may be applied to determining attachment rates.

1.2.2 Resistance to detachment. While enumeration of surface-associated cells is more useful for understanding Phase I adhesion (where bacteria form a loose association with the surface), studying resistance to detachment lends information on the reinforcement of adhesion that accompanies Phase II. The adhesion strength that results from the multitude of specific and/or non-specific interactions between the bacterium and the substrate may be assessed by applying a measurable force along the surface until the interactions are physically disrupted and the bacteria detach. This is key to understanding how difficult the removal of pathogenic bacteria from a bare surface (e.g., a device prior to implantation) may be once adhesion occurs, or how bacteria adhered to a protein-coated material (e.g., an implanted device) behave when exposed to biologically relevant forces such as the shear stresses of blood flow or the mechanical impact resulting from patient movement. Additionally, determining how adhesion strength changes as a function of time yields important information on the fundamental behavior of bacterial interactions with surfaces.

Lateral forces may be applied using techniques such as micromanipulation to induce mechanical disruption (particularly useful for measurement of biofilm adhesion strength),[54,70,71] the air-liquid interface introduced by a passing air bubble,[72] or most commonly by applying shearing forces with laminar flow.[19,61,73-75] As bacteria are essentially charged colloids, an electrophoretic technique has also been reported for determining the strength of adhesion based upon the applied electric field required to detach cells.[76] These techniques are limited by the inability to simultaneously control both the magnitude and

location of applied forces, with the exception of micromanipulation, which possesses a limit of force detection that exceeds that achieved by individual bacteria.

The same principle behind the dynamic systems (e.g., PPFC and RSPF) used to study bacterial attachment rates may be modified to apply lateral forces to detach adhered bacteria using laminar flow, and detachment is easily monitored using light microscopy. Using a microjet impingement technique closely related to RSPF, the adhesion strength of *Pseudomonas stutzeri* was shown to be 2- to 3-fold greater on hydrophobic indium tin oxide coated substrates relative to bare hydrophilic glass, agreeing well with theoretical predictions.[73] A PPFC was used to evaluate the effect of shear stress on receptor mediated adhesion of *S. aureus* to collagen coated substrates as a function of flow rate and densities of both receptor and ligand.[77] Another hydrodynamic approach involves the use of a spinning disk, where the applied shear stress during rotation is a function of the density and viscosity of the fluid as well as the angular velocity, which varies linearly with the radial distance.[74]

Recently, atomic force microscopy (AFM) has emerged as the prominent technique for studying the forces of bacterial adhesion. Overall, AFM has surpassed flow cells in publications related to bacterial adhesion after the year 2000 (138 vs. 129), while among the techniques used to study individual forces of adhesion, it far exceeds the publication numbers for optical tweezers (25). AFM has gained this prominence through being particularly versatile. Traditionally, AFM has been used to probe interaction forces perpendicular to the substrate, generating curves of force felt by the AFM probe as a function of distance between the probe and the surface measured in the z-direction. In terms of understanding bacterial adhesion, surface-adhered bacteria have been probed using bare or modified AFM tips.[57,78-80] Conversely, bacteria have been used to probe various surfaces by covalently crosslinking

them either directly onto the AFM probe[81-83] or to a colloid that is subsequently attached to the tip of a cantilever.[84,85] Of particular interest, bacteria-modified cantilevers can be used to survey for low-biofouling surfaces.[86]

While the versatility and control over the interactions investigated using AFM is unprecedented, force measurements acquired normal to the surface have generally been restricted to acquiring data in the early stage of adhesion, ranging from attractive or repulsive interactions felt during approach to the force of detachment following physical contact over perhaps the first few seconds or minutes. Bond strengthening has been shown over the short term using AFM force spectroscopy.[87-89] Long-term adhesive forces have not been evaluated using this method, primarily due to low throughput. Only one vertical force measurement may be obtained per increment of time over which adhesion strength is to be evaluated.

More recently, a technique for applying a lateral force to adhered bacteria using AFM has been reported.[90-93] Here, bacteria adhered to a substrate are mechanically detached by an AFM probe scanning over the substrate, and this technique allows for analysis of many bacteria simultaneously, while maintaining control over the applied force. Detection of bacteria and bacterial detachment can be simultaneously monitored if the lateral forces are applied while imaging (contact mode). This method has been used to compare the effect of surface roughness/topography[91,93] and surface hydrophobicity[92] on the strength of bacterial adhesion, drawing empirical relationships between the normal force between the probe and the underlying substrate (assumed constant due to feedback loop adjustment). Later modifications to this technique introduced a more quantitative approach for determining the force applied to bacteria, applying it to monitor the long-term (Phase II) kinetics of adhesion

strength of *P. aeruginosa* and *S. aureus* over an 8 h time period (18-26 h after initial attachment).[90]

1.3 Antibacterial agents

It wasn't until the revolutionary introduction of germ theory in the latter half of the 19th century, spearheaded by such luminaries as Louis Pasteur and Robert Koch, when the connection was finally made between microorganisms and disease. Infections were relatively common occurrences, but rarely treatable and frequently deadly, and, therefore, viewed with a degree of superstition. Once microbes, invisible to the naked eye, were finally recognized as causative agents, doctors could begin to search for strategies to circumvent and treat infection. Vaccination against disease is one ingenious stratagem that obtained prominence with the acceptance of germ theory and has resulted in the prevention of countless infections.[94] Injection of a small amount of antigenic material (attenuated or inactivated pathogen) stimulates the immune system to produce antibodies that quickly recognize and bind to characteristic epitopes, tagging the microbe for destruction.[94] More frequently used to prevent viral infection, immunization has also enjoyed some success in preventing bacterial infection (e.g., tetanus, anthrax).

With the introduction of penicillin into clinical practice, hailed as the so-called 'magic bullet,' it seemed like bacterial infection was under control for the first time.[1] The *Penicillium* fungi had evolved the production of this molecule specifically to elicit bactericidal action, and penicillin could be used to rapidly cure infections caused by Gram-positive pathogens with no toxic effects. The natural products of thousands of microorganisms were intensively screened and additional drug candidates identified.

Ironically, it soon became evident that these drugs, when used inappropriately, became the selective pressure responsible for promoting the emergence of resistant species. Thus, there is always a drive for the discovery of new antibacterial agents and the identification of novel treatment options in the ongoing race to fight infection.

1.3.1 General overview of antibiotics. Antibiotics are a broad class of antimicrobial agent derived directly from microbial species that inhibit the growth of other microbial species. The production of antibiotics evolved as a partial solution to microbial competition for space by poisoning nearby microorganisms that vie for the same nutrients.[95] While conferring a selective advantage to antibiotic-producers, biofilm formation and other resistance mechanisms co-evolved as a protective response.[45] Classification as an antibiotic also requires that the natural products possess low molecular weights and efficacy at low concentrations.[95] Hence, neither lysozyme nor ethanol, both products of microorganisms with biocidal effects, is considered to be an antibiotic. Although antibiotics technically refer to an inhibitor of the growth of any microbe (e.g., bacteria, fungi, protozoa), only bactericidal antibiotics are considered here.

For therapeutic application in treating infectious disease, antibacterial agents should possess certain characteristics.[95] Of primary importance is a high level of efficacy (the ability to efficiently eradicate infectious pathogens) combined with minimal harmful side effects to the patient. A drug should also possess good bioavailability, or distribution to the infected part of the body, and elimination properties. The overall risk and toxicity to the patient should be low. Other preferable characteristics include that the drug be inexpensive to produce and exhibit activity against a range of pathogens. Around 10,000 antibiotics have been discovered, although only a small percentage of them have proven useful in treating

infectious disease. Antibiotics function by molecular recognition of and specific binding to a macromolecule or cellular component that performs a vital function within the bacteria. If the effects are lethal, the antibiotic is bactericidal, while if the growth of the bacteria is only inhibited (usually reversibly), the antibiotic is bacteriostatic. The major targets for antibiotic action are cell wall biosynthesis, protein biosynthesis, and DNA replication and repair.

Antibiotics are frequently classified into families based upon common chemical structure and biological properties, which are generally named after the first antibiotic of the family to be discovered.[95] The principle classes included β-lactams (penicillins), tetracyclines, aminoglycosides, macrolides, ansamycins, as well as certain peptides and glycopeptides. In order to improve action, bioavailability, or circumvent resistance to these natural products, pharmaceutical scientists have introduced minor modifications while preserving the structure of the active regions, and many semi-synthetic analogs have been successfully used to treat infection. For example, ampicillin and methacillin are two well known variants of penicillin, all three possessing the β-lactam ring structure that inhibits peptidoglycan synthesis. Finally, there are three families of fully-synthetic antibiotics used clinically: the sulfonamides, introduced in the 1930s; quinolones, introduced in the 1960s, and oxazolidanone, approved by the FDA in 2000.[95] To date, a virtual encyclopedia of information has been accumulated on biometabolism, structure/function relationships, mechanisms of action and of antibiotic resistance, bioavailability, therapeutic uses and treatment protocols of the various antibiotics.[95,96]

Antibiotics are popularly prescribed due to their high selectivity and low-dosage requirement, but due to the tendency for overuse, the co-evolution of numerous genetic resistance traits, and rapid adaptability of bacteria when faced with new stressors, it now

appears that antibiotic use in the sense we know it today will be of limited use.[1] The discovery of new antibiotics is slow. Identification of key bacterial targets helps direct attempts at developing new synthetic antibiotics, but with limited success. Furthermore, the introduction of a safe and effective new antibiotic has historically led to widespread use and subsequent development of resistance.[95] It is evident that antibiotics are losing their effectiveness for fighting infection, and other therapeutic options must be developed. Two candidates with proven antibacterial efficacy, ionic silver (Ag^+) and nitric oxide (NO), are discussed in detail below.

1.3.2 Ionic silver and silver compounds. With records dating back thousands of years, silver is perhaps the antimicrobial with the longest history of use by man.[97] Nano- to micromolar concentrations exhibit broad-spectrum bactericidal activity, showing efficacy against Gram-negative and -positive species including those resistant to traditional antibiotics.[98-101] Ag^+ reacts covalently with electron-donating groups (e.g., cysteine) and electostatically with negatively charged molecules (e.g., DNA). While the promiscuous reactivity of this species raises questions of toxicity to the host, centuries of use combined with modern clinical studies indicate that therapeutic doses of Ag^+ do not pose a serious health risk for humans.[97,98] For example, the minimum dose of silver nitrate ($AgNO_3$) causing inhibition of respiration in skin tissue culture was shown to be 25-fold greater than the quantity required to inhibit growth of *P. aeruginosa*,[102] a common pathogen in burn patients. The broad-spectrum activity exhibited against a wide range of microorganisms, including antibiotic-resistant species, ensures the continued interest in developing novel silver treatments, particularly for topical applications (e.g., burn and wound management).[100]

Storage of water in silver vessels was a common practice in ancient times. Silver in its solid, metallic (Ag^0) form is unreactive, and bacterial toxicity is limited by the rate of oxidation to the biologically active state (Ag^+). While this rate may be adequate to neutralize the relatively few microbes that might be present in drinking water to a sanitary level, bacterial infections are characterized by microbial densities of at least 10^5 organisms per gram of tissue mass.[99] The clinical solution for effective topical delivery of Ag^+ has been the use of silver compounds, particularly $AgNO_3$ (Fig 1.4A) and silver sulfadiazine (AgSD) (Fig 1.4B). These compounds, used clinically for over 40 years, represent the gold standard in silver delivery systems, releasing 3.8×10^4 (0.5% solution) and 1.6×10^4 (1% solution) μg Ag^+ in^{-2} d^{-1}, respectively.[99] Their nearest market competitor (in levels of Ag^+ released) is nanocrystalline silver, a metallic solid possessing high surface-to-volume ratios, though the quantity of Ag^+ delivered is almost two orders of magnitude lower.[99] The primary advantage of the nanocrystalline delivery formulation relates to its anti-inflammatory properties,[103,104] as prolonged inflammation can be deleterious to the wound healing process.[99]

Gram-negative bacteria are typically more susceptible to the effects of Ag^+.[100,105-107] Feng et al. attributed this to the protective nature of the thicker peptidoglycan layers possessed by Gram-positive species.[105] A screen of the efficacy of AgSD against 657 clinical isolates representing 22 bacterial species clearly demonstrated the susceptibility of Gram-negative species.[100] The authors pointed out the remarkable resistance displayed by *Enterococci* as a group, though surprisingly did not comment further on the overall trend of higher Gram-negative susceptibility evident in their data.[100] They did conclude that the most relevant pathogens for burn and wound infections were susceptible to doses of AgSD that

A

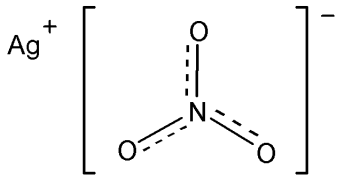

silver nitrate

B

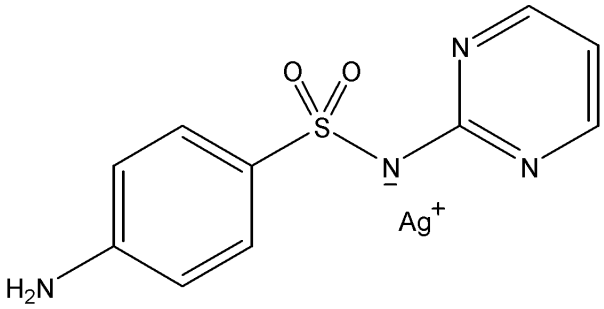

silver sulfadiazine

Figure 1.4 Molecular structures of the compounds (A) silver nitrate ($AgNO_3$) and (B) silver sulfadiazine (AgSD), commonly used for the topical delivery of Ag^+.

were easily achieved topically. Unfortunately, despite its efficacy, resistance to Ag^+ has been documented.[97,108-110] As with antibiotics, the expression of Ag^+-resistance primarily becomes a problem when the infection is treated with sub-bactericidal levels.[99] Li et al. showed that silver-resistant mutants of *Eschericia coli* could be cultivated in vitro through a step-wise exposure and selection procedure using low levels of $AgNO_3$.[108] The mechanism of Ag^+ resistance is thought to lie at the cell envelope level[111] and there is evidence of both porin deficiency and active efflux of Ag^+ in *E. coli*.[108]

The mechanism of bactericidal action of Ag^+ is still not clear. This is partially due to the broad level of reactivity, with numerous target sites and subsequent chains of cause-and-effect that are potentially interwoven. To complicate the elucidation process, the changes elicited from in vitro experiments with $AgNO_3$ differ somewhat from those observed when AgSD is used.[111-113] However, significant progress has been made in elucidating certain aspects of Ag^+ toxicity. One comprehensive set of studies aimed at elucidating the mechanism of AgSD activity utilized radioactive elements to trace the presence of ^{110}Ag in various cellular components (i.e., lipids, proteins and polysaccharides, and nucleic acids) of *P. aeruginosa* and verified that the majority of Ag^+ reacts with proteinaceous functional groups.[114,115] It is well known that thiol groups readily bind covalently to heavy metals such as Ag^+, and Liau et al. showed that the addition of compounds containing free thiol groups neutralized the bactericidal activity of $AgNO_3$ against the same species.[116] Adsorption to proteins inhibits their ability to function, and Ag^+ has been implicated in causing both structural and metabolic disruption to bacteria.[112,117]

Most of the bacterial target sites of Ag^+ probably lie in the vicinity of the cell membrane.[117,118] It has been shown that Ag^+ associates with cell wall components.[105,117]

After treatment with $AgNO_3$, electron-rich conglomerations on the order of tens of nanometers deposited around the cell wall of *E. coli* were visualized using transmission electron microscopy (TEM).[105] Images of *E. coli* and *S. aureus* treated with $AgNO_3$ also clearly showed detachment of the cytoplasmic membrane from the cell wall structure.[105] Using the same technique, AgSD-sensitive *Enterobacter cloacae* and *P. aeruginosa* demonstrated abnormal morphologies (e.g., blebbing) after exposure to this compound, while AgSD-resistant strains did not exhibit these changes.[111,119]

The effects of broad-scale membrane-oriented protein deactivation are not limited to structural damage. Importantly, a number of studies indicate that low concentrations of Ag^+ ($\leq$ 10 μM) inhibit cellular respiration in bacteria by decoupling the respiratory chain from oxidative phosphorylation, resulting in a lethal deenergization of the cell.[118,120-122] Dibrov et al. showed that treatment of *Vibrio cholerae* membrane vesicles with $AgNO_3$ caused a massive proton leakage and subsequent collapse of the proton gradient across the membrane ultimately dissipating the proton motive force.[120] Further evidence that Ag^+ affects electron transport at the membrane was provided by Holt and Bard,[118] who demonstrated that $AgNO_3$ caused an initial stimulation followed by a complete cessation of respiration in *E. coli*.

In addition to adsorption at the cell membrane level, some studies indicate that Ag^+ penetrates the bacterial cell and interacts directly with cytoplasmic proteins and DNA. TEM showed condensation of chromosomal DNA after treatment with $AgNO_3$, purportedly inhibiting replication and division.[105,119] Complementary analyses of electron-dense granules in the vicinity using X-ray microanalysis positively identified both Ag and S, suggesting that Ag^+ interacts with intracellular protein thiols as well.[105] Cell fractionation experiments of *P. aeruginosa* treated with radiolabeled silver compounds showed a positive correlation

between growth inhibition and the quantity of DNA-associated Ag^+, despite the low level of interaction relative to Ag bound to the protein fraction.

1.3.3 Nitric oxide and NO-donors. Nitric oxide is a highly reactive, diatomic free radical endogenously produced by the enzyme nitric oxide synthase (NOS), which catalyzes the oxidation of L-arginine to L-citrulline.[123] NO has been implicated as a mediator in diverse physiological processes, ranging from regulatory roles in the cardiovascular and nervous system to the inducible host response to infection.[124,125] Various therapeutic properties attributed to NO, including tumor cytotoxicity,[126,127] vasodilation, and improved wound healing and tissue integration at implant sites[128] may prove beneficial in a number of pharmacological applications.[129,130] In particular, the antimicrobial properties of NO, an essential part of the body's endogenous first line defense against foreign pathogens,[131,132] are of interest as a therapeutic option for the treatment of infection. The very fact that this role is conserved[133] yet continually effective implies a limited ability on the part of bacteria to develop resistance to the antimicrobial action of NO. In terms of NO-tolerance, low molecular weight thiols play a role in scavenging NO in bacterial cells,[131] while *E. coli*, *S. aureus*, and *Salmonella typhimurium* bacteria have been shown to upregulate the production of certain proteins in the presence of NO in order to resist NO-mediated damage.[134-137] However, it is unlikely that bacteria possess mechanisms sufficient to tolerate therapeutic doses of NO, as these are much higher than the quantities produced endogenously by the host's immune system.

Like Ag^+, NO is a broad-spectrum antibacterial agent of somewhat dubious mechanisms and is known to react either directly or indirectly with cysteine residues and transition-metal centers of proteins, DNA, and lipids.[131,138,139] The effects of direct NO-modification are

more prominent at low concentrations (<1 μM) and include reaction with metal and metal-oxygen complexes (including hemoglobin) as well as other high energy radicals.[138] At concentrations in the micromolar range and above, NO elicits indirect effects through the formation of reactive nitrogen oxide species (RNOS) that then render nitrosative and oxidative stresses upon biomolecules.[138] Oxidative stresses involve hydroxylation reactions as well as the withdrawal of 1 to 2 electrons from a substrate.[138] Nitrosative stress may refer either to nitrosation by the addition of NO^+ to an amine or thiol or to nitration of aromatic groups by the addition of an equivalent of NO_2^+.[138] When NO reacts with oxygen (O_2) or superoxide (O_2^-), species commonly encountered near bacteria lipid membranes, highly reactive RNOS intermediates are formed.[131,138,140] Reaction with O_2 forms nitrogen dioxide (NO_2) and dinitrogen trioxide (N_2O_3), which primarily function via deamination of nucleotides and nitrosation of thiols and amines.[138,140,141] The strong oxidant peroxynitrite ($ONOO^-$) is formed by reaction with O_2^- and has been implicated in the radical lipid peroxidation leading to membrane degradation in addition to deleterious modification of proteins and DNA.[131,138] Despite a solid understanding of the types of reactions undergone by NO and RNOS, it is not clear which target sites are critical for bactericidal activity.[131] Considering the lipophilic nature of NO and the proximity of O_2 and O_2^- to the cytoplasmic membrane,[140] it is likely that many targets are concentrated in this vicinity.

Due to its high level of reactivity, diverse regulatory roles, diffusibility,[142] and short half-life in blood (< 1 s),[143] the ability to target therapeutic NO delivery locally is critical. Gaseous NO (gNO), delivered from a cylinder of compressed gas, has been evaluated for topical application[144] and as a potential treatment of pulmonary infections via direct, intermittant inhalation of gNO diluted in medical-grade air.[145,146] For treatment of infections

that are not directly available for gNO exposure, a NO-delivery system is needed. Nitric oxide donating compounds, such as *S*-nitrosothiols[147,148] and *N*-diazeniumdiolates,[129] decompose to release NO and hence serve as vehicles for its storage and transport (Fig. 1.5). As the name suggests, *S*-nitrosothiol functionalities, usually abbreviated RSNO, consist of an NO group bonded directly to a sulfur atom and embody the endogenous solution to the problem of NO storage (Fig. 1.5A). Release of NO from RSNO is catalyzed by light, heat, metal ions, or via direct transfer to a second thiol.[148,149] Most RSNO also decompose spontaneously, and their inherent instability limits their shelf life.[148,149] *N*-Diazeniumdiolates (NONO-ates) represent a second class of NO-donor functionality that store NO on primary or secondary amines (Fig 1.5B).[143] Stable at low temperatures and in aprotic environments, diazeniumdiolate moieties rapidly decompose into two equivalents of NO under physiological pH and temperature (regenerating the parent amine), a characteristic of clinical significance.[129]

A number of materials, including nanoparticles,[150,151] films and coatings,[152,153] and small molecules,[154,155] have employed diazeniumdiolate chemistry with varied physicochemical and NO-release properties that are dependent upon the structure of the NONO-ate as well as the chemical environment provided by the material backbone.[156] Stabilizing effects may be provided, for example, by nearby positively charged amines or by protection of the moiety from solvent (e.g., within a xerogel polymer matrix), slowing decomposition according to the rate of water permeability. By contrast, many small molecule donors such as diazeniumdiolate-modified proline (PROLI/NO)[155] possess a very short half life in water since the protic solvent has ready access to the diazeniumdiolate moiety. Tuneable NO-release properties are a key feature of diazeniumdiolate-modified materials as it allows

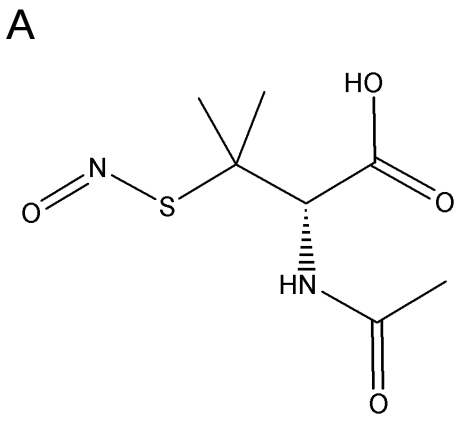

Figure 1.5 Molecular structures of representative NO-donor compounds. (A) *S*-Nitrosothiol-modified penicillamine (SNAP) and (B) *N*-diazeniumdiolate-modified proline (PROLI/NO) store one and two equivalents of NO per molecule, respectively.

control over both duration and dose of therapeutic NO delivered.[156]

The antimicrobial properties of NONO-ate materials have been characterized against a number of pathogenic bacterial species, including Gram-negative, -positive, and antibiotic-resistant species.[107,157-159] Nitric oxide released from xerogel coatings have been shown to reduce the rate of bacterial attachment[158,160,161] while killing those that do adhere.[158] As would be expected, a positive correlation exists between the dose of NO and the level of antibacterial activity.[107,157,158] Short-term delivery of NO via a bolus results in a higher degree of cellular damage than equivalent doses delivered more slowly as a sustained, but localized, surface flux.[157] However, a localized bolus delivery of NO from nanoparticles was shown to be more effective than a dissipated, but higher concentration, bolus dose from PROLI/NO.[159] Therefore, both the dose of NO and the proximity of NO release to the pathogens appears to be important for antibacterial efficacy. Nitric oxide-releasing nanoparticles have also proven effective against day-old biofilms of Gram-negative and -positive species in addition to an infectious species of yeast (*Candida albicans*).[162] At bactericidal levels, the toxicity of NO against mammalian cells is low,[145,159] and in some cases has been shown to promote proliferation of epithelial cells and increase survival of macrophages.[145] Therefore, materials that store and release NO are very promising for their potential to both reduce the likelihood of initial bacterial attachment and treat established infection.

1.4 Techniques for evaluating antimicrobial activity

1.4.1 Morphology. Bacteria, though invisible to the naked eye, are of very convenient dimensions for viewing microscopically. Further, healthy cells of a particular species have a

relatively standard outer appearance. Thus, with the introduction of high-resolution microscopes such as SEM, TEM, and AFM, scientists have the tools to directly observe antibacterial effects. Morphological analyses of bacteria aid in understanding mechanisms of antibiotic action by allowing visualization of changes in the appearance of the microbe undergone subsequent to treatment. The images obtained using electron microscopy are primarily utilized to obtain qualitative comparisons. For example, dose-dependence can be monitored as a function of concentration or exposure time. In addition, antimicrobials that function by similar mechanisms can be compared. With the introduction of AFM for morphological evaluation, semi-quantitative information on changes in bacterial surface roughness could be obtained simultaneously with high-resolution three-dimensional reconstructions of cell morphology.[157,163] An added benefit of AFM is the flexible and adaptable nature of cantilevers as transducers that allow detection of other physical (e.g., elasticity) or chemical (e.g., charge distribution) surface parameters simultaneously with the acquisition of height information.[57,78,163,164]

Changes in appearance, or morphology, of bacteria exposed to various antimicrobials have been frequently reported since the 1970s.[105,111,112,165-168] As described in Section 1.3.2, TEM was vital for demonstrating the structural damage wrought by Ag^+ on Gram-negative and -positive species and well as visualizing adsorption to DNA.[105,111,112] Klainer and Russell[166] used SEM analysis to show that two antibiotics that inhibit protein synthesis (chloramphenicol and streptomycin) rendered a similar spectrum of morphological changes on *E. coli*. Another study compared the effects of two β-lactam antibiotics amoxicillin and ampicillin on *E. coli*, and found a correlation between morphology and the superior activity of amoxicillin.[168]

While electron microscopy has been employed toward this end for decades, atomic force microscopy (AFM) has recently been used with increasing frequency.[169-174] As a surface characterization tool, AFM is ideal for morphological studies of surface-adhered bacteria as it allows cells to be imaged in situ with high resolution without requiring chemical drying, metal coating, or exposure to ultra-high vacuum. Atomic force microscopy has been applied to visualizing the antimicrobial action of peptides,[169,171,173] chitosan,[170] quantum dots,[172] and the β-lactam antibiotics penicillin and amoxicillin.[174] It has also been used to monitor the dose-dependence of NO on cell roughness and to compare the efficacy of two NO-donor delivery methods.[157]

1.4.2 Efficacy. While microscopy is very useful for visualizing the effects of biocides, it is very important from a clinical standpoint to evaluate antimicrobial efficacy in quantitative terms. To be clinically effective, it is essential that therapeutic drug concentrations are achieved at the site of infection. Pharmacodynamics represent the dose of an antibacterial agent necessary to elicit bacteriostatic (inhibitory) or bactericidal effects.[175] The interaction between the drug and the patient's body, or the pharmacokinetics, also plays a role in overall efficacy. Pharmacokinetics encompasses absorption, biodistribution, metabolism and elimination of the drug by the patient.[175] Parameters describing the pharmacokinetics and pharmacodynamics of an antibiotic help quantify the degree to which a treatment will be effective against infection.

Due to the broad medical application and need for consistency, there are relatively standardized techniques for evaluating the efficacy of an antibacterial.[176] In determining the pharmacodynamic interplay between a target microorganism and antibacterial agent in vitro, the minimum inhibitory concentration (MIC) and/or the minimum bactericidal concentration

(MBC) are generally determined.[177] The classical approach for evaluating the antibacterial efficacy of a biocide is determination of the MIC, or the drug concentration sufficient to arrest further growth of the bacteria in nutrient broth. A common technique is the microdilution broth method, where the MIC is determined by inoculating a vial of bacteria (at concentrations below detection via optical density) with a series of concentrations of the drug and allowing growth at 37 °C overnight.[177] The MIC falls between the lowest concentration vial retaining transparent media and the highest concentration vial exhibiting visible turbidity.[177] A similar approach utilizes solid media prepared with two-fold, stepwise dilutions of the antibacterial. Bacteria are spread upon the agar surface, and inhibition is determined by the lowest concentration that inhibits colony growth.[96]

Inhibition of growth, however, does not indicate bactericidal doses. In fact, inhibitory doses often have reversible effects, and treating infection-causing bacteria with sub-bactericidal levels tends to select for and allow further growth of mutants and naturally resistant strains. Common methods for evaluating the bactericidal activity of an antimicrobial are killing curves and determination of minimum bactericidal concentration (MBC).[177] Determination of the MBC is more clinically useful, though more work intensive, than the MIC. The MBC, usually conducted by counting colony-forming units (cfu) grown on agar plates before and after treatment, was historically determined by plating an aliquot of each vial containing transparent media following an MIC assay. The lowest concentration of bactericidal agent capable of eliciting a 3-log reduction in viable bacteria is the MBC, and any higher concentration should be bactericidal as well.[177]

Evaluating efficacy using in vitro infection models is fast and inexpensive, and the main disadvantage lays in the simplicity of the system (also an advantage). For instance the

conspicuous absence of the immune system means that contributions to efficacy from endogenous defenses cannot be evaluated in concert with the antibiotic.[175] It is also known that bacteria in vitro grow faster and express decreased levels of virulence.[178] Additionally, the microdilution broth methods to determine MIC and MBC values evaluate inhibition and viability of planktonic cells, which are faster-growing and more susceptible to antimicrobials that disrupt metabolic processes than would their sessile, slow-growing counterparts. Although it is more convenient to study planktonic cells, it is also important to evaluate antimicrobial efficacy on biofilms.

Biofilms (Section 1.1.4), characterized by sessile communities of bacteria, are commonly associated with recurrent, chronic, and device-related infection and are responsible for an estimated 60% of human infections.[45] The evolution of matrix-encased, cooperative community organizations that reduce susceptibility to antibiotics (natural products) was certainly advantageous in the microbial competition for space in nature. This protective advantage has been carried over to infectious biofilms,[45] rendering them notoriously difficult to treat. The underlying causes of reduced susceptibility of biofilms is multifactorial and not fully understood: the EPS encapsulating the biofilm renders them relatively impermeable to most antibacterials; cells in a biofilm exhibit decreased rates of growth and metabolism; alterations in phenotypic and genotypic expression of sessile bacteria may affect their sensitivity; and, finally, the rather ambiguous theory of the persister cell that expresses a temporary tolerance to antibacterials due to the necessity to survive under stress.

Biofilms often require from 10 to 1,000-fold greater concentrations than planktonic bacteria to achieve efficacy.[179-182] Based upon the poor correlation in efficacies obtained for planktonic vs. biofilm bacteria and subsequent difficulties in predicting the therapeutic

outcome of treating suspected biofilm-related infections using planktonic (MIC or MBC) determinations, a new procedure was necessary to present quantitative information regarding the reduced susceptibility of biofilms.[45] The minimum biofilm eradication concentration (MBEC) assay was thus designed to assess antimicrobial efficacy against these surface-associated communities.[45,179,182,183] Briefly, equivalent biofilms are grown simultaneously in each well of a 96-well microtitre plate. After exposure to antibacterial agents for 24 h, the biofilm is removed via sonication and transferred to sterile nutrient broth. The MBEC is the lowest dilution of biocide at which bacteria fail to regrow.

1.4.3 Combination therapy. Resistance to standard antibiotic treatments is a growing problem and resistance to all clinically used antibiotics has been documented, while the discovery of novel antibiotics or synthetic antibacterial agents is a slow process.[1] Elucidation of the genes and proteins essential for bacterial vitality allows us to pinpoint specific targets in order to intelligently design and assay potential new treatment options.[95] Bacteria faced with a new antibacterial agent must adapt or die. Unfortunately for us, the rate at which bacteria divide is exceptionally fast. Though adaptation through mutation is slow for most organisms, bacteria quickly adapt to new agents, developing resistance mechanisms that allow them to flourish. As bacteria often share genetic material, the genes that code for resistance may be passed not only to the offspring of the resistant mutant, but also to other bacterial species, particularly those that reside in close proximity either on the body of the patient or in the nearby community.[1,184] Due to the pressing problem of resistance, there is a continual need for the introduction of novel treatment options. Until the time that it becomes possible to prevent infections from forming, it is necessary to treat infections that do form while taking care to stave off developing resistance.

One approach is combination therapy, the concerted use of two or more antibacterial agents. There are numerous benefits to using antimicrobial combinations. One reason is to enhance the spectrum of activity through multiple mechanisms of action, and this may be particularly useful when treating polymicrobial infections, such as wound beds, or seriously ill patients.[185] The presence of multiple bactericidal mechanisms also reduces the likelihood for resistance to develop, in addition to allowing treatment of infections that may already express some resistance to one of the agents. One final advantage to combination therapy is the potential to minimize any toxic effects imposed by the individual antibacterial agents.[185] If the effects of combined usage are at least additive, then only half the dose of each individual biocide in combination would be necessary to elicit the response garnered from the full dose of either agent independently.

Synergy between agents is another possible outcome of combination therapy. Synergism is achieved when the coincident use of two agents is characterized by a greater than additive effect than when the agents are dosed individually. This may be expressed as a greater rate of action or in the absolute magnitude of bacterial killing.[186] In order to intelligently predict advantageous combinations, knowledge of the mechanisms of action of individual agents is important.[187] Synergistic combinations represent a particularly attractive avenue for slowing the rate of emerging resistance, possessing all the advantages of combination therapy in addition to further reducing potential toxicity by requiring even smaller doses. Depending upon the mechanism of action, the use of synergistic combinations may also further reduce the probability of emerging resistance.[186]

One route to attain synergy involves combining a cell permeabilizer with an agent that functions primarily within the cytoplasm, with the end goal of improving the accessibility of

the target to the biocide. For example, the combined use of penicillin, a cell wall-active agent, and the aminoglycoside streptomycin has synergistic activity against most Gram-positive bacteria, including *Enterococci*,[188,189] *Streptococci*,[190] and *Staphylococci*,[191] as well as some Gram-negative bacteria.[192,193] Other agents that enhance membrane permeability, such as *p*-aminobenzoic acid (PABA)[194] and positively charged glycopeptides,[195] have successfully been combined with intracellularly active agents to produce synergy.

Another synergistic mechanism is brought about if one agent serves to protect the second agent, for example, through inhibition of a modifying enzyme. One resistance determinant currently expressed by many bacteria is the β-lactamase enzyme, which hydrolyzes and cleaves the β-lactam ring of penicillin-like antibiotics. In an attempt to circumvent the detrimental effect of this enzyme, much research has focused on developing analogs that express a lower affinity for the β-lactamase and numerous generations of β-lactam family have been generated.[95] Another approach to overcoming the β-lactam resistance utilizes the synergistic combination of a β-lactamase inhibitor, a molecule possessing a higher affinity for the enzyme, used in concert with a typical β-lactam antibiotic.[196]

The sequential blockage of steps in a metabolic pathway has also been shown to elicit synergistic activity. The combination of trimethoprim with a sulfa drug such as sulfamethoxazole or sulfadiazine exhibits synergistic activity by inhibiting two important enzymes that synthesize folic acid (dihydropteroate synthetase and dihydrofolate reductase).[197,198] While each agent is typically bacteriostatic when used independently, the combination elicits bactericidal activity and is effective against a wide range of pathogens (both Gram-negative and -positive species).[185,199]

The synergistic activity between two biocides is typically evaluated using a checkerboard assay to determine the ideal combined concentration to elicit either inhibitory or bactericidal effects.[185] This technique is carried out by creating an array of all possible combinations of two antibiotics serially diluted within a desired range.[200] The endpoint is typically evaluated at the lowest concentrations that inhibit growth (as determined by turbidity) and is expressed as the fractional inhibitory concentration (FIC) as determined from Equation 1.1:[200,201]

$$FIC = \frac{MIC_{AB}}{MIC_{A}} + \frac{MIC_{BA}}{MIC_{B}} \qquad \text{Eq. (1.1)}$$

where MIC_A and MIC_B are the inhibitory concentrations for the individual agents and MIC_{AB} and MIC_{BA} are the lowest combined concentrations to elicit an inhibitory effect. The endpoint of the assay can be modified to require bactericidal activity, and can be combined with the principle of time-kill techniques[200] to determine dose-dependency by evaluating viability as a function of time.[107]

1.5 Summary of dissertation research

My dissertation research has focused on the improvement and implementation of bioanalytical techniques to investigate non-specific bacterial adhesion and characterize the antimicrobial properties of NO. The specific aims of my research included:

1. the development of an improved AFM methodology for quantifying the lateral force required to detach bacteria adhered to a surface;

2. characterization of the kinetics of adhesion strength exhibited by *P. aeruginosa* and *S. aureus* to a hydrophobic xerogel coating in late stages of adhesion (> 18 h after attachment);
3. the application of high-resolution AFM imaging to qualitatively visualize the morphological changes of two Gram-negative pathogens, *E. coli* and *P. aeruginosa*, after exposure to NO;
4. determination of the concentration-dependent effects of NO released as a bolus from a small-molecule donor and time-dependent effects of NO released via a sustained surface flux from a xerogel coating using a quantitative analysis of membrane roughness; and
5. the evaluation of the bactericidal efficacy elicited by NO and AgSD in combination against a wide range of pathogenic bacteria, including two antibiotic-resistant strains, using modified viability assays that require bactericidal efficacy within 2 h.

The goal of this introduction (Chapter 1) was to provide background on the problem and process of infection as well as an overview of infection treatment in order to generate a context for understanding the motivation and potential applications of my dissertation research. Chapter 2 introduces an improved technique for measuring the adhesion strength of bacteria and its application toward observing late-stage adhesion kinetics. Chapter 3 discusses the implementation of AFM to qualitatively observe changes in bacterial morphology after treatment with NO and compare with the effects of treatment with a cell wall-active agent, amoxicillin. In addition, quantitative measurements of membrane roughness used to evaluate the dose-dependence of NO and compare two NO-delivery

methods are described. Chapter 4 focuses on the use of stringent efficacy assays to determine the antimicrobial activity of NO and AgSD alone and in combination, while potential mechanisms to account for the observed synergistic activity are postulated. Finally, Chapter 5 summarizes my dissertation research and suggests several interesting avenues for future research based upon both lateral force measurements acquired with AFM and the antimicrobial properties of NO.

1.6 References

(1) Levy, S. B. *The Antibiotic Paradox*; 2nd ed.; Perseus: Cambridge, 2002.

(2) Kreier, J. P. Host-Parasite Relationships. *Infection, Resistance, and Immunity*; 2nd ed.; Taylor & Francis: Ann Arbor, MI, 2002; pp 13-26.

(3) Baldwin, C. Constitutive Host Response. *Infection, Resistance, and Immunity*; 2nd ed.; Taylor & Francis: Ann Arbor, MI, 2002.

(4) Dugan, P. R. Bacteria. *Infection, Resistance, and Immunity*; 2nd ed.; Taylor & Francis: Ann Arbor, MI, 2002; pp 283-318.

(5) Seltmann, G.; Holst, O. *The Bacterial Cell Wall*; Springer: Berlin, 2002; 280.

(6) Winter, L. Pathogenicity and Virulence. *Infection, Resistance, and Immunity*; 2nd ed.; Taylor & Francis: Ann Arbor, MI, 2002; pp 265-282.

(7) Coico, R. Gram staining. *Curr. Protoc. Immunol.* **2001**, *Appendix 3O*.

(8) Beveridge, T. J. Use of the gram stain in microbiology. *Biotech. Histochem.* **2001**, *76*, 111-118.

(9) Apicella, M. A.; Griffiss, J. M.; Schneider, H. Isolation and characterization of lipopolysaccharides, lipooligosaccharides, and lipid A. *Meth. Enzymol.* **1994**, *235*, 242-252.

(10) Tsujimoto, H.; Gotoh, N.; Nishino, T. Diffusion of macrolide antibiotics through the outer membrane of *Moraxella catarrhalis*. *J. Infect. Chemother.* **1999**, *5*, 196-200.

(11) Nikaido, H. Isolation of outer membranes. *Meth. Enzymol.* **1994**, *235*, 225-234.

(12) Jiang, X.; Pace, J. L. Microbial biofilms. *Biofilms, Infection, and Antimicrobial Therapy*; Taylor & Francis: Boca Raton, 2006; pp 3-20.

(13) An, Y. H.; Friedman, R. J. Concise Review of Mechanisms of Bacterial Adhesion to Biomaterial Surfaces. *J. Biomed. Mater. Res. (Appl. Biomater.)* **1998**, *43*, 338-348.

(14) Dankert, J.; Hogt, A. H.; Feijen, J. Biomedical polymers: Bacterial adhesion, colonization, and infection. *CRC Crit. Rev. Biocompat.* **1986**, *2*, 219-301.

(15) Katsikogianni, M.; Missirlis, Y. F. Concise review of mechanisms of bacterial adhesion to biomaterials and of techniques used in estimating bacteria-material interactions. *Eur. Cells Mater.* **2004**, *8*, 37-57.

(16) Li, B.; Logan, B. E. Bacterial adhesion to glass and metal-oxide surfaces. *Colloids Surf., B* **2004**, *36*, 81-90.

(17) Hogt, A. H.; Dankert, J.; Feijen, J. Adhesion of *Staphylococcus epidermidis* and *Staphylococcus saprophyticus* to a hydrophobic biomaterial. *J. Gen. Microbiol.* **1985**, *131*, 2485-2491.

(18) Chin, M. Y. H.; Sandham, A.; Pratten, J.; de Vries, J.; van der Mei, H. C. et al. Multivariate analysis of surface physico-chemical properties controlling biofilm formation on orthodontic adhesives prior to and after fluoride and chlorhexidine treatment. *J. Biomed. Mater. Res. (Appl. Biomater.)* **2006**, *78B*, 401-408.

(19) Dickinson, R. B.; Nagel, J. A.; Proctor, R. A.; Cooper, S. L. Quantitative comparison of shear-dependent *Staphylococcus aureus* adhesion to three polyurethane ionomer analogs with distinct surface properties. *J. Biomed. Mater. Res.* **1997**, *36*, 152-162.

(20) Tang, H.; Cao, T.; Wang, A.; Liang, X.; Salley, S. O. et al. Effect of surface modification of siliconeon to *Staphylococcus epidermidis* adhesion and colonization. *J. Biomed. Mater. Res.* **2006**, *80A*, 885-894.

(21) Dickinson, R. B.; Nagel, J. A.; McDevitt, D.; Foster, T. J.; Proctor, R. A. et al. Quantitative comparison of clumping factor- and coagulase-mediated *Staphylococcus aureus* adhesion to surface-bound fibrinogen under flow. *Infect. Immun.* **1995**, *63*, 3143-3150.

(22) Kussela, P. Fibronectin binds to *Staphylococcus aureus*. *Nature* **1978**, *276*, 718-720.

(23) Morris, E. J.; McBride, B. C. Adherence of *Streptococcus sanguis* to saliva-coated hydroxyapatite: Evidence for two binding sites. *Infect. Immunol.* **1984**, *43*, 656-663.

(24) Paulsson, M.; Kober, M.; Freij-Larsson, C.; Stollenwerk, M.; Wesslen, B. et al. Adhesion of *Staphylococci* to chemically modified and native polymers, and the influence of preadsorbed fibronectin, vitronectin and fibrinogen. *Biomaterials* **1993**, *14*, 845-853.

(25) Orstavik, D. Sorption of *Streptococcus faecium* to glass. *Acta Pathol. Microbiol. Scand.* **1977**, *85B*, 38-46.

(26) Dudderiege, J. E.; Cent, C. A.; Laws, J. E. Effect of surface shear stress on the attachment of *Pseudomonas fluorescens* to stainless steel under defined flow conditions. *Biotechnol. Bioeng.* **1982**, *24*, 153-164.

(27) McWhirter, M. J.; McQullan, A. J.; Bremer, P. J. Influence of ionic strength and pH on the first 60 min of *Pseudomonas aeruginosa* attachment to ZnSe and to TiO_2 monitored by ATR-IR spectroscopy. *Colloids Surf., B* **2002**, *26*, 365-372.

(28) Walker, S. L.; Redman, J. A.; Elimelech, M. Influence of Growth Phase on Bacterial Deposition: Interaction Mechanisms in Packed-Bed Column and Radial Stagnation Point Flow Systems. *Environ. Sci. Technol.* **2005**, *39*, 6405-6411.

(29) An, Y. H.; Dickinson, R. B.; Doyle, R. J. Mechanisms of Bacterial Adhesion and Pathogenesis of Implant and Tissue Infections. *Handbook of Bacterial Adhesion: Principles, Methods, and Applications*; Humana Press Inc.: Totowa, NJ, 2000; pp 1-27.

(30) Gristina, A. G. Biomaterial-centered infection: Microbial adhesion versus tissue integration. *Science* **1987**, *237*, 1588-1595.

(31) Marshall, K. C. Mechanisms of bacterial adhesion at solid-water interfaces. *Bacterial adhesion: mechanisms and physiological significance*; Plenum Press: New York, 1985; pp 133-161.

(32) Vacheethasanee, K.; Marchant, R. E. Nonspecific *Staphylococcus epidermidis* Adhesion: Contributions of Biomaterial Hydrophobicity and Charge. *Handbook of Bacterial Adhesion*; Humana Press: Totowa, NJ, 2000; pp 73-90.

(33) van Loosdrecht, M. C.; Lyklema, J.; Norde, W.; Zehnder, A. J. Influence of interfaces on microbial activity. *Microbiol. Rev.* **1990**, *54*, 75-87.

(34) Veenstra, G. J.; Cremers, F. F.; van Dijk, H.; Fleer, A. Ultrastructural organization and regulation of a biomaterial adhesin in *Staphylococcal epidermidis*. *J. Bacteriol.* **1996**, *178*, 537-541.

(35) O'Toole, G.; Kolter, R. Flagellar and twitching motility are necessary for *Pseudomonas aeruginosa* biofilm development. *Mol. Microbiol.* **1998**, *30*, 295-304.

(36) Hermann, M.; Vaudaux, P.; Pittet, D.; Auckenthaler, R.; Lew, D. P. et al. Fibronectin, fibrinogen and laminin act as mediators of adherence of clinical *Staphylococcal* isolates to foreign material. *J. Infect. Dis.* **1988**, *158*, 693-701.

(37) Boyd, A.; Chakrabarty, A. M. Role of alginate lyase in cell detachment of *Pseudomonas aeruginosa*. *Appl. Environ. Microbiol.* **1994**, *60*, 2355-2359.

(38) Davies, D. G.; Geesey, G. G. Regulation of the alginate biosynthesis gene algC in *Pseudomonas aeruginosa* during biofilm development in continuous culture. *Appl. Environ. Microbiol.* **1995**, *61*, 860-867.

(39) Sharon, N.; Lis, H. Lectins as cell recognition molecules. *Science* **1989**, *246*, 227-234.

(40) Mandrell, R. E.; Apicella, M. A.; Lindstedt, R.; Leffler, H. Possible interaction between animal lectins and bacterial carbohydrates. *Meth. Enzymol.* **1994**, *234*, 231-254.

(41) Burne, R. A.; Quivey, R. G.-J. Use of transposons to dissect pathogenic strategies of Gram-positive bacteria. *Meth. Enzymol.* **1994**, *235*, 405-426.

(42) Ofek, I.; Beachey, E. H. General concepts and principles of bacterial adherence in animals and man. *Bacteria Adherence*; Chapman and Hall: London, 1980; pp 1-29.

(43) Costerton, J. W.; Lewandowski, Z.; Caldwell, D. E.; Korber, D. R.; Lappin-Scott, H. M. Microbial biofilms. *Annu. Rev. Microbiol.* **1995**, *49*, 711-745.

(44) Lawrence, J. R.; Neu, T. R. Confocal laser scanning microscopy for analysis of microbial biofilms. *Meth. Enzymol.* **1999**, *310*, 131-144.

(45) Ceri, H.; Olson, M. E.; Morck, D. W.; Storey, D. G. Minimal Biofilm Eradication Concentration (MBEC) Assay: Susceptibility Testing for Biofilms. *Biofilms, Infection, and Antimicrobial Therapy*; Taylor & Francis: Boca Raton, 2006; pp 257-269.

(46) Donlan, R. M.; Costerton, J. W. Biofilms: Survival mechanisms of clinically relevant microorganisms. *Clin. Microbiol. Rev.* **2002**, *15*, 167-193.

(47) Costerton, J. W.; Stewart, P. S.; Greenberg, E. P. Bacterial biofilms: A common cause of persistent infections. *Science* **1999**, *284*, 1318-1322.

(48) Black, S. J. Introduction to Infection, Resistance, and Immunity. *Infection, Resistance, and Immunity*; 2nd ed.; Taylor & Francis: Ann Arbor, MI, 2002; pp 1-12.

(49) Otto, K. Biophysical approaches to study the dynamic process of bacterial adhesion. *Res. Microbiol.* **2008**, *159*, 415-422.

(50) An, Y. H.; Friedman, R. J. Laboratory methods for studies of bacterial adhesion. *J. Microbiol. Methods* **1997**, *30*, 141-152.

(51) O'Toole, G.; Kolter, R. Initiation of biofilm formation in *Pseudomonas fluorescens* WCS365 proceeds via multiple, convergent signalling pathways: A genetic analysis. *Mol. Microbiol.* **1998**, *28*, 449-461.

(52) Darouiche, R. O. Treatment of infections associated with surgical implants. *New Engl. J. Med.* **2004**, *250*, 1422-1429.

(53) Weinstein, R. A. Special Issue: Nosocomial Infection Update. *Emerging Infectious Diseases* **1998**, *4*, 416-420.

(54) Garrett, T. R.; Bhakoo, M.; Zhang, Z. Characterisation of bacterial adhesion and removal in a flow chamber by micromanipulation measurements. *Biotechnol. Lett.* **2008**, *30*, 427-433.

(55) Walker, S. L.; Hill, J. E.; Redman, J. A.; Elimelech, M. Influence of growth phase on adhesion kinetics of *Escherichia coli* D21g. *Appl. Environ. Microbiol.* **2005**, *71*, 3093-3099.

(56) Liu, Y. Adhesion kinetics of nitrifying bacteria on various thermoplastic supports. *Colloids Surf., B* **1995**, *5*, 213-219.

(57) Camesano, T. A.; Logan, B. E. Probing bacterial electrosteric interactions using atomic force microscopy. *Environ. Sci. Technol.* **2000**, *34*, 3354-3362.

(58) Otto, K.; Elwing, H.; Hermansson, M. Effect of ionic strength on the initial interactions of *Escherichia coli* with surfaces studied on-line by a novel quartz crystal microbalance. *J. Bacteriol.* **2004**, *181*, 5210-5218.

(59) Pitt, W. G.; McBride, M. O.; Barton, A. J.; Sagers, R. D. Air-water interface displaces adsorbed bacteria. *Biomaterials* **1993**, *14*, 605-608.

(60) Prince, J. L.; Dickinson, R. B. Kinetics and forces of adhesion for a pair of capsular/unencapsulated *Staphylococcus* mutant strains. *Langmuir* **2003**, *19*, 154-159.

(61) Bakker, D. P.; Busscher, H. J.; van der Mei, H. C. Bacterial deposition in a parallel plate and a stagnation point flow chamber: microbial adhesion mechanisms depend on the mass transport conditions. *Microbiology* **2002**, *148*, 597-603.

(62) Bosch, J. A.; Veerman, E. C.; Turkenburg, M.; Hartog, K.; Bolscher, J. G. et al. A rapid solid-phase fluorimetric assay for measuring bacterial adherence, using DNA-binding stains. *J. Microbiol. Methods* **2003**, *53*, 51-56.

(63) Olofsson, A. C.; Zita, A.; Hermansson, M. Floc stability and adhesion of green-fluorescent-protein-marked bacteria to flocs in activated sludge. *Microbiology* **1998**, *144 (Part 2)*, 519-528.

(64) Emerson, R. J.; Camesano, T. A. Nanoscale investigation of pathogenic microbial adhesion to a biomaterial. *Appl. Environ. Microbiol.* **2004**, *70*, 6012-6022.

(65) Vesterlund, S.; Paltta, J.; Karp, M.; Ouwehand, A. C. Measurement of bacterial adhesion - in vitro evaluation of different methods. *J. Microbiol. Methods* **2005**, *60*, 225-233.

(66) Cooper, M. A.; Singleton, V. T. A survey of the 2001 to 2005 quartz crystal microbalance biosensor literature: applications of acoustic physics to the analysis of biomolecular interactions. *J. Mol. Recognit.* **2007**, *20*, 154-184.

(67) Pavey, K. D.; Barnes, L.-M.; Hanlon, G. W.; Olliff, C. J.; Ali, Z. et al. A rapid, non-destructive method for the determination of *Staphylococcus epidermidis* adhesion to surfaces using quartz crystal resonant sensor technology. *Lett. Appl. Microbiol.* **2001**, *33*, 344-348.

(68) Oli, M. W.; McArthur, W. P.; Brady, L. J. A whole cell BIAcore assay to evaluate P1-mediated adherence of *Streptococcus mutans* to human salivary agglutinin and inhibition by specific antibodies. *J. Microbiol. Methods* **2006**, *65*, 503-511.

(69) Pourshafie, M. R.; Marklund, B.-I.; Ohlson, S. Binding interactions of *Escherichia coli* with globotetraosylceramide (globoside) using a surface plasmon resonance biosensor. *J. Microbiol. Methods* **2004**, *58*, 313-320.

(70) Chen, M. J.; Zhang, Z.; Bott, T. R. Direct measurement of the adhesive strength of biofilms in pipes by micromanipulation. *Biotechnol. Techn.* **1998**, *12*, 875-880.

(71) Tsang, P. H.; Li, G.; Brun, Y. V.; Freund, L. B.; Tang, J. X. Adhesion of single bacterial cells in the micronewton range. *Proc. Natl. Acad. Sci. USA* **2006**, *103*, 5764-5768.

(72) Gomez-Suarez, C.; Busscher, H. J.; van der Mei, H. C. Analysis of bacterial detachment from substratum surfaces by the passage of air-liquid interfaces. *Appl. Environ. Microbiol.* **2001**, *67*, 2531-2537.

(73) Bayoudh, S.; Ponsonnet, L.; Ben Ouada, H.; Bakhrouf, A.; Othmane, A. Bacterial detachment from hydrophilic and hydrophobic surfaces using microjet impingement. *Colloids Surf., A* **2005**, *266*, 160-167.

(74) Bowen, W. R.; Fenton, A. S.; Lovitt, R. W.; Wright, C. J. The measurement of *Bacillus mycoides* spore adhesion using atomic force microscopy, simple counting methods, and a spinning disk technique. *Biotechnol. Bioeng.* **2001**, *79*, 170-179.

(75) Dickinson, R. B.; Cooper, S. L. Analysis of shear-dependent bacterial adhesion kinetics to biomaterial surfaces. *AIChE J.* **1995**, *41*, 2160-2174.

(76) Parent, M. E.; Velegol, D. *E. coli* adhesion in the presence of humic acid. *Colloids Surf., B* **2004**, *39*, 45-51.

(77) Mohamed, N.; Rainier, T. R., Jr.; Ross, M. R. Novel experimental study of receptor-mediated bacterial adhesion under the influence of fluid shear. *Biotechnol. Bioeng.* **2000**, *68*, 628-636.

(78) Velegol, S. B.; Logan, B. E. Contributions of bacterial surface polymers, electrostatics, and cell elasticity to the shape of AFM force curves. *Langmuir* **2002**, *18*, 5256-5262.

(79) Dupres, V.; Verbelen, C.; Dufrene, Y. F. Probing molecular recognition sites on biosurfaces using AFM. *Biomaterials* **2007**, *28*, 2393-2402.

(80) Hinterdorfer, P.; Dufrene, Y. F. Detection and localization of single molecular recognition events using atomic force microscopy. *Nat. Methods* **2006**, *3*, 347-355.

(81) Liu, Y.; Strauss, J.; Camesano, T. A. Adhesion forces between *Staphylococcus epidermidis* and surfaces bearing self-assembled monolayers in the presence of model proteins. *Biomaterials* **2008**, *29*, 4374-4382.

(82) Razatos, A.; Ong, Y.-L.; Sharma, M. M.; Georgiou, G. Molecular determinants of bacterial adhesion monitored by atomic force microscopy. *Proc. Natl. Acad. Sci. USA* **1998**, *95*, 11059-11064.

(83) Ong, Y.-L.; Razatos, A.; Georgiou, G.; Sharma, M. M. Adhesion forces between *E. coli* bacteria and biomaterial surfaces. *Langmuir* **1999**, *15*, 2719-2725.

(84) Lower, S. K.; Hochella, M. F.-J.; Beveridge, T. J. Bacterial recognition of mineral surfaces: Nanoscale interactions between *Shewanella* and α-FeOOH. *Science* **2001**, *292*, 1360-1363.

(85) Lower, S. K.; Tadanier, C. J.; Hochella, M. F.-J. Measuring interfacial and adhesion forces between bacteria and mineral surfaces with biological force microscopy. *Geochim. Cosmochim. Acta* **2000**, *64*, 3133-3139.

(86) Bowen, W. R.; Hilal, N.; Lovitt, R. W.; Wright, C. J. Characterisation of membrane surfaces: direct measurement of biological adhesion using an atomic force microscope. *J. Membr. Sci.* **1999**, *154*, 205-212.

(87) Boks, N. P.; Busscher, H. J.; van der Mei, H. C.; Norde, W. Bond-strengthening in *Staphylococcal* adhesion to hydrophilic and hydrophobic surfaces using atomic force microscopy. *Langmuir* **2008**, *24*, 12990-12994.

(88) Vadillo-Rodríguez, V.; Busscher, H. J.; Norde, W.; de Vries, J.; van der Mei, H. C. Atomic force microscopic corroboration of bond aging for adhesion of *Streptococcus thermophilus* to solid substrata. *J. Colloid Interface Sci.* **2004**, *278*, 251-254.

(89) van der Mei, H. C.; Rustema-Abbing, M.; de Vries, J.; Busscher, H. J. Bond strengthening in oral bacterial adhesion to salivary conditioning films. *Appl. Environ. Microbiol.* **2008**, *74*, 5511-5515.

(90) Deupree, S. M.; Schoenfisch, M. H. Quantitative method for determining the lateral strength of bacterial adhesion and application for characterizing adhesion kinetics. *Langmuir* **2008**, *24*, 4700-4707.

(91) Boyd, R. D.; Verran, J. Use of the atomic force microscope to determine the effect of substratum surface topography on bacterial adhesion. *Langmuir* **2002**, *18*, 2343-2346.

(92) Senechal, A.; Carrigan, S. D.; Tabrizian, M. Probing surface adhesion forces of *Enterococcus faecalis* to medical-grade polymers using atomic force microscopy. *Langmuir* **2004**, *20*, 4172-4177.

(93) Whitehead, K. A.; Rogers, D.; Colligon, J.; Wright, C.; Verran, J. Use of the atomic force microscope to determine the effect of substratum surface topography on the ease of bacterial removal. *Colloids Surf., B* **2006**, *51*, 44-53.

(94) Sorensen, R. A. The Inducible System: History of Development of Immunology as a Component of Host-Parasite Interactions. *Infection, Resistance, and Immunity*; 2nd ed.; Taylor & Francis: Ann Arbor, MI, 2002.

(95) Walsh, C. *Antibiotics: actions, origins, resistance*; ASM Press: Washington, D. C., 2003; 335.

(96) Lancini, G.; Parenti, F.; Gallo, G. G. *Antibiotics: A Multidisciplinary Approach*; Plenum Press: New York, 1995.

(97) Silver, S.; Phung, L. T.; Silver, G. Silver as biocides in burn and wound dressings and bacterial resistance to silver compounds. *J. Ind. Microbiol. Biotechnol.* **2006**, *33*, 627-634.

(98) Russell, A. D.; Hugo, W. B. Antimicrobial activity and action of silver. *Prog. Med. Chem.* **1994**, *31*, 351-371.

(99) Warriner, R.; Burrell, R. Infection and the chronic wound: A focus on silver. *Advances in Skin & Wound Care* **2005**, *18, Suppl. 1*, 2-12.

(100) Carr, H. S.; Wlodkowski, T. J.; Rosenkranz, H. S. Silver sulfadiazine: In vitro antibacterial activity. *Antimicrob. Agents Chemother.* **1973**, *4*, 585-587.

(101) Thomas, S. MRSA and the use of silver dressings: overcoming bacterial resistance. In *World Wide Wounds*, 2004.

(102) Ricketts, C. R.; Lowbury, J. L.; Lawrence, J. C.; Hall, M.; Wilkins, M. D. Mechanism of prophylaxis by silver compounds against infection of burns. *Br. Med. J.* **1970**, *2*, 444-446.

(103) Kirsner, R. S.; Orstead, H.; Wright, J. B. Matrix metalloproteinases in normal and impaired wound healing: A potential role for nanocrystalline silver. *Wounds* **2001**, *13 (3 Suppl C)*, 5-12.

(104) Wright, J. B.; Lam, K.; Buret, A.; Olson, M. E.; Burrell, R. E. Early healing events in a porcine model of contaminated wounds: Effects of nanocrystalline silver on matrix metalloproteinsases, cell apoptosis, and healing. *Wound Repair Regen.* **2002**, *10*, 141-151.

(105) Feng, Q. L.; Wu, J.; Chen, G. Q.; Cui, F. Z.; Kim, T. N. et al. A mechanistic study of the antibacterial effect of silver ions on *Escherichia coli* and *Staphylococcus aureus*. *J. Biomed. Mater. Res.* **2000**, *52*, 662-668.

(106) Ip, M.; Lui, S. L.; Poon, V. K. M.; Lung, I.; Burd, A. Antimicrobial activities of silver dressings: An in vitro comparison. *J. Med. Microbiol.* **2006**, *55*, 59-63.

(107) Deupree, S. M.; Johnson, C. B.; Schoenfisch, M. H. Synergy of nitric oxide and silver sulfadiazine against Gram-negative, -positive, and antibiotic-resistant bacteria. *J. Antimicrob. Chemother.* **2009**, *(submitted)*.

(108) Li, X.-Z.; Nikaido, H.; Williams, K. E. Silver-resistant mutants of *Escherichia coli* display active efflux of Ag^+ and are deficient in porins. *J. Bacteriol.* **1997**, *179*, 6127-6132.

(109) Modak, S. M.; Fox, J., C. R. Sulfadiazine silver-resistant *Pseudomonas* in burns. *Arch. Surg.* **1981**, *116*, 854-857.

(110) Silver, S. Bacterial silver resistance: Molecular biology and uses and misuses of silver compounds. *FEMS Microbiol. Rev.* **2003**, *27*, 341-353.

(111) Rosenkranz, H. S.; Coward, J. E.; Wlodkowski, T. J.; Carr, H. S. Properties of silver sulfadiazine-resistant *Enterobacter cloacae*. *Antimicrob. Agents Chemother.* **1973**, *5*, 199-201.

(112) Coward, J. E.; Carr, H. S.; Rosenkranz, H. S. Silver sulfadiazine: Effect on the ultrastructure of *Pseudomonas aeruginosa*. *Antimicrob. Agents Chemother.* **1973**, *3*, 621-624.

(113) Rosenkranz, H. S.; Rosenkranz, S. Silver sulfadiazine: interaction with isolated DNA. *Antimicrob. Agents Chemother.* **1972**, *2*, 373-383.

(114) Modak, S. M.; Fox, J., C. L. Binding of silver sulfadiazine to the cellular components of *Pseudomonas aeruginosa*. *Biochem. Pharmacol.* **1973**, *22*, 2391-2404.

(115) Fox, J., C. L.; Modak, S. M. Mechanism of silver sulfadiazine action of burn wound infections. *Antimicrob. Agents Chemother.* **1974**, *5*, 582-588.

(116) Liau, S. Y.; Read, D. C.; Pugh, W. J.; Furr, J. R.; Russell, A. D. Interaction of silver nitrate with readily identifiable groups: Relationship to the antibacterial action of silver ions. *Lett. Appl. Microbiol.* **1997**, *25*, 279-283.

(117) Rosenkranz, H. S.; Carr, H. S. Silver sulfadiazine: Effect on the growth and metabolism of bacteria. *Antimicrob. Agents Chemother.* **1972**, *2*, 367-372.

(118) Holt, K. B.; Bard, A. J. Interaction of silver (I) ions with the respiratory chain of *Escherichia coli*: An electrochemical and scanning electrochemical microscopy study of the antimicrobial mechanism of micromolar Ag^+. *Biochemistry* **2005**, *44*, 13214-13223.

(119) Coward, J. E.; Carr, H. S.; Rosenkranz, H. S. Silver sulfadiazine: Effect of the ultrastructure of *Pseudomonas aeruginosa*. *Antimicrob. Agents Chemother.* **1973**, *3*, 621-624.

(120) Dibrov, P.; Dzioba, J.; Gosink, K. K.; Häse, C. C. Chemiosmotic mechanism of antimicrobial activity of Ag^+ in *Vibrio cholerae*. *Antimicrob. Agents Chemother.* **2002**, *46*, 2668-2670.

(121) Bragg, P. D.; Rainnie, D. J. The effect of silver ions on the respiratory chain of *Escherichia coli*. *Can. J. Microbiol.* **1974**, *20*, 883-889.

(122) Schreurs, W. J. A.; Rosenberg, H. Effect of silver ions on transport and retention of phosphate by *Escherichia coli*. *J. Bacteriol.* **1982**, *152*, 7-13.

(123) Marletta, M. A.; Hurshman, A. R.; Rusche, K. M. Catalysis by nitric oxide synthase. *Curr. Opin. Chem. Biol.* **1998**, *2*, 656-663.

(124) Lowenstein, C. J.; Dinerman, J. L.; Snyder, S. H. Nitric oxide: A physiologic messenger. *Ann. Intern. Med.* **1994**, *120*, 227-237.

(125) Bogdan, C. Nitric oxide and the immune response. *Nat. Immunol.* **2001**, *2*, 907-916.

(126) Bonavida, B.; Khineche, S.; Huerta-Yepez, S.; Garbán, H. Therapeutic potential of nitric oxide in cancer. *Drug Resistance Updates* **2006**, *9*, 157-173.

(127) Buga, G. M.; Ignarro, J. L. Nitric Oxide and Cancer. *Biology and Pathobiology*; Academic Press: San Diego, 2000; pp 895-920.

(128) Hetrick, E. M.; Prichard, H. L.; Klitzman, B.; Schoenfisch, M. H. Reduced foreign body response at nitric oxide-releasing subcutaneous implants. *Biomaterials* **2007**, *28*, 4571-4580.

(129) Keefer, L. K. Progress toward clinical application of the nitric oxide-releasing diazeniumdiolates. *Annu. Rev. Pharmacol. Toxicol.* **2003**, *43*, 585-607.

(130) Napoli, C.; Ignarro, L. J. Nitric oxide-releasing drugs. *Annu. Rev. Pharmacol. Toxicol.* **2003**, *43*, 97-123.

(131) Fang, F. C. Host/pathogen interactions: Mechanisms of nitric oxide-related antimicrobial activity. *J. Clin. Invest.* **1997**, *99*, 2818-2825.

(132) MacMicking, J.; Xie, Q. W.; Nathan, C. Nitric oxide and macrophage function. *Annu. Rev. Immunol.* **1997**, *15*, 323-350.

(133) Foley, E.; O'Farrell, P. H. Nitric oxide contributes to induction of innate immune responses to Gram-negative bacteria in Drosophila. *Genes Dev.* **2003**, *17*, 115-125.

(134) Nunoshiba, T.; de Rojas-Walker, T.; Wishnok, J. S.; Tannenbaum, S. R.; Demple, B. Activation by nitric oxide of an oxidative-stress response that defends *Escherichia coli* against activated macrophages. *Proc. Natl. Acad. Sci. USA* **1993**, *90*, 9993-9997.

(135) Hausladen, A.; Gow, A. J.; Stamler, J. S. Nitrosative stress: Metabolic pathway involving the flavohemoglobin. *Proc. Natl. Acad. Sci. USA* **1998**, *95*, 14100-14105.

(136) Richardson, A. R.; Libby, S. J.; Fang, F. C. A nitric oxide-inducible lactate dehydrogenase enables *Staphylococcus aureus* to resist innate immunity. *Science* **2009**, *319*, 1672-1676.

(137) Crawford, M. J.; Goldberg, D. E. Role for the *Salmonella* flavohemoglobin in protection from nitric oxide. *J. Biol. Chem.* **1998**, *273*, 12543-12547.

(138) Wink, D. A.; Mitchell, J. B. Chemical biology of nitric oxide: Insights into regulatory, cytotoxic, and cytoprotective mechanisms of nitric oxide. *Free Radic. Biol. Med.* **1998**, *25*, 434-456.

(139) Zaki, M. H.; Akuta, T.; Akaike, T. Nitric oxide-induced nitrative stress involved in microbial pathogenesis. *J. Pharmacol. Sci.* **2005**, *98*, 117-129.

(140) Moller, M. N.; Li, Q.; Lancaster, J. R. J.; Denicola, A. Acceleration of nitric oxide autooxidation and nitrosation by membranes. *Life* **2007**, *59*, 243-248.

(141) Tamir, S.; Burney, S.; Tannenbaum, S. R. DNA damage by nitric oxide. *Chem. Res. Toxicol.* **1996**, *9*, 821-827.

(142) Lancaster, J. R. J. A tutorial on the diffusibility and reactivity of free nitric oxide. *Nitric Oxide: Biology and Chemistry* **1997**, *1*, 18-30.

(143) Smith, D. J.; Chakravarthy, D.; Pulfer, S.; Simmons, M. L.; Saavedra, J. E. et al. Nitric oxide-releasing polymers containing the [N(O)NO]- group. *J. Med. Chem.* **1996**, *39*, 1148-1156.

(144) Ghaffari, A.; Miller, C. C.; McMullin, B.; Ghahary, A. Potential application of gaseous nitric oxide as a topical antimicrobial agent. *Nitric Oxide* **2006**, *14*, 21-29.

(145) Miller, C.; McMullin, B.; Ghaffari, A.; Stenzler, A.; Pick, N. et al. Gaseous nitric oxide bactericidal activity retained during intermittent high-dose short duration exposure. *Nitric Oxide* **2009**, *20*, 16-23.

(146) Long, R.; Light, B.; Talbot, J. A. Mycobacteriocidal action of exogenous nitric oxide. *Antimicrob. Agents Chemother.* **1999**, *43*, 403-405.

(147) Lyn, D.; Williams, H. The chemistry of *S*-nitrosothiols. *Acc. Chem. Res.* **1999**, *32*, 869-876.

(148) Butler, A. R.; Rhodes, P. Chemistry, analysis, and biological rolse of *S*-nitrosothiols. *Anal. Biochem.* **1997**, *249*, 1-9.

(149) Wang, P. G.; Xian, M.; Tang, X.; Wu, X.; Wen, Z. et al. Nitric oxide donors: Chemical activities and biological applications. *Chem. Rev.* **2002**, *102*, 1091-1134.

(150) Shin, J. H.; Metzger, S. K.; Schoenfisch, M. H. Synthesis of nitric oxide-releasing silica nanoparticles. *J. Am. Chem. Soc.* **2007**, *129*, 4612-4619.

(151) Shin, J. H.; Schoenfisch, M. H. Inorganic/organic hybrid silica nanoparticles as a nitric oxide delivery scaffold. *Chem. Mater.* **2008**, *20*, 239-249.

(152) Marxer, S. M.; Rothrock, A. R.; Nablo, B. J.; Robbins, M. E.; Schoenfisch, M. H. Preparation of nitric oxide (NO)-releasing sol-gels for biomaterial applications. *Chem. Mater.* **2003**, *15*, 4193-4199.

(153) Robbins, M. E.; Hopper, E. D.; Schoenfisch, M. H. Synthesis and characterization of nitric oxide-releasing sol-gel microarrays. *Langmuir* **2004**, *20*, 10296-10302.

(154) Hrabie, J. A.; Klose, J. R.; Wink, D. A.; Keefer, L. K. New nitric oxide-releasing zwitterions derived from polyamines. *J. Org. Chem.* **1993**, *58*, 1472-1476.

(155) Saavedra, J. E.; Southan, G. J.; Davies, K. M.; Lundell, A.; Markou, C. et al. Localizing antithrombotic and vasodilatory activity with a novel, ultrafast nitric oxide donor. *J. Med. Chem.* **1996**, *39*, 4361-4365.

(156) Hrabie, J. A.; Keefer, L. K. Chemistry of the nitric oxide-releasing diazeniumdiolate ("nitrosohydroxylamine") functional group and its oxygen-substituted derivatives. *Chem. Rev.* **2002**, *102*, 1135-1154.

(157) Deupree, S. M.; Schoenfisch, M. H. Morphological analysis of the antimicrobial action of nitric oxide on Gram-negative pathogens using atomic force microscopy. *Acta Biomater.* **2009**, *(in press)*.

(158) Hetrick, E. M.; Schoenfisch, M. H. Antibacterial nitric oxide-releasing xerogels: Cell viability and parallel plate flow cell adhesion studies. *Biomaterials* **2007**, *28*, 1948-1956.

(159) Hetrick, E. M.; Shin, J. H.; Stasko, N. A.; Johnson, B. A.; Wespe, D. A. et al. Bactericidal efficacy of nitric oxide-releasing silica nanoparticles. *ACS Nano* **2007**, *2*.

(160) Nablo, B. J.; Chen, T.-Y.; Schoenfisch, M. H. Sol-gel derived nitric-oxide releasing materials that reduce bacterial adhesion. *J. Am. Chem. Soc.* **2001**, *123*, 9712-9713.

(161) Nablo, B. J.; Rothrock, A. R.; Schoenfisch, M. H. Nitric oxide-releasing sol-gels as antibacterial coatings for orthopedic implants. *Biomaterials* **2005**, *26*, 917-924.

(162) Hetrick, E. M.; Shin, J. H.; Paul, H. S.; Schoenfisch, M. H. Anti-biofilm efficacy of nitric oxide-releasing silica nanoparticles. *Biomaterials* **2009**, *(in press)*.

(163) Camesano, T. A.; Natan, M. J.; Logan, B. E. Observation of changes in bacterial cell morphology using tapping mode atomic force microscopy. *Langmuir* **2000**, *16*, 4563-4572.

(164) Yao, X.; Walter, J.; Burke, S.; Stewart, S.; Jericho, M. H. et al. Atomic force microscopy and theoretical considerations of surface properties and turgor pressures of bacteria. *Colloids Surf., B* **2002**, *23*, 213-230.

(165) Waisbren, S. J.; Hurley, D. J.; Waisbren, B. A. Morphological expression of antibiotic synergism against *Pseudomonas aeruginosa* as observed by scanning electron microscopy. *Antimicrob. Agents Chemother.* **1980**, *18*, 969-975.

(166) Klainer, A. S.; Russell, R. R. B. Effect of the inhibition of protein synthesis on the *Escherichia coli* cell envelope. *Antimicrob. Agents Chemother.* **1974**, *6*, 216-224.

(167) Iida, K.; Koike, M. Cell wall alterations of Gram-negative bacteria by aminoglycoside antibiotics. *Antimicrob. Agents Chemother.* **1974**, *5*, 95-97.

(168) Comber, K. R.; Boon, R. J.; Sutherland, R. Comparative effects of amoxycillin and ampicillin on the morphology of *Escherichia coli* in vivo and correlation with activity. *Antimicrob. Agents Chemother.* **1977**, *12*, 736-744.

(169) Da Silva, A.; Teschke, O. Effects of the antimicrobial peptide PGLa on live *Escherichia coli*. *Biochim. Biophys. Acta* **2003**, *1643*, 95-103.

(170) Eaton, P.; Fernandes, J. C.; Pereira, E.; Pintado, M. E.; Malcata, F. X. Atomic force microscopy study of the antibacterial effects of chitosans on *Escherichia coli* and *Staphylococcus aureus*. *Ultramicroscopy* **2008**, *108*, 1128-1134.

(171) Li, A.; Lee, P. Y.; Ho, B.; Ding, J. L.; Lim, C. T. Atomic force microscopy study of the antimicrobial action of Sushi peptides on Gram-negative bacteria. *Biochim. Biophys. Acta* **2007**, *1768*, 411-418.

(172) Lu, Z.; Li, C. M.; Bao, H.; Qiao, Y.; Toh, Y. et al. Mechanism of antimicrobial activity of CdTe quantum dots. *Langmuir* **2008**, *24*, 5445-5452.

(173) Meincken, M.; Holroyd, D. L.; Rautenbach, M. Atomic force microscopy study of the effect of antimicrobial peptides on the cell envelope of *Escherichia coli*. *Antimicrob. Agents Chemother.* **2005**, *49*, 4085-4092.

(174) Yang, L.; Wang, K.; Tan, W.; He, X.; Jin, R. et al. Atomic force microscopy study of different effects of natural and semisynthetic β-lactam on the cell envelope of *Escherichia coli*. *Anal. Chem.* **2006**, *78*, 7341-7345.

(175) Finch, R. G.; Gander, S. Pharmacodynamics of the Treatment of IMD-Related Infections. *Biofilms, Infection, and Antimicrobial Therapy*; Taylor & Francis: Boca Raton, 2006; pp 331-351.

(176) Lorian, V. *Antibiotics in Laboratory Medicine*; 4th ed.; Williams & Wilkins: Baltimore, 1996.

(177) Amsterdam, D. Susceptibility Testing of Antimicrobials in Liquid Media. *Antibiotics in Laboratory Medicine*; 4th ed.; Williams & Wilkins: Baltimore, 1996; pp 52-111.

(178) Li, R. C. New pharmacodynamic parameters for antimicrobial agents. *Int. J. Antimicrob. Agents* **2000**, *13*, 229-235.

(179) Ceri, H.; Olson, M. E.; Stremick, C.; Read, R. R.; Morck, D. W. et al. The Calgary Biofilm Device: A new technology for the rapid determination of antibiotic susceptibility of bacterial biofilms. *J. Clin. Microbiol.* **1999**, *37*, 1771-1776.

(180) Wilson, M. Susceptibility of oral bacterial biofilms to antimicrobial agents. *J. Med. Microbiol.* **1996**, *44*, 79-87.

(181) Kumon, H.; Ono, N.; Iida, M.; Nickel, J. C. Combination effect of fosfomycin and ofloxacin against *Pseudomonas aeruginosa* growing in a biofilm. *Antimicrob. Agents Chemother.* **1995**, *39*, 1038-1044.

(182) Olson, M. E.; Ceri, H.; Morck, D. W.; Buret, A.; Read, R. R. Biofilm bacteria: Formation and comparative susceptibility to antibiotics. *Can. J. Vet. Res.* **2002**, *66*, 86-92.

(183) Ceri, H.; Olson, M. E.; Morck, D. W.; Storey, D.; Read, R. R. et al. The MBEC™ Assay System: multiple equivalent biofilms for antibiotic and biocide susceptibility testing. *Methods Enzymol.Microbial Growth in Biofilms, Part B*; Academic Press: San Diego, 2001; pp 377-385.

(184) Levy, S. B.; Marshall, B.; Schluederberg, S.; Rowse, D.; Davis, J. High frequency of antimicrobial resistance in human fecal flora. *Antimicrob. Agents Chemother.* **1988**, *32*, 1801-1806.

(185) Eliopoulos, G. M.; Eliopoulos, C. T. Antibiotic combinations: Should they be tested? *Clin. Microbiol. Rev.* **1988**, *1*, 139-156.

(186) Gribble, M. J.; Chow, A. W.; Naiman, S. C.; Smith, J. A.; Bowie, W. R. et al. Prospective randomized trial of piperacillin monotherapy versus carboxpenicillin-aminoglycoside combination regimens in the empirical treatment of serious bacterial infections. *Antimicrob. Agents Chemother.* **1983**, *24*, 388-392.

(187) Denyer, S. P. Mechanisms of action of antibacterial biocides. *Int. Biodeterior. Biodegrad.* **1996**, 227-245.

(188) Jawetz, E.; Gunnison, J. B.; Coleman, V. R. The combined acion of penicillin with streptomycin or chloromycetin on *Enterococci* in vitro. *Science* **1950**, *111*, 254-256.

(189) Moellering, R. C., Jr.; Weinberg, A. N. Studies on antibiotic synergism against enterococci. II. Effect of various antibiotics on the uptake of ^{14}C-labeled streptomycin by *Enterococci*. *J. Clin. Invest.* **1971**, *50*, 2580-2584.

(190) Yee, Y.; Farber, B.; Mates, S. Mechanism of penicillin-streptomycin synergy for clinical isolates of viridans *Streptococci*. *J. Infect. Dis.* **1986**, *154*, 531-534.

(191) Watanakunakorn, C.; Glotzbecker, C. Enhancement of the effects of anti-*Staphylococcal* antibiotics by aminoglycosides. *Antimicrob. Agents Chemother.* **1974**, *6*, 802-806.

(192) Giamarellou, H. Aminoglycosides plus beta-lactams against Gram-negative organisms. Evaluation of in vitro synergy and chemical interactions. *Am. J. Med.* **1986**, *80 (Suppl. 6B)*, 126-137.

(193) Glew, R. H.; Pavuk, R. A. Early synergistic interaction between semisynthetic penicillins and aminoglycosidic aminocyclitiols against *Enterobacteriaceae*. *Antimicrob. Agents Chemother.* **1983**, *23*, 902-906.

(194) Richards, R. M. E.; Xing, D. K. L. Enhancement of antibacterial activity by *p*-aminobenzoic acid and sulphadiazine. *Inter. J. Pharm.* **1992**, *82*, 107-115.

(195) Baltch, A. L.; Smith, R. P.; Ritz, W. J.; Bopp, L. H. Comparison of inhibitory and bactericidal activities and postantibiotic effects of LY333328 and ampicillin used

singly and in combination against vancomycin-resistant *Enterococcus faecium*. *Antimicrob. Agents Chemother.* **1998**, *42*, 2564-2568.

(196) Bornside, G. H. Synergistic antibacterial activity of ampicillin-cloxicillin mixtures against *Proteus morganii*. *Appl. Microbiol.* **1968**, *16*, 1507-1511.

(197) Cockerill, F. R., III; Edson, R. S. Trimethoprim-sulfamethoxazole. *Mayo Clin. Proc.* **1983**, *58*, 147-153.

(198) Richards, R. M. E.; Xing, J. Z.; Gregory, D. W.; Marshall, D. Mechanism of sulphadiazine enhancement of trimethoprim activity against sulphadiazine-resistant *Enterococcus faecalis*. *J. Antimicrob. Chemother.* **1995**, *36*, 607-618.

(199) Harvey, R. J. Synergism in the folate pathway. *Rev. Infect. Dis.* **1982**, *4*, 255-260.

(200) Eliopoulos, G. M.; Moellering, J., R. C. Antimicrobial Combinations. *Antibiotics in Laboratory Medicine*; 4th ed.; Williams & Wilkins: Baltimore, 1996; pp 330-396.

(201) Elion, G. B.; Singer, S.; Hitchings, C. H. Antagonists of nucleic acid derivitives. VIII. Synergism in combinations of biochemically related antimetabolites. *J. Biol. Chem.* **1954**, *208*, 477-488.

Chapter 2:

Quantitative method for determining the lateral strength of bacterial adhesion and application for characterizing adhesion kinetics

2.1 Introduction

Elucidation of the mechanisms of bacterial adhesion at surfaces is required to improve methods for preventing and treating implant-related infection. As a necessary step in the pathogenesis of local infection, bacteria attach to the surface of medical devices and/or nearby host tissue. The complicated mechanisms involved in bacterial adhesion to material surfaces have been reviewed previously.[1-3] The type, number, and strength of the interactions involved in adhesion depend on multiple factors including microbial species,[4,5] surface properties,[4,6-8] the presence of proteins or other conditioning layers on the surface,[5,9-12] experimental system parameters (e.g., temperature, exposure time and conditions),[13,14] and the culture environment (e.g., growth phase, ionic strength, pH)[2,4,15,16] under which adhesion occurred.

The process of non-specific bacterial adhesion is often described as consisting of two distinct phases where initial, reversible physicochemical attachment precedes irreversible adhesion through molecular binding interactions (Section 1.1.3).[17-20] In Phase I, the cell approaches the surface through a combination of mechanical processes (e.g., Brownian motion, gravity, motility structures) and long- and short-range reversible chemical interactions (e.g., electrostatic and hydrophobic interactions, and attractive van der Waals

forces). Once association has been established, the cell fortifies its attachment during Phase II via cellular and molecular interactions between macromolecules present on the exterior of the bacterium and the substratum in a complex and time-dependent process (>1-3 h). The two phases of adhesion differ distinctly. While Phase I involves interactions occurring away from and along vectors perpendicular to the surface and eventually leads to reversible attachment, Phase II is characterized by lateral reinforcement of adhesion through numerous irreversible binding interactions serving to establish a firm adherence of the cell to the underlying substrate after it reaches the surface.

Two physical characteristics of bacterial adhesion, each related to either Phase I or Phase II, readily lend themselves to quantitative study: the affinity for association and the resistance to dissociation. The proclivity of bacteria to interact and form associations with a surface is typically evaluated by determination of surface coverage of adhered cells. While enumeration of surface-associated cells is more useful for understanding Phase I adhesion (where bacteria form a loose association with the surface), information on the lateral reinforcement or strength of adhesion that accompanies Phase II may be assessed by applying a measurable, physical force to dislodge the cells from the surface. Lateral adhesion strength, studied by applying forces along a surface until the interactions are disrupted and the bacteria detach, is a measure of the friction force established between the cell and a surface due to a multitude of specific and non-specific chemical interactions. Previous studies have employed laminar flow[21] and the application of an air-liquid interface via passage of air bubbles[22] to dislodge bacteria attached to a surface and quantify lateral adhesion strength. Both methods are limited by the inability to apply both controlled and

directed forces at a specific location. Furthermore, the forces applied by laminar flow may be insufficient to detach all cells from the surface.[21]

More recently, atomic force microscopy (AFM) has been used to apply forces with a probe while scanning in contact mode.[23-25] Indeed, the ability to simultaneously detect the presence of single cells, apply a controlled and measurable force at a known location, and detect subsequent detachment of each adhered cell, all under pseudo-physiological conditions (i.e., in buffer) make AFM a useful tool for studying adhesion of living cells. Atomic force microscopy has been used previously to evaluate the effect of surface roughness/topography[23,25] and surface hydrophobicity[24] on the strength of bacterial adhesion. These studies assumed a constant normal force between the probe and the underlying substrate (due to feedback loop adjustment) without determining the actual force applied by the probe to the cell at the time of its detachment. Herein, we present a rigorous quantitative method for calculating the lateral strength of the adhesion of individual cells to a surface using AFM by determining the total cantilever compression (deflection) at each detachment event and accounting for probe geometry.

While the kinetics of Phase I adhesion strength have been previously examined,[26,27] a logical, and heretofore unexplored, application of AFM is the characterization of Phase II kinetics, the rate at which bacteria are capable of establishing lateral reinforcement and resistance to detachment. The ability of cells to irreversibly enhance their stability against lateral or shear forces applied during relevant processes such as blood flow, the blinking of an eyelid, or wiping/scrubbing of a surface during a cleansing process are essential in their pathogenesis and the development of infections. To this end, we apply the quantitative

method introduced to elucidate the kinetics of Phase II adhesion strength by observing the strength of adhesion as a function of time for *P. aeruginosa* and *S. aureus*.

2.2 Experimental

2.2.1 Materials. Ethanol (absolute) was purchased from Fisher Scientific (Pittsburgh, PA). *N*-(6-aminohexyl)aminopropyltrimethoxysilane (AHAP3) was obtained from Gelest (Tullytown, PA). Isobutyltrimethoxysilane (BTMOS) was purchased from Aldrich (St. Louis, MO). The amino- and alkoxysilanes were stored over dessicant. The above chemicals were used without further purification. Distilled water was purified with a Millipore Milli-Q UV Gradient A-10 system (Bedford, MA) to a resistivity of 18.2 MΩ*cm. *P. aeruginosa* (ATCC #19143) and *S. aureus* (ATCC #29213) were obtained from American Type Culture Collection (Manassas, VA).

2.2.2 Substrate preparation. Glass slides were coated with optically clear xerogel polymer films formed via sol-gel chemistry. Briefly, a 40% (v:v total silane content) mixture of AHAP3/BTMOS was prepared via a 2-step process.[28] First, 120 µl BTMOS was mixed with 60 µl water, 200 µl ethanol, and 10 µl of 0.5 M HCl for 1 h. Then, 80 µl of AHAP3 was added, and the solution was mixed for an additional hour. To cast a film, 40 µl of the polymer precursor solution was pipetted onto clean glass slides (dim. 13 x 17.5 mm) and allowed to dry at 85 °C for 3 d. The xerogel-coated slides were stored in dessicators at room temperature until used.

2.2.3 Cell culture. *P. aeruginosa* and *S. aureus* were cultured separately at 37 °C in sterile tryptic soy broth (TSB) while shaking, centrifuged for 10 min at 4500 g, rinsed with ultrapure water, resuspended in 15% (v:v) glycerol, and stored as stock suspensions at -80

°C. Bacterial cultures for daily use were grown from the -80 °C stock overnight at 37 °C. Next, 1 mL of overnight culture was inoculated in 100 mL of TSB and incubated at 37 °C for 3-5 h until the culture reached a target optical density at 600 nm ($OD_{600} \approx 0.2 \pm 0.1$ for *P. aeruginosa* and $OD_{600} \approx 0.5 \pm 0.1$ for *S. aureus*) corresponding to mid-exponential log phase as determined by growth curves (data not shown).

2.2.4 Substrate characterization. Xerogel films have been used extensively in our laboratory to study bacterial adhesion[28-30] and possess several suitable characteristics for AFM analysis of non-specific cell adhesion strength. The xerogel coatings (40% (v:v) AHAP3/BTMOS) are hydrophobic (water contact angle ~90°).[28,29] In addition, xerogel films resist the physical damage and deformation common to softer polymers. AFM images of bare xerogels indicated a topologically featureless surface, providing a homogenous substratum for adherence. The average RMS roughness of three separate regions of three independently prepared 40% (v:v) AHAP3/BTMOS xerogel films was 0.75 ± 0.47 nm over 40 μm^2 areas and 0.14 ± 0.02 nm over 1 μm^2 areas. The former is representative of the scan sizes evaluated for adhesion measurements while the latter represents surface roughness on the scale of a single bacterium.

2.2.5 Bacterial adhesion. Xerogel-coated substrates were rinsed with ultrapure water and ethanol, and dried under a stream of nitrogen. A 200-µL aliquot of bacterial suspension in nutrient broth was pipetted directly onto the substrate and incubated at room temperature for 1 h. The substrate with adhered bacteria was immersed into a dish of PBS (pH = 7.4, I_c = 0.16 M) for 3 h, rinsed with ultrapure water, and dried under a gentle stream of nitrogen. The surface coverage of cells on the substrate was determined by imaging representative 40 μm^2 regions of the surface using contact mode AFM. After 1 h in ambient air, the substrate was

placed into a fresh PBS solution at room temperature until analysis. The short drying step, modeling the type of cellular transfer that might occur prior to in vivo implantation of a medical device, proved necessary to initiate firmly-adhered cells.

2.2.6 CFU viability count. To determine the viability of adhered cells under experimental conditions, prepared substrates were briefly sonicated for 5 min in PBS, and rinsed with an additional 5 mL of PBS to remove cells loosened, but not detached, by sonication. Serial dilutions of the sonicant were prepared, 100-μL aliquots spread onto nutrient agar plates, and incubated at 37 °C overnight. Observed colonies were then counted. The total number of viable cells removed from the substrate was back-calculated.

2.2.7 AFM imaging. Simultaneous AFM height, deflection, and lateral images were obtained in contact mode using an Asylum MFP-3D atomic force microscope (Santa Barbara, CA) with manufacturer provided software. Silicon nitride (Si_3N_4) triangle-shaped cantilevers with nominal spring constants of 0.06, 0.12, and 0.32 N/m were used to obtain images and measure forces (DNP-S, Veeco, Santa Barbara, CA). Root mean square (RMS) measurements of xerogel surface roughness were obtained in air using the most rigid cantilever. Images for force measurement were acquired in PBS at a scan rate of 1 Hz and scan size of 40 μm^2 with a 512 x 512 line/pixel resolution. The scan size and resolution were optimized to collect data from multiple cells during a single run while maintaining sufficient resolution to observe single cells for positive identification and force determination (e.g., ~10 pixels across the width of the cell).

2.2.8 Force calculation. The tip-surface force applied by an AFM probe to the underlying substrate during scanning was calculated using Hooke's Law, $F_z = k\ d$, where the cantilever is approximated as a spring with an associated spring constant, k, and is

compressed (deflected) by a distance, d, as it interacts with the surface during scanning (Fig. 2.1A). Direct application of Hooke's Law gives the applied force normal to the compression of the spring, which in the case of AFM is the force applied by the tip of the probe. However, when the probe interacts with a large feature such as a bacterium, the point of interaction moves from the tip to the side of the probe, and the applied force normal to the plane of interaction is calculated from Equation 2.1

$$F_{app} = k\, d \sin(\theta + \Phi) \qquad \text{Eq. (2.1)}$$

where the angles θ and Φ are parameters of the probe geometry and cantilever orientation, respectively (Fig. 2.1B). The lateral component (F_{lat}) of the applied force (F_{app}) is responsible for applying the shear force to detach adhered cells and is determined using Equation 2.2

$$F_{lat} = F_{app} \cos(\theta). \qquad \text{Eq. (2.2)}$$

The cantilever deflection, d, for any point in an image was determined by $d = \Delta V\, S^{-1}$, where the total change in the output signal due to vertical movement of the laser on the photodiode detector resulting from compression, ΔV, is multiplied by the inverse optical lever sensitivity (S^{-1}), a calibration factor relating the deflection-detector sensitivity. The inverse optical lever sensitivity (S^{-1}), the value of the slope in the constant compliance region of a force curve (deflection (nm) versus output signal (V)), was determined before each experiment using a clean mica substrate.

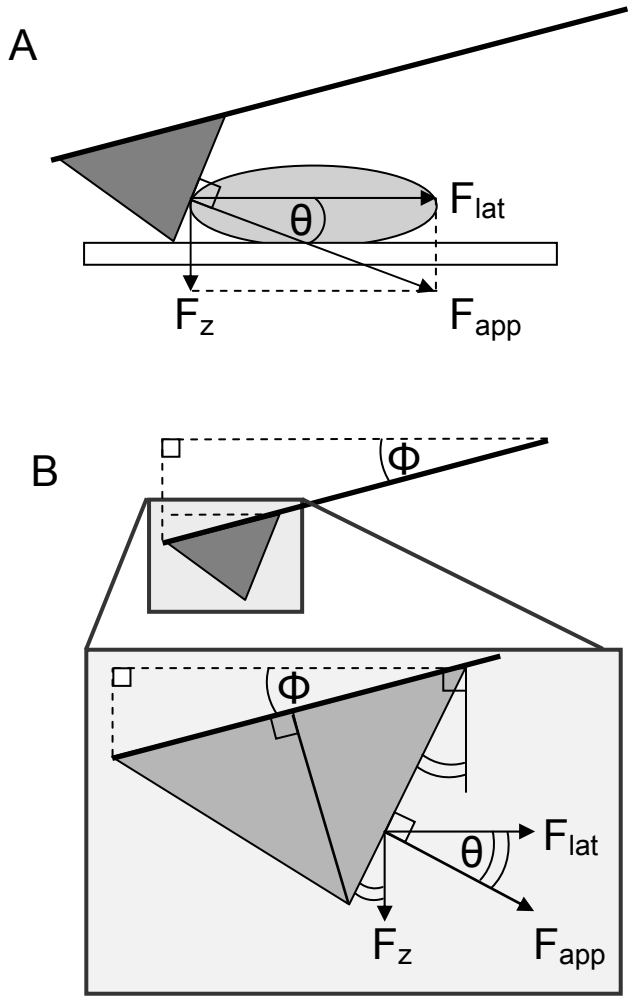

Figure 2.1 (A) The vertical and lateral components of the normal force applied by an AFM probe to an adhered cell are illustrated schematically. The latter component is responsible for applying the lateral force to detach cells, and is directly related to the normal force by the angle θ. (B) By modeling the slightly compressed cantilever as a straight line, a direct relationship can be drawn between Φ, which varies with the distance of compression, and θ.

2.2.9 Kinetic assay. A kinetic assay was designed to identify a time frame of dynamic change in adhesion strength. An initial image of adhered bacteria was obtained in contact mode in PBS at a setpoint (user-defined change in output signal maintained by the feedback loop through cantilever compression and corresponding to an approximate tip-surface force) near the limit of detection. For our system, the limit of detection was approximately 0.2 nN with k = 0.06 N/m. Of note, the limit of detection will vary directly with k and S^{-1} and is a function of detector sensitivity. The imaged cells were counted to establish the baseline number of total cells detected. The ability of these cells to withstand scanning at higher tip-surface forces (F_z) was tested by adjusting the setpoint to predetermined low and high F_z of 2.5 nN and 15 nN, respectively, and rescanning the same region at each threshold. The percentage of cells able to withstand detachment at each threshold was then determined. The assay was repeated at different regions of the substrate every 6 h for 48 h after exposure of the substrate to the bacterial suspension.

2.2.10 Measurement of adhesion kinetics. To observe detailed changes in bacterial adhesion strength, an analogous process of acquiring consecutive images over a region was employed. In contrast to the kinetic assay, however, the actual lateral force applied to each individual bacterium at the time of detachment was determined. As before, an initial image was obtained at a low setpoint (~ 5 nN) to establish the number of cells present within a 40 μm^2 scan region. This starting threshold force was empirically determined for our system (e.g., adhesion conditions, substrate) to select for securely adhered bacteria representative of Phase II bacterial adhesion, while removing loosely attached cells. Of note, scanning at lower tip-surface forces did not yield significantly more cells. The setpoint was increased incrementally for subsequent scans so that increasingly higher forces were applied until all

cells in the scan region were removed. No cell was imaged in subsequent scans that did not appear in the first scan. After displacement, cells likely become planktonic, at least briefly, as the imaging artifacts observed (i.e., streaks) clearly indicate that rolling or pushing of cells does not extend to the periphery of the scan. After all cells in a scan region were displaced, the probe was systematically moved to a different location on the substrate several millimeters away from the previous analysis area, and the process was repeated.

To calculate the force applied for removal of a cell, the set of height and deflection scans consisting of a run was visually examined to identify the image in which each cell was last detected (partially imaged cell) (Fig. 2.2A-C). Cell removal was indicated by greater error in setpoint deflection relative to previous line scans and was occasionally accompanied by a streaking artifact. Such streaks originate from temporary continued association of the cell with the tip as the cell moves away from the location of its attachment. The error in setpoint deflection is easily visualized in the deflection image, and the force responsible for bacterial detachment likely originates from an accumulation of cantilever bending prior to feedback loop correction (Fig. 2.2D-E). Thus, the line where detachment occurred was identified for each bacterium. The total compression of the cantilever at the time of detachment was calculated by summing the distance of compression required to obtain the setpoint from the free air deflection (i.e., position of the laser on the photodiode before the probe contacts the surface) with the additional error from the setpoint at detachment (Fig. 2.3). Upon determining the total cantilever compression responsible for cell detachment on an individual basis and the geometrical analysis of the system, F_{lat} was calculated independently for each bacterium, using Eq. 2.2.

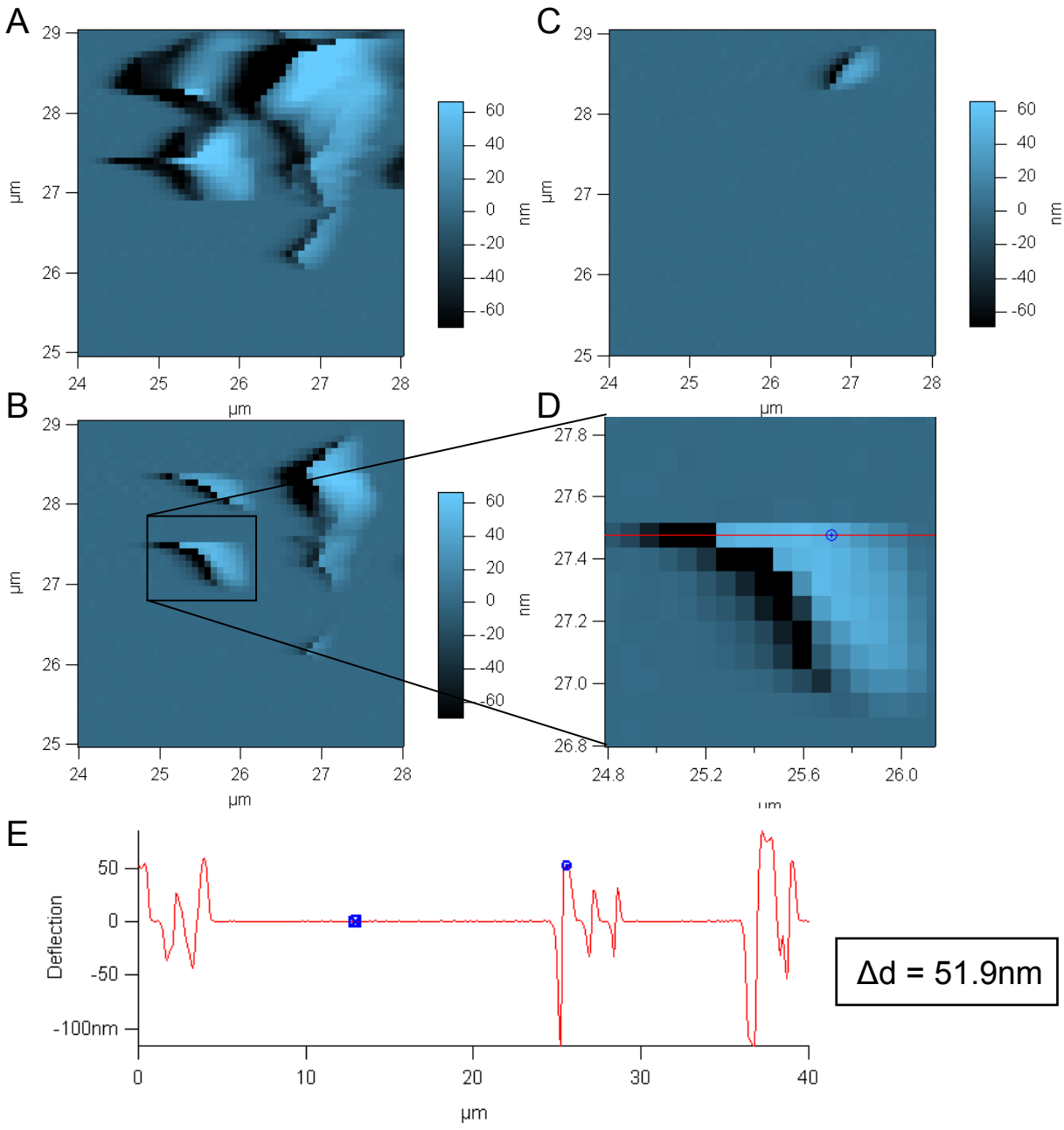

Figure 2.2 In three consecutive AFM scans, *S. aureus* cells are imaged at $\Delta V_{setpoint}$ of (A) 0.80 V, (B) 1.35 V, and (C) 3.00 V. The partially imaged cell highlighted in (B) is an example of a bacterium undergoing detachment. This cell is imaged completely in (A) and is no longer visible in (C). The scale bar indicates error from setpoint deflection, where increased cantilever compression corresponds to positive values. (D-E) From the deflection values of the scan line where the cell detaches, the change in deflection (Δd) is determined, which is directly related to $\Delta V_{deflection\ error}$ by a factor of S^{-1}. Δd is calculated as the difference between the baseline (setpoint) deflection and the peak in deflection error (indicated by the round cursor) and can be converted to the additional force applied by cantilever compression beyond the setpoint.

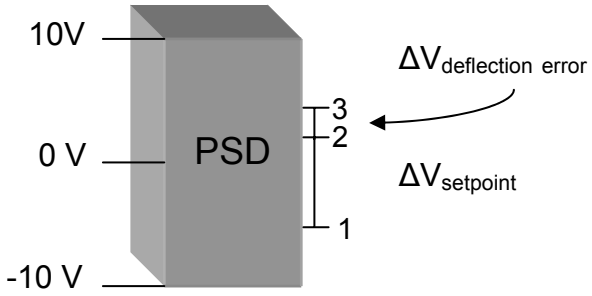

Figure 2.3 The laser position on the position sensitive diode (PSD) changes in response to cantilever compression. Position 1 represents the laser position at free air deflection. When the tip engages with the surface, the cantilever is compressed to the setpoint (position 2) and the total change in output signal is $\Delta V_{setpoint}$. During scanning when the probe encounters a raised feature, the cantilever is compressed past the setpoint. This additional compression is termed deflection error and is illustrated as the change in output signal, $\Delta V_{deflection\ error}$, between position 2 and 3 on the PSD. The total compression of the cantilever, deflecting the laser from position 1 to 3, is used to determine the force applied at detachment.

2.3 Results

2.3.1 Long-term observation of adhesion kinetics. A kinetic assay of bacterial adhesion strength was utilized to monitor the adhesion dynamics of *P. aeruginosa* in PBS over 2 d. First introduced by Boyd et al.,[23] the technique involves determining the number of cells capable of withstanding probe interaction at pre-set vertical tip-surface forces (setpoints). However, neither the lateral component of the applied force nor the applied force for individual cell removal based on total cantilever compression was determined. Instead, all cells remaining after scanning at a particular setpoint (F_z) were assigned an empirical threshold adhesive force related to the setpoint. This simple assay allowed efficient observation of increasing adhesion strength trends over time and was useful in identifying a time window of interest for in-depth kinetic studies. Nevertheless, it does lack the accuracy of the more time-consuming method based on determining the total cantilever compression at the time of detachment (used later in our study).

The percentages of surface-adhered *P. aeruginosa* cells that withstood probe interaction at both low and high threshold probe-surface forces as a function of time are shown in Figure 2.4. At 18 h after initial adhesion, two significant and related observations were made. The percentage of cells with adhesion strength greater than the lateral force applied by a setpoint of 2.5 nN began to increase at an accelerated rate. Furthermore, some cells had generated sufficient adhesion strength to withstand a six-fold greater scanning force (i.e., 15 nN). Between 18 and 42 h, the percentage of cells remaining attached continued to increase, with the most drastic rise occurring 24–30 h after exposure, where the amount of cells remaining adhered was approximately six- fold higher than that achieved in the 6 h period immediately prior. The percentage of cells capable of withstanding 15 nN of tip-surface force increased

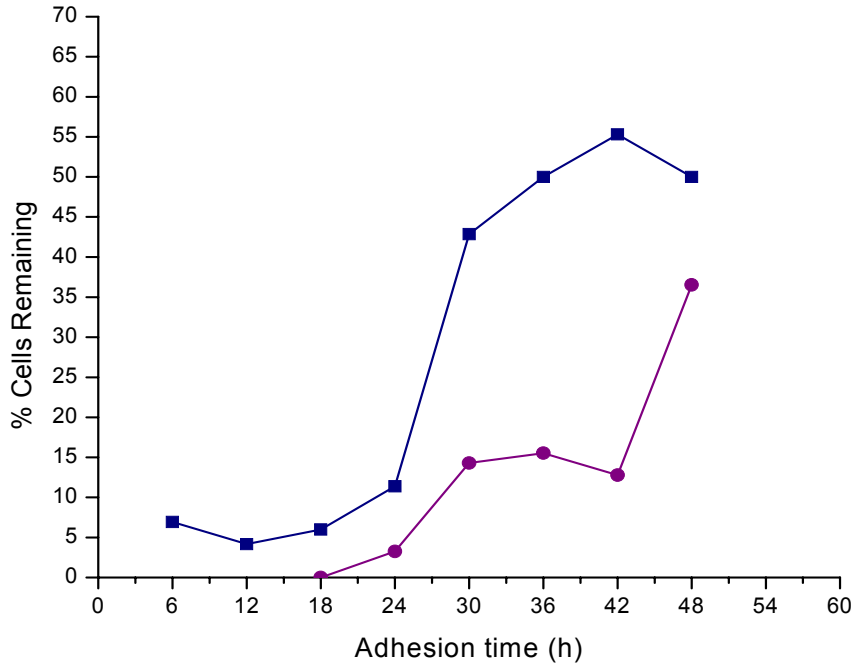

Figure 2.4 The percentage of *P. aeruginosa* cells which remain adhered to the substrate after scanning the surface at threshold tip-surface setpoint forces of 2.5 (■) and 15 nN (●).

~ four-fold during the same 6 h time window compared to the previous period (14.3% and 3.3%, respectively). Based on these observations, the most notable adhesion dynamics occurred over an 8 h period.

2.3.2 Quantitative measurement of adhesion kinetics. The quantitative method for determining the strength of bacterial adhesion was used to study the adhesion strengths of individual adhered *P. aeruginosa* and *S. aureus* cells over similar periods to compare the non-specific adhesion of two distinct pathogenic strains of bacteria. The experiments were conducted from different cultures in triplicate for each species. The average lateral force required to remove all cells within a scan region is shown in Figure 2.5. As the majority of cells detected were typically removed during the first half of the run, the points in the graph representing the average force for a region correspond to the length of time after exposure associated with the lowest setpoint scan. The overall magnitude of forces required to detach *P. aeruginosa* (Fig. 2.5A) was significantly greater than for *S. aureus* (Fig. 2.5B). In fact, the cantilevers were no longer capable of applying sufficient force to remove every *P. aeruginosa* cell from the xerogel substrate after ~26 h. Table 2.1 lists both the average adhesion strength rates measured for independent experiments and the overall average and standard deviation for each species. The average rate of adhesion strength increase was almost seven-fold faster for *P. aeruginosa* (3.36 ± 0.08 nN/h) than for *S. aureus* (0.50 ± 0.09 nN/h).

Figure 2.6A shows the average lateral forces necessary to detach *S. aureus* in a single experiment. Examination of the component measurements used in calculating these average forces revealed two additional trends in adhesion kinetics that could not be resolved from the

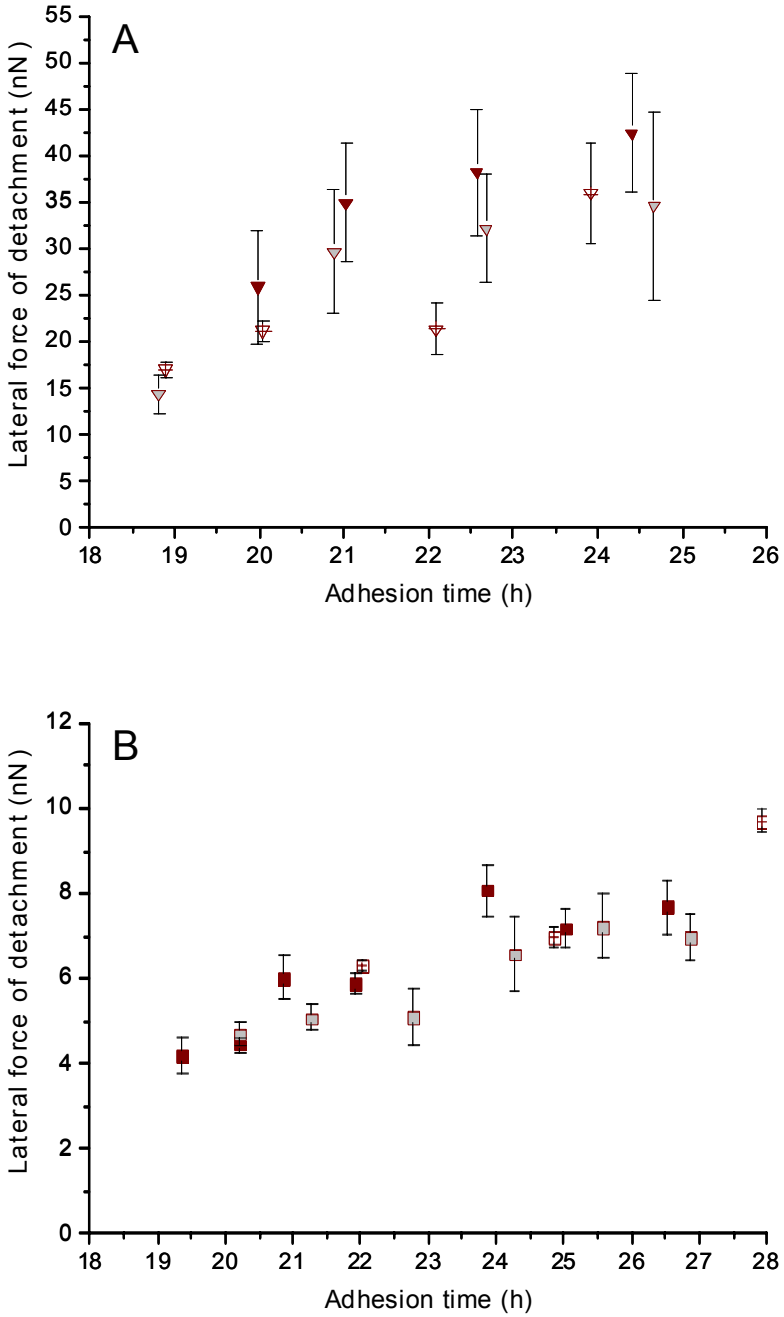

Figure 2.5 The average lateral force required for cell detachment measured for each (A) *P. aeruginosa* (▼) and (B) *S. aureus* (■) cell within a scan region between 19 and 27 h after substrate exposure to cell suspension. The error bars indicate the standard error over all measurements taken with a scan area. Data points obtained during duplicate and triplicate experiments are indicated by the open and cross-hatched symbols, respectively.

Table 2.1 Average, basal and elite adhesion rates for *P. aeruginosa* 19 – 26 h after initial adhesion and *S. aureus* 19 – 28 h after initial adhesion from three independent kinetics experiments per species. After 26 h, the cantilevers used in this study were no longer able to apply sufficient lateral force to detach all *P. aeruginosa* cells from the substrate.

species	average (nN/h)	basal (nN/h)	elite (nN/h)
P. aeruginosa	3.36 ± 0.08	0.0 ± 0.2	9 ± 1
S. aureus	0.50 ± 0.09	0.17 ± 0.09	1.4 ± 0.4

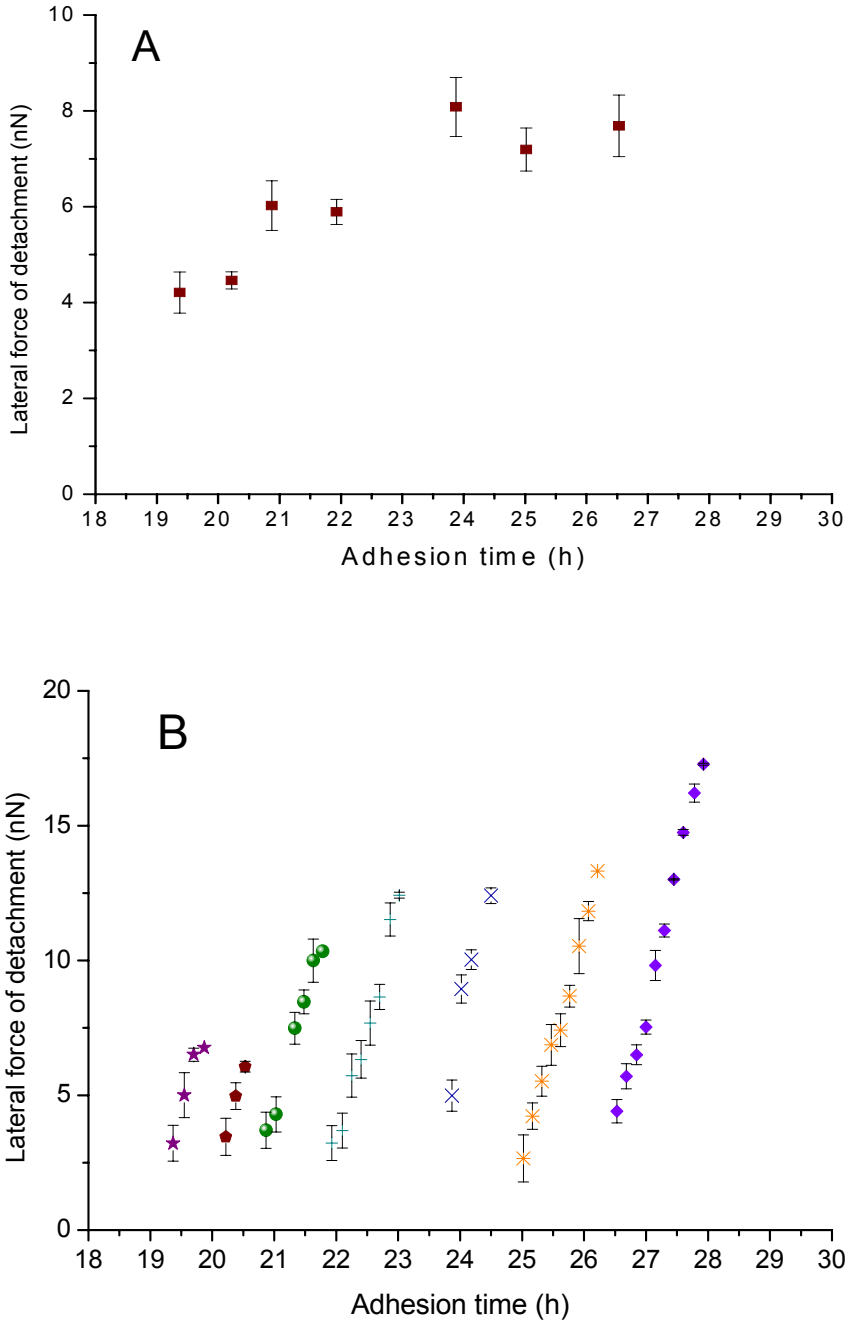

Figure 2.6 (A) The average force of detachment measured for *S. aureus* per scan region (■) as a function of time for a single experiment. The error bars indicate the standard error of all measurements taken within the scan region. (B) The average force of detachment measured for *S. aureus* per scan in the same experiment at the following timepoints: 19 h (★), 20 h (⬟), 21 h (●), 22 h (+), 24 h (x), 25 h (✳), and 26 h (◆). The error bars indicate the standard deviation over all measurements taken with a single scan.

average values alone. By breaking down the average lateral forces measured in each scan region during an entire run into adhesion measurement averages for each scan (Fig. 2.6B), a large range of detachment forces were evident in each region. Furthermore, the range of forces broadened with time. Though example data is provided for a single *S. aureus* experiment, similar trends were observed for all other experiments involving both species of bacteria. The trends indicate that adhesion strength increases vary with bacteria species.

A population of cells whose detachment occurs in the first scan of each run was always apparent. In contrast, another population of cells, the last to be removed from each scan area, became increasingly more difficult to detach over time. Examining only those cells that were detached in the first and last scan of each run in relation to the average over the entire region (Fig. 2.7) allowed for the deterimination of adhesion kinetics for "basal" and "elite" cell populations, respectively (Table 2.1). The elite *S. aureus* population was characterized having a ten-fold larger rate of adhesion over the basal cells (1.4 ± 0.4 nN/h and 0.17 ± 0.09 nN/h, respectively). The basal *P. aeruginosa* population exhibited no appreciable increase in adhesion rate (0.0 ± 0.2 nN/h), while the adhesion strength kinetics of the elite population increased at 9 ± 1 nN/h, a value significantly greater than that observed for elite *S. aureus*. Additional plots of basal and elite *P. aeruginosa* and *S. aureus* populations are provided in Figure 2.8.

2.3.3 Intercellular interactions. To evaluate the effect of cell-cell interactions on force measurements, standard statistical analysis was employed. Only *S. aureus* were examined as such cells have a tendency to grow and adhere in clusters. In contrast, *P. aeruginosa* cells were observed to adhere more typically as single cells. Forces in a particular run were grouped as either clustered or independent, and an Anova single-factor analysis was

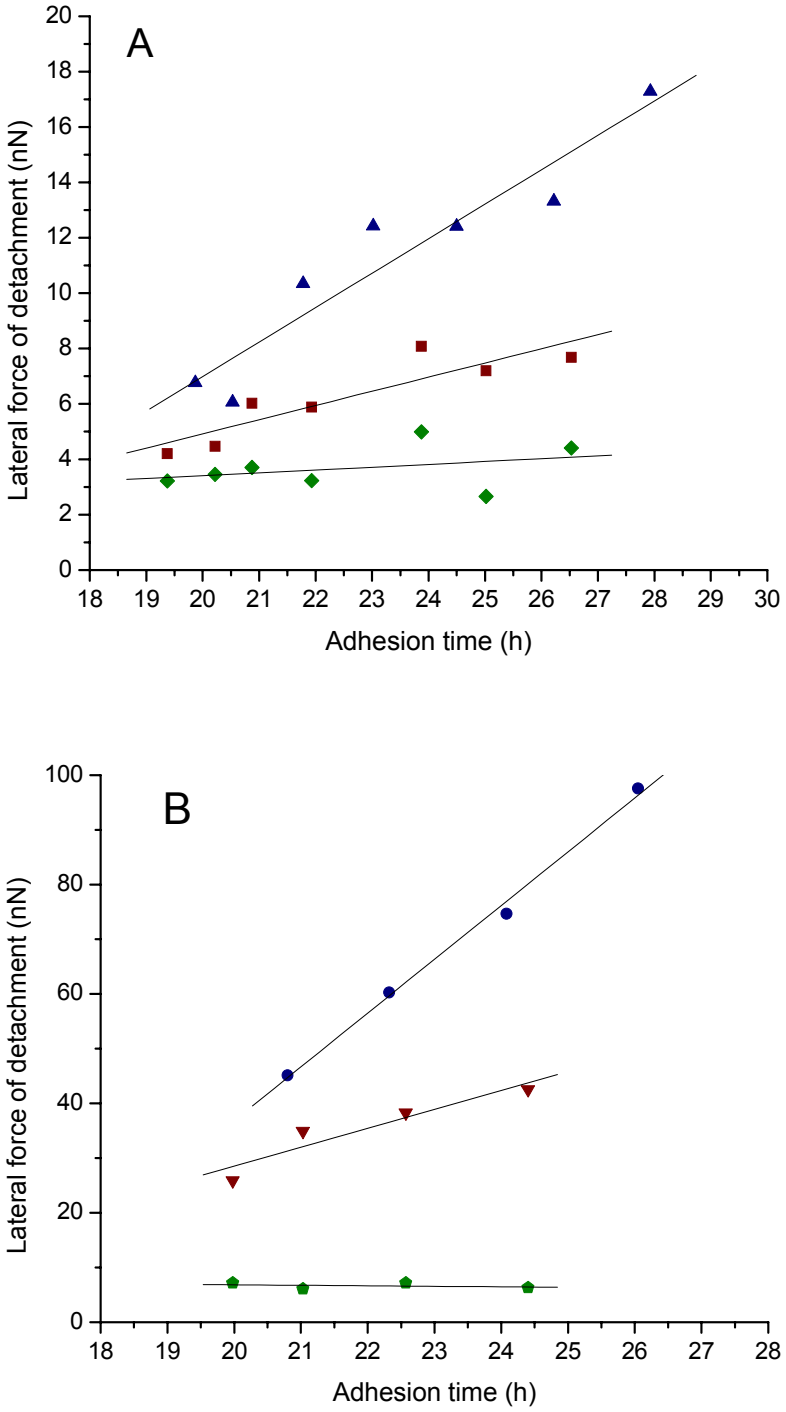

Figure 2.7 Adhesion kinetics from a single experiment for (A) *S. aureus* basal (♦), average (■), and elite (▲) population of cells and (B) *P. aeruginosa* basal (⬟), average (▼), and elite (●) cell populations.

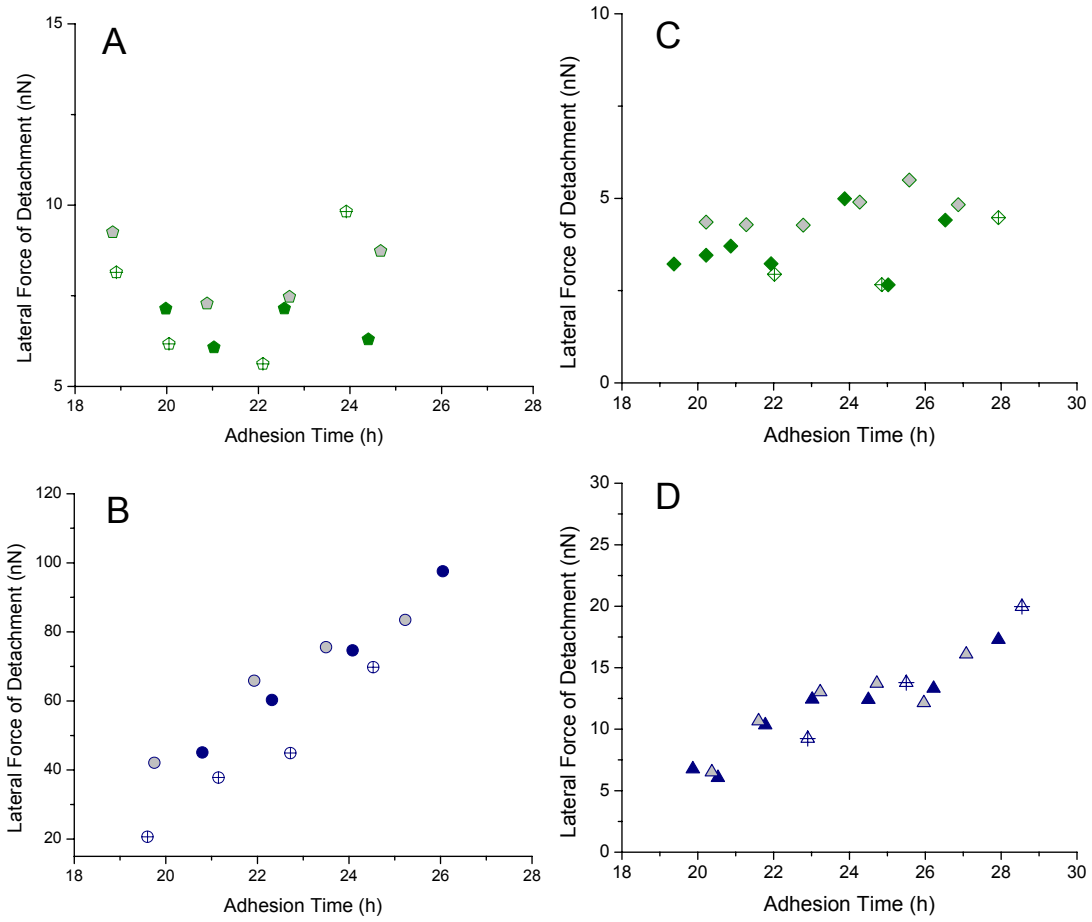

Figure 2.8 Average measured (A) basal and (B) elite detachment forces for replicate *P. aeruginosa* experiments. Average measured (C) basal and (D) elite detachment forces for replicate *S. aureus* experiments.

conducted. Cells with a neighbor oriented perpendicular to the applied lateral force were evaluated separately from those with a neighbor oriented in line with the direction of probe movement. No statistical difference in force measurements existed between independent cells and those in close proximity to neighboring cells. At least three runs encompassing both high and low setpoints were evaluated for each neighbor orientation.

2.3.4 Cell viability. The viability of *P. aeruginosa* and *S. aureus* was evaluated after 30 h resident adhesion time by sonication of the colonized surfaces, and subsequent plating and growth on agar nutrient medium. The number of viable cells removed per surface area was calculated from the number of colonies observed after overnight incubation at 37 °C (Table 2.2). The numbers of viable colonies observed were in close agreement with the average number of cells detected during an experimental run.

2.4 Discussion

The primary aim of our studies was to develop an improved method for more accurately measuring and comparing the strength of adhesion of bacterial cells in situ via AFM. By employing a geometrical analysis of the applied force vectors coupled with quantification of the total cantilever compression responsible for applying the detachment force for each individual cell, the lateral force (F_{lat}) necessary to overcome the force of adhesion was determined on a per cell basis. The method is broadly applicable to any number of species, substrates, and preparation procedures. Upon evaluating changes in bacterial adhesion strength as a function of time, a number of interesting observations became evident.

Table 2.2 Comparison of the number of viable cells recovered after 30 h adherence in PBS to the average number of cells detected using AFM. The number of cfu counted was back-calculated to determine the average number of viable cells recovered from a 40 μm^2 region of the substrate.

species	viable cells recovered[a]	cells detected[a]
P. aeruginosa	14.4	14.6 ± 7.5
S. aureus	35.5	32.2 ± 20.0

[a]per 40 μm^2 surface area of the substrate

2.4.1 Variation in interspecies kinetics. Regardless of the time adhered to our model substrate, the adhesion of *P. aeruginosa* was significantly greater relative to *S. aureus*. Assessing the differences in cell-surface properties that exist between the two species may be helpful in understanding the gap in measured adhesion strength. Both the size and shape of the bacteria differ significantly. *P. aeruginosa* is a rod-shaped bacterium (1 x ~3 μm) while *S. aureus* is spherically shaped (d ~ 1 μm). Larger, rod-shaped bacteria would be expected to contact the substrate to a greater extent due to their size and degree of curvature. Gomez-Suarez et al. also reported superior adhesion of rod-shaped bacteria over coccal species upon exposure to low-velocity air bubbles.[22]

Another likely contributing factor for the differences in adhesion strength may stem from the intrinsic flexibility, or lack thereof, inherent in the varying component layers of the cell wall. The gram-positive cell wall is coated with a thick peptidoglycan layer that is rigid in nature. In contrast, the gram-negative cell wall is characterized by a thinner layer of peptidoglycan matrix surrounded by a flexible outer phospholipid bilayer. Thus, not only is *P. aeruginosa* capable of establishing a larger footprint of contact, but its added flexibility allows additional freedom to conform or expand against the substrate to further increase its surface area of interaction. The effect of flexibility on increasing surface contact area has been observed previously for *Bacillus mycoides* spores on a similarly modified glass substrate.[31]

In addition to cell morphology, the polymeric and proteinaceous structures present on the exterior of the cell differ between species and strains. In general, it is difficult to predict the mediating effect of these variations on non-specific attachment, but recent studies have shown increasing adhesion forces over short surface-resident time periods (~100 s) between

colloids and protein coated surfaces.[32,33] Additionally, greater surface contact between features of the cell and the substrate presumably lead to an increase in the number of potential interactions (e.g., van der Waals interactions) that may be established to reinforce adhesion strength. While the contribution to adhesion of each individual non-covalent bond is small, the combined effect generates an essentially irreversible attachment. A number of studies point to the roles of proteins and polysaccharides at the exterior of the cell on bacterial adhesion.[34,35] In addition to having filimentous proteinaceous features termed fimbriae, or pili, *P. aeruginosa* is known to produce an alginate extracellular polysaccharide slime (glycocalyx) that facilitate both non-specific and specific adhesion. Likewise, *S. aureus* produces a microcapsule that with other external components, such as lipoteicoic acid and a variety of specific protein receptors plays a role in the adhesive mechanisms of the species.[36] The importance of surface-adsorbed matrix proteins such as fibrinogen and fibronectin for promoting *S. aureus* colonization of biomaterial surfaces has been reported previously and may partially explain the lower measured adhesive forces observed for *S. aureus* relative to *P. aeruginosa* using bare biomaterial substrates.[37-40]

2.4.2 Intraspecies population kinetics. As evidenced by our data, not all cells of the same species and culture are equally capable of establishing the ability to withstand detachment from the same surface. Dickenson and Cooper observed a similar phenomenon while studying the detachment rate of *S. aureus* adhered to different polymeric surfaces in a laminar flow field as a function of shear stress.[41] They reported that cell attachment followed first-order rate kinetics. However, the detachment rate of adhered cells at early periods was more rapid, slowing with time. The range of shear stresses used in their experiments was insufficient to remove all cells adhered to the substrates. These results correspond with our

observation that most cells were detached when subjected to low tip-cell forces, while a certain population of cells required much larger applied forces to initiate cell detachment. Dickenson and Cooper proposed that a homogeneous cell population exhibiting a heterogeneous adhesion energy distribution may result from a combination of the small surface contact area established by each cell and the variation in molecular components existing in this contact region. Other researchers have reported similar heterogeneity in the detachment of receptor-coated beads that model cells.[41-43]

The wide range of adhesion forces measured for cell detachment may also be attributed to the complex combinations of changes in metabolic processes resulting from surface adhesion or proximate cell signaling. Sauer et al. described a number of changes in gene regulation for *P. aeruginosa* at discrete stages of biofilm development following initial attachment, including 57 specific proteins expressed in cell populations at the irreversible attachment stage (Phase II) that were absent or weakly detected in planktonic cells.[44] While some of the changes in gene regulation were linked directly to quorum sensing, the authors suggested additional surface-induced expression of proteins that might play a role in increasing adhesion strength after initial attachment. The heterogeneity in adhesion strength observed in this study may be an observation of such physiological changes that occur after bacteria attach to a surface.

Local variations in substrate properties may also influence bacterial adhesion. Deviations from theoretical predictions of adhesion behavior have previously been attributed to heterogeneity in surface properties. Using AFM force-mapping, Vadillo-Rodríguez et al. reported the presence of a small number of randomly distributed high-adhesion sites on silica and metal oxide surfaces.[45] The model surfaces used in our study were partially composed of

aminosilanes whose amines are protonated at physiological pH. While we assumed that these charges were distributed across the surface due to repulsive interaction, it is possible that higher densities of aminosilanes may exist locally. Bacteria with negatively charged functional groups present on the exterior of the membrane would be attracted to such regions. Such interactions would likely yield greater adhesion to the surface over time due to increased water exclusion and hydrophobic interactions.

2.4.3 Quantitative force determination. The premise of previous reports relies on the principle that when imaging a surface in contact mode, the applied force between the probe and substrate is held constant by a feedback loop. Thus, empirical relationships were drawn between the tip-surface setpoint force maintained by the feedback loop of the AFM and the number of cells withstanding imaging at such applied forces to evaluate bacterial adhesion strength.[23-25] While this method has merit for preliminary studies of bacterial adhesion kinetics, we believe it is not adequate for quantitative determination of the actual force that is applied at cell detachment. Rather, the feedback loop response occurs after a finite time. When a large feature such as a cell is encountered, an instantaneous increase in cantilever deflection is unavoidable. This phenomenon may be observed in real time and collected as an image by directing an AFM channel to record the difference between setpoint deflection and actual deflection (i.e., deflection error) for each point corresponding with the height image. The effect is exacerbated by using cantilevers with low spring constants and low setpoints where additional force due to deflection error contributes a significant percentage of the overall force applied to the cell by the probe. By examining the total force applied to all cells removed at representative low (0.10 V) and high (5.00 V) setpoint scans (Table 2.3), the contribution to normal force calculation from deflection error becomes evident. Without

Table 2.3 Comparison of the actual normal force applied to the cell and the tip-surface force adjusted for by the feedback loop for both small and large setpoints.

setpoint (V)	deflection error (nm)	total compression (nm)	normal force[a] (nN)	setpoint force[a] (nN)	percent error[b] (nN)
0.100	24.1	106	12.8	9.32	-27.2
0.100	24.8	107	12.9	9.32	-27.8
0.100	41.7	127	15.3	9.32	-39.1
5.00	15.0	706	84.7	82.5	-2.60
5.00	35.1	730	87.6	82.5	-5.82

[a]Nominal spring constant = 0.12 N/m
[b]Percent error from the normal force (calculated from the total compression of the cantilever) obtained by using the setpoint force

correcting for setpoint deflection error, the values calculated for the applied forces within each scan would all be equivalent and systematically underrepresented.

While determining total cantilever compression was a key improvement to the method introduced herein, other modifications were made in force measurement and data acquisition procedures to further improve accuracy of bacterial adhesion strength values. First, the free air deflection of the probe was measured before and after each scan to account for thermal drift. Large areas (40 μm^2) were scanned to observe the adhesion strength of many cells (~10 to 50) simultaneously, improving the statistical significance of the data generated. In addition, proper orientation of the cantilever and tip during imaging scans was maintained. Only deflection data accumulated from the 'retrace' (i.e., movement of the probe from tip end along the long axis of the cantilever toward the cantilever holder) was used in acquiring force measurements. If scanning along the long axis in the opposite direction, buckling of the cantilever may occur. Changes in the output signal due to buckling would be indistinguishable from those resulting from bending. In contrast, scanning laterally (along the short axis of the cantilever) torsional force is applied by twisting in the cantilever due to tip-cell interactions twist the cantilever. Buckling and twisting of the cantilever deviate from the spring model and Hooke's Law.

In addition to assuring that our force application system can be approximated by Hooke's Law, it is much more relevant to determine and report the actual force responsible for detachment (F_{lat}) versus the applied force (F_{app}) or setpoint force (F_z). By approximating the slightly bent cantilever as a straight line, geometrical analysis showed that the directional change of the normal force applied by a pyramidal probe at a known tilt was not significant over the range of cantilever compression used in this study (Fig. 2.2B, Appendix). As such,

the lateral forces reported herein were calculated using the known tilt of the cantilever and geometry of the AFM probe.

2.5 Conclusions

A quantitative method for measuring the strength of bacterial adhesion was described enabling the discrimination of adhesion forces measured by AFM at a single setpoint by determining total cantilever compression from deflection error image analysis. Compared to previous methods, this method allowed for more accurate measurement of the actual normal and lateral force applied to bacteria while imaging in contact mode. We thus describe a useful tool for characterizing changes in non-specific adhesion strength of bacteria that may be easily applied to evaluating the effect of a number of variables including protein mediation and substrate properties on bacterial adhesion.

Analysis of adhesion forces measured for *P. aeruginosa* and *S. aureus* as a function of time indicated that the strength of bacterial adhesion is both dynamic and non-uniform for both species. *P. aeruginosa* demonstrated significantly greater overall adhesion forces and rates of increasing adhesion strength than *S. aureus*. The size, shape, and cell wall structure of *P. aeruginosa* contribute to its superior ability to adhere non-specifically to a substrate. The apparent heterogeneity in the adhesion of cells of the same species under similar conditions may be attributed to variation in the states of adhesion energy attained, local variation in surface characteristics, and/or metabolic changes in gene regulation after surface attachment.

2.6 References

(1) An, Y. H.; Friedman, R. J. Concise review of mechanisms of bacterial adhesion to biomaterial surfaces. *J. Biomed. Mater. Res. (Appl. Biomater.)* **1998**, *43*, 338-348.

(2) Dankert, J.; Hogt, A. H.; Feijen, J. Biomedical polymers: Bacterial adhesion, colonization, and infection. *CRC Crit. Rev. Biocompat.* **1986**, *2*, 219-301.

(3) Katsikogianni, M.; Missirlis, Y. F. Concise review of mechanisms of bacterial adhesion to biomaterials and of techniques used in estimating bacteria-material interactions. *Eur. Cells Mater.* **2004**, *8*, 37-57.

(4) Li, B.; Logan, B. E. Bacterial adhesion to glass and metal-oxide surfaces. *Colloids Surf., B* **2004**, *36*, 81-90.

(5) Hogt, A. H.; Dankert, J.; Feijen, J. Adhesion of *Staphylococcus epidermidis* and *Staphylococcus saprophyticus* to a hydrophobic biomaterial. *J. Gen. Microbiol.* **1985**, *131*, 2485-2491.

(6) Dickinson, R. B.; Nagel, J. A.; Proctor, R. A.; Cooper, S. L. Quantitative comparison of shear-dependent *Staphylococcus aureus* adhesion to three polyurethane ionomer analogs with distinct surface properties. *J. Biomed. Mater. Res.* **1997**, *36*, 152-162.

(7) Chin, M. Y. H.; Sandham, A.; Pratten, J.; de Vries, J.; van der Mei, H. C. et al. Multivariate analysis of surface physico-chemical properties controlling biofilm formation on orthodontic adhesives prior to and after fluoride and chlorhexidine treatment. *J. Biomed. Mater. Res. (Appl. Biomater.)* **2006**, *78B*, 401-408.

(8) Tang, H.; Cao, T.; Wang, A.; Liang, X.; Salley, S. O. et al. Effect of surface modification of siliconeon to *Staphylococcus epidermidis* adhesion and colonization. *J. Biomed. Mater. Res.* **2006**, *80A*, 885-894.

(9) Dickinson, R. B.; Nagel, J. A.; McDevitt, D.; Foster, T. J.; Proctor, R. A. et al. Quantitative comparison of clumping factor- and coagulase-mediated *Staphylococcus aureus* adhesion to surface-bound fibrinogen under flow. *Infect. Immun.* **1995**, *63*, 3143-3150.

(10) Kussela, P. Fibronectin binds to *Staphylococcus aureus*. *Nature* **1978**, *276*, 718-720.

(11) Morris, E. J.; McBride, B. C. Adherence of *Streptococcus sanguis* to saliva-coated hydroxyapatite: Evidence for two binding sites. *Infect. Immunol.* **1984**, *43*, 656-663.

(12) Paulsson, M.; Kober, M.; Freij-Larsson, C.; Stollenwerk, M.; Wesslen, B. et al. Adhesion of *Staphylococci* to chemically modified and native polymers, and the influence of preadsorbed fibronectin, vitronectin and fibrinogen. *Biomaterials* **1993**, *14*, 845-853.

(13) Orstavik, D. Sorption of *Streptococcus faecium* to glass. *Acta Pathol. Microbiol. Scand.* **1977**, *85B*, 38-46.

(14) Dudderiege, J. E.; Cent, C. A.; Laws, J. E. Effect of surface shear stress on the attachment of *Pseudomonas fluorescens* to stainless steel under defined flow conditions. *Biotechnol. Bioeng.* **1982**, *24*, 153-164.

(15) McWhirter, M. J.; McQullan, A. J.; Bremer, P. J. Influence of ionic strength and pH on the first 60 min of *Pseudomonas aeruginosa* attachment to ZnSe and to TiO_2 monitored by ATR-IR spectroscopy. *Colloids Surf., B* **2002**, *26*, 365-372.

(16) Walker, S. L.; Redman, J. A.; Elimelech, M. Influence of growth phase on bacterial deposition: Interaction mechanisms in packed-bed column and radial stagnation point flow systems. *Environ. Sci. Technol.* **2005**, *39*, 6405-6411.

(17) An, Y. H.; Dickinson, R. B.; Doyle, R. J. Mechanisms of Bacterial Adhesion and Pathogenesis of Implant and Tissue Infections. *Handbook of Bacterial Adhesion: Principles, Methods, and Applications*; Humana Press Inc.: Totowa, NJ, 2000; pp 1-27.

(18) Gristina, A. G. Biomaterial-centered infection: Microbial adhesion versus tissue integration. *Science* **1987**, *237*, 1588-1595.

(19) Marshall, K. C. Mechanisms of bacterial adhesion at solid-water interfaces. *Bacterial adhesion: mechanisms and physiological significance*; Plenum Press: New York, 1985; pp 133-161.

(20) Vacheethasanee, K.; Marchant, R. E. Nonspecific *Staphylococcus epidermidis* Adhesion: Contributions of Biomaterial Hydrophobicity and Charge. *Handbook of Bacterial Adhesion*; Humana Press: Totowa, NJ, 2000; pp 73-90.

(21) Dickinson, R. B.; Cooper, S. L. Analysis of shear-dependent bacterial adhesion kinetics to biomaterial surfaces. *AIChE J.* **1995**, *41*, 2160-2174.

(22) Gomez-Suarez, C.; Busscher, H. J.; van der Mei, H. C. Analysis of bacterial detachment from substratum surfaces by the passage of air-liquid interfaces. *Appl. Environ. Microbiol.* **2001**, *67*, 2531-2537.

(23) Boyd, R. D.; Verran, J. Use of the atomic force microscope to determine the effect of substratum surface topography on bacterial adhesion. *Langmuir* **2002**, *18*, 2343-2346.

(24) Senechal, A.; Carrigan, S. D.; Tabrizian, M. Probing surface adhesion forces of *Enterococcus faecalis* to medical-grade polymers using atomic force microscopy. *Langmuir* **2004**, *20*, 4172-4177.

(25) Whitehead, K. A.; Rogers, D.; Colligon, J.; Wright, C.; Verran, J. Use of the atomic force microscope to determine the effect of substratum surface topography on the ease of bacterial removal. *Colloids Surf., B* **2006**, *51*, 44-53.

(26) Meinders, J. M.; van der Mei, H. C.; Busscher, H. J. Physicochemical aspects of deposition of *Streptococcus thermophilus* B to hydrophobic and hydrophilic substrata in a parallel plate flow chamber. *J. Colloid Interface Sci.* **1994**, *164*, 355-363.

(27) Vadillo-Rodríguez, V.; Busscher, H. J.; Norde, W.; de Vries, J.; van der Mei, H. C. Atomic force microscopic corroboration of bond aging for adhesion of *Streptococcus thermophilus* to solid substrata. *J. Colloid Interface Sci.* **2004**, *278*, 251-254.

(28) Marxer, S. M.; Rothrock, A. R.; Nablo, B. J.; Robbins, M. E.; Schoenfisch, M. H. Preparation of nitric oxide (NO)-releasing sol-gels for biomaterial applications. *Chem. Mater.* **2003**, *15*, 4193-4199.

(29) Nablo, B. J.; Schoenfisch, M. H. Antibacterial properties of nitric oxide-releasing sol-gels. *J. Biomed. Mater. Res.* **2003**, *67A*, 1276-1283.

(30) Hetrick, E. M.; Schoenfisch, M. H. Antibacterial nitric oxide-releasing xerogels: Cell vialility and parallel plate flow cell adhesion studies. *Biomaterials* **2007**, *28*, 1948-1956.

(31) Bowen, W. R.; Fenton, A. S.; Lovitt, R. W.; Wright, C. J. The measurement of *Bacillus mycoides* spore adhesion using atomic force microscopy, simple counting methods, and a spinning disk technique. *Biotechnol. Bioeng.* **2001**, *79*, 170-179.

(32) Xu, L.; Logan, B. E. Interaction forces measured using AFM between colloids and surfaces coated with both dextran and protein. *Langmuir* **2006**, *22*, 4720-4727.

(33) Xu, L.; Logan, B. E. Adhesion forces between functionalized latex microspheres and protein-coated surfaces evaluated using colloid probe atomic force microscopy. *Colloids Surf., B* **2006**, *48*, 84-94.

(34) Kwon, K. D.; Vadillo-Rodriguez, V.; Logan, B. E.; Kubicki, J. D. Interactions of biopolymers with silica surfaces: Force measurements and electronic structure calculation studies. *Geochim. Cosmochim. Acta* **2006**, *70*, 3803-3819.

(35) Xu, L.; Logan, B. E. Interaction forces between colloids and protein-coated surfaces measured using an atomic force microscope. *Environ. Sci. Technol.* **2005**, *39*, 3592-3600.

(36) Montanaro, L.; Arciola, C. R. Studying Bacterial Adhesion to Irregular or Porous Surfaces. *Handbook of Bacterial Adhesion: Principles, Methods, and Applications*; Humana Press Inc.: Totowa, NJ, 2000; pp 331-343.

(37) Cheung, A. L.; Fischetti, V. A. The role of fibrinogen in Staphylococcal adherence to catheters in vitro. *J. Infect. Dis.* **1990**, *161*, 1177-1186.

(38) Hermann, M.; Vaudaux, P.; Pittet, D.; Auckenthaler, R.; Lew, D. P. et al. Fibronectin, fibrinogen and laminin act as mediators of adherence of clinical *Staphylococcal* isolates to foreign material. *J. Infect. Dis.* **1988**, *158*, 693-701.

(39) Vaudaux, P.; Pittet, D.; Haeberli, A.; Huggler, E.; Nydegger, U. E. et al. Host factors selectively increase *Staphylococcal* adherence on inserted catheters: A role for fibronectin and fibrinogen/fibrin. *J. Infect. Dis.* **1989**, *160*, 865-875.

(40) Vaudaux, P.; Yasuda, H.; Velazco, M. I.; Huggler, E.; Ratti, I. et al. Role of host and bacterial factors in modulating *Staphylococcal* adhesion to implanted polymer surfaces. *J. Biomater. Appl.* **1990**, *5*, 134-153.

(41) Cozens-Roberts, C.; Lauffenburger, D. A.; Quinn, J. A. Receptor-mediated cell attachment and detachment kinetics: II. Experimental model studies with the radial-flow detachment assay. *Biophys. J.* **1990**, *58*, 857-872.

(42) Cozens-Roberts, C.; Lauffenburger, D. A.; Quinn, J. A. Receptor-mediated cell attachment and detachment kinetics. I. Probabilistic model and analysis. *Biophys. J.* **1990**, *58*, 841-856.

(43) Saterbak, A.; Kuo, S. C.; Lauffenburger, D. A. Heterogeneity and probabilistic binding contributions to receptor-mediated cell detachment kinetics. *Biophys. J.* **1993**, *65*, 243-252.

(44) Sauer, K.; Camper, A. K.; Ehrlich, G. D.; Costerton, J. W.; Davies, D. G. *Pseudomonas aeruginosa* displays multiple phenotypes during development as a biofilm. *J. Bacteriol.* **2002**, *184*, 1140-1154.

(45) Vadillo-Rodríguez, V.; Logan, B. E. Localized attraction correlates with bacterial adhesion to glass and metal oxide substrata. *Environ. Sci. Technol.* **2006**, *40*, 2983-2988.

Chapter 3:

Morphological analysis of the antimicrobial action of nitric oxide on Gram-negative pathogens using atomic force microscopy

3.1 Introduction

Nitric oxide (NO) is a highly reactive diatomic radical endogenously produced by the enzyme-catalyzed oxidation of L-arginine to L-citrulline. It has been implicated as a mediator in multiple physiological processes, ranging from regulatory roles in the cardiovascular and nervous system to the inducible host response to infection.[1,2] Various therapeutic properties attributed to NO, including tumor cytotoxicity,[3,4] antimicrobial activity, and improved wound healing and tissue integration at implant sites,[5] may prove beneficial in a number of pharmacological applications.[6,7] Due to its reactivity, diverse regulatory roles, and short half-life in blood (< 1 sec),[8] the ability to target therapeutic NO delivery locally is critical. Nitric oxide donating compounds, such as *N*-diazeniumdiolates[6] and *S*-nitrosothiols,[9,10] decompose to release NO and hence serve as vehicles for its storage and transport. A number of materials, including nanoparticles,[11,12] films and coatings,[13,14] and small molecules,[15,16] have employed NO-donor chemistry with varied physicochemical and NO-release properties.

The role of NO in the innate immune response is a conserved feature through a wide range of species, from *Drosophila* to human.[17] In mammals, macrophages and other immune cells produce NO in response to invading pathogens.[18] The antimicrobial properties of NO

may be elicited by direct modification of biomacromolecules or by formation of reactive nitrogen species (RNS) via reaction with oxygen (O_2) or superoxide (O_2^-).[19] These RNS may render nitrosative stress by the formation of compounds such as dinitrogen trioxide (N_2O_3) and oxidative stress via the formation of peroxynitrite ($ONOO^-$).[19-22] The spectrum of potential bactericidal mechanisms is thus broad, encompassing DNA damage resulting from deamination of deoxyribonucleotides, protein damage via numerous potential reactive sites (e.g. heme groups, thiols, amines) that disrupts normal cellular transport and metabolism, and membrane damage propagated by radical lipid peroxidation. The local physiological environment plays a key role in determining the metabolic pathways available to NO, and it would thus be expected that the bactericidal mechanism(s) of NO produced endogenously in phagosomal compartments would differ from NO released extracellularly (e.g., from an implanted biomaterial) as a result of differences in local conditions and substrates available in the biological milieu.

In vitro, NO has proven a potent antimicrobial agent effective against a range of microorganisms, including both Gram-negative and Gram-positive bacteria. Gaseous NO was found to be toxic against a number of pathogenic species, including *C. albicans* and methacillin-resistant *S. aureus*.[23] *N*-Diazeniumdiolate-modified NO-releasing surfaces have been shown to reduce initial *P. aeruginosa* adhesion relative to controls,[24-26] and kill those that do adhere.[27] Nitric oxide release from silica nanoparticles has been characterized by significant toxicity to bacterial cells with reduced toxicity to L929 mouse fibroblasts.[28] While the bactericidal effects of NO and NO-releasing biomaterials have been demonstrated repeatedly, details on the primary targets resulting in bacterial cytotoxicity and the corresponding cellular effects of NO on microbial species remain speculative.

Morphological analyses of bacteria aid in understanding mechanisms of antibiotic action by allowing visualization of changes in the appearance of the microbe undergone subsequent to treatment. While electron microscopy has been employed toward this end for decades,[29-31] atomic force microscopy (AFM) has been used with increasing frequency.[32-37] As a surface characterization tool, AFM is ideal for morphological studies of surface-adhered bacteria as it allows cells to be imaged in situ with high resolution without requiring chemical drying, metal coating, or exposure to ultra-high vacuum. An added benefit of AFM is the flexible and adaptable nature of cantilevers as transducers that allow detection of other physical (e.g., elasticity) or chemical (e.g., charge distribution) surface parameters simultaneously with the acquisition of height information. Atomic force microscopy has been applied to visualizing the antimicrobial action of peptides,[32,34,36] chitosan,[33] quantum dots,[35] and the β-lactam antibiotics penicillin and amoxicillin.[37]

Herein, we report a morphological analysis of *P. aeruginosa* and *Escherichia coli* after exposure to NO released from two *N*-diazeniumdiolate-modified materials: a small molecule NO-donor derived from proline (PROLI/NO) and a NO donor-modified xerogel surface coating. The diazeniumdiolate moiety stores two molecules of the antimicrobial agent NO on each functionalized amine. Exposure to proton sources such as buffer and blood catalyzes the release of NO. Using topographical surface mapping and nanometer-scale height resolution, changes in bacteria shape and surface roughness were studied as a function of exposure time, material, and quantity of NO released.

3.2 Experimental

3.2.1 Materials. Ethanol and methanol were purchased from Fisher Scientific (Pittsburgh, PA). Argon, NO, nitrogen (N_2), and a 25.7 ppm gaseous NO standard in N_2 were purchased from National Welders (Raleigh, NC). *N*-(6-aminohexyl) aminopropyltrimethoxysilane (AHAP3) was obtained from Gelest (Tullytown, PA). Amoxicillin was obtained from Fluka (Buchs, Switzerland). Isobutyltrimethoxysilane (BTMOS), L-proline, sodium methoxide, and dimethylsulfoxide (DMSO) were purchased from Sigma-Aldrich (St. Louis, MO). The amino- and alkoxysilanes were stored over desiccant. The above chemicals were used without further purification. Distilled water was purified with a Millipore Milli-Q UV Gradient A-10 system (Bedford, MA) to a resistivity of 18.2 MΩ cm.

3.2.2 Cell culture. *P. aeruginosa* (ATCC #19143) and *E. coli* (ATCC #53323) were obtained from American Type Culture Collection (Manassas, VA) and cultured in tryptic soy broth (TSB). Stock cultures were prepared and stored at -80 °C for subsequent experiments. A 1-mL aliquot from an overnight culture was inoculated in ~100 mL of TSB and incubated at 37 °C for 3-5 h until the culture reached mid-exponential log phase as determined from optical density at 600 nm (OD_{600} = 0.2 ± 0.1), corresponding to ~10^8 colony forming units (cfu) mL^{-1}.

3.2.3 Synthesis of xerogel films. Glass slides were coated with a 40% (v:v total silane content) AHAP3/BTMOS xerogel film via a 2-step process as described by Marxer et al.[13] Briefly, 120 µl BTMOS was mixed with 60 µl water, 200 µl ethanol, and 10 µl of 0.5 M HCl for 1 h. Then, 80 µl of AHAP3 was added, and the solution was mixed for an additional hour. Glass slides were cut into sections (dim. 13 x 17.5 mm), rinsed with ultrapure water

and ethanol, dried under a stream of nitrogen, and cleaned for 30 min in a UV-ozone cleaner (BioForce, Ames, IA). To cast a film, 40 μl of the sol was pipetted onto clean glass slides, dried for 30 min at ambient temperature, and cured at 85 °C for 3 d. Control xerogel films were stored in desiccators at 22 °C.

3.2.4 NO-donor synthesis and characterization. Xerogels were modified to release NO by exposing the films to 5 atm of NO for 72 h as previously described.[13] The NO chamber was flushed twice with 5 atm Ar to remove atmospheric impurities (e.g., oxygen, water) prior to introducing NO gas. After 3 d, unreacted NO was removed by flushing the vessel with Ar.

L-proline was converted to PROLI/NO following a procedure previously reported by Saavedra et al.[16] Briefly, 10 g of L-proline was dissolved in 39 mL of 25% sodium methoxide in methanol. This solution was combined with an additional 20 mL of methanol, and exposed to NO gas (5 atm) as described above. The resulting PROLI/NO formed as a white precipitate that was collected via filtration, washed with ether, and vacuum dried. All NO-releasing materials (i.e., PROLI/NO and xerogels) were stored in vials purged with nitrogen at -20 °C until use in order to stabilize the NO donor.

A chemiluminescent nitric oxide analyzer (NOA) (Sievers Model 280, Boulder, CO) was used to measure NO release in real time. A known quantity of the NO-release material was placed in a flask containing phosphate buffered saline (PBS, pH = 7.4) positioned in a water bath maintained at 37 °C. The NO generated via diazeniumdiolate decomposition was carried into the analyzer via a stream of N_2 bubbled into the solution at a flow rate of 80 mL min^{-1}. The detector was calibrated by a 2-point curve using an atmospheric sample passed through an NO zero filter and a 25.7 ppm NO standard.

3.2.5 Bacterial adhesion to control and NO-releasing xerogels. Prior to use, the NO-releasing xerogels were allowed to reach ambient temperature. Control and NO-releasing films were rinsed briefly with ultrapure water and dried under a stream of nitrogen immediately prior to bacterial adhesion. After diluting bacterial suspensions in TSB (1:2 in PBS), a 200-μL aliquot of the solution was beaded directly onto the xerogel surface. Substrates were covered to reduce evaporation and incubated for either 1 h (in preparation for treatment in antibiotic solutions) or 2 h (NO-releasing xerogels) at 37 °C to allow for bacterial adhesion.

3.2.6 Antimicrobial treatment. For time points exceeding 2 h, NO-releasing xerogels with adhered bacteria were placed in vials containing 5 mL of PBS and incubated at 37 °C for the remainder of the exposure period. For treatment with PROLI/NO, the appropriate mass was first weighed into chilled, dry vials. The correct volume of PBS (~5 mL) was added to obtain the desired concentration, vortexed briefly, and a control (unmodified) xerogel with adhered, untreated bacteria was immediately added to the PROLI/NO solution and incubated for 2 h at 37 °C. Amoxicillin treatment was achieved by preparing a 1 μg mL^{-1} solution in PBS from a 9.6 mg mL^{-1} stock solution in DMSO, into which a control xerogel (with adhered bacteria) was placed and incubated for 2 h at 37 °C. Each xerogel time point and antibiotic concentration was replicated for each species studied. A detailed description of the substrate rinsing process is provided below.

3.2.7 Substrate preparation technique. A gentle-rinse procedure was developed to ensure that adhered cells remained relatively undisturbed for subsequent treatment and/or imaging experiments. A rinse step was accomplished by pipetting a single, 300-μL aliquot of the appropriate rinse solution onto the substrate. Immediately thereafter, the solution was

removed with a narrow-tipped pipette in 100-μL increments. Of note, the pipette was only applied to the outer edge of the substrate to remove residual rinse solution so as not to disturb the surface to be imaged.

For both control and NO-releasing xerogels, excess cell suspension in TSB was removed from the surface after the adhesion period, followed by five consecutive rinses with PBS to remove TSB, non-adhered cells, and trace cellular components. If adhered cells were subsequently treated, the substrate was added to a vial containing the appropriate concentration of antimicrobial agent in PBS (PROLI/NO, amoxicillin) for 2 h or PBS (40% AHAP3/BTMOS xerogel time points exceeding 2 h) at 37 °C. The final rinse steps consisted of 5 washes with ultrapure water to remove antibiotic and/or salts, after which the substrate was dried using capillary action by placing absorbent paper at the edge of the substrate to draw excess water off the surface. A thin layer of water remained, which was allowed to evaporate prior to imaging. It has previously shown that the process of drying bacteria at xerogel surfaces does not affect their viability.[38]

3.2.8 AFM imaging. Simultaneous AFM height, amplitude, and phase images were obtained in AC mode on the air-dried substrates using an Asylum MFP-3D AFM (Santa Barbara, CA). Olympus AC240TS silicon beam cantilevers (Center Valley, PA) with a spring constant of 2 N m^{-1} and resonant frequency of 70 kHz were used to image bacteria in air. At least three 20 μm^2 survey images were obtained at random locations at an interior region of each substrate. Additional images captured control and antibiotic treated cells at greater magnifications. Images were acquired at a resolution of 512 x 512 pixels and scan speed of 1 Hz. Individual root-mean-square (rms) roughness of cell membranes was calculated using the MFP-3D software from 500 and 800 nm^2 regions of *P. aeruginosa* and

E. coli, respectively. Images used for roughness determination were acquired in the central part of a cell and were flattened by one order to reduce contributions from cell curvature at the edges of the image. Membrane roughness values were averaged from at least 3 different cells per species, agent, and dose. Artificial color and light were added to the three-dimensional reconstructions of height data to aid visualization of image detail.

3.3 Results and Discussion

3.3.1 Material characterization and experimental design. Bacterial cells were exposed to two NO-releasing materials that differ in their kinetic release profiles. A representative NO-release profile and the average integrated dose delivered from a 40% AHAP3/BTMOS xerogel film as a function of time are provided in Figure 3.1 and Table 3.1, respectively. Nitric oxide is released from these films via a surface flux, increasing rapidly upon exposure to aqueous solution and reaching a maximum within half an hour. Thereafter, the NO release gradually reduces to a flux averaging ~50 pmol cm^{-2} s^{-1} over 24 h. Hetrick, et al.[27] reported that a total dose of NO between 375 and 425 nmol cm^{-2} delivered from 40 % AHAP3/BTMOS xerogels 5 – 7 h after initial bacterial adhesion was sufficient to eradicate all adhered *P. aeruginosa* cells at room temperature. By contrast, PROLI/NO is a water-soluble, small molecule diazeniumdiolate NO donor derived from the amino acid proline. PROLI/NO releases a bolus of nitric oxide upon breakdown by water. Due to a short half-life ($t_{1/2}$ = 100 s), the majority of stored NO (10.4 ± 2.1 μmol NO mg^{-1}) is released within 300 s (Table 3.1). Standard plating experiments indicated a minimum bactericidal concentration of 4 and 8 mg mL^{-1} PROLI/NO after 2 h (MBC_{120}) for *E. coli* and *P. aeruginosa*, respectively (3-log reduction in cfu).

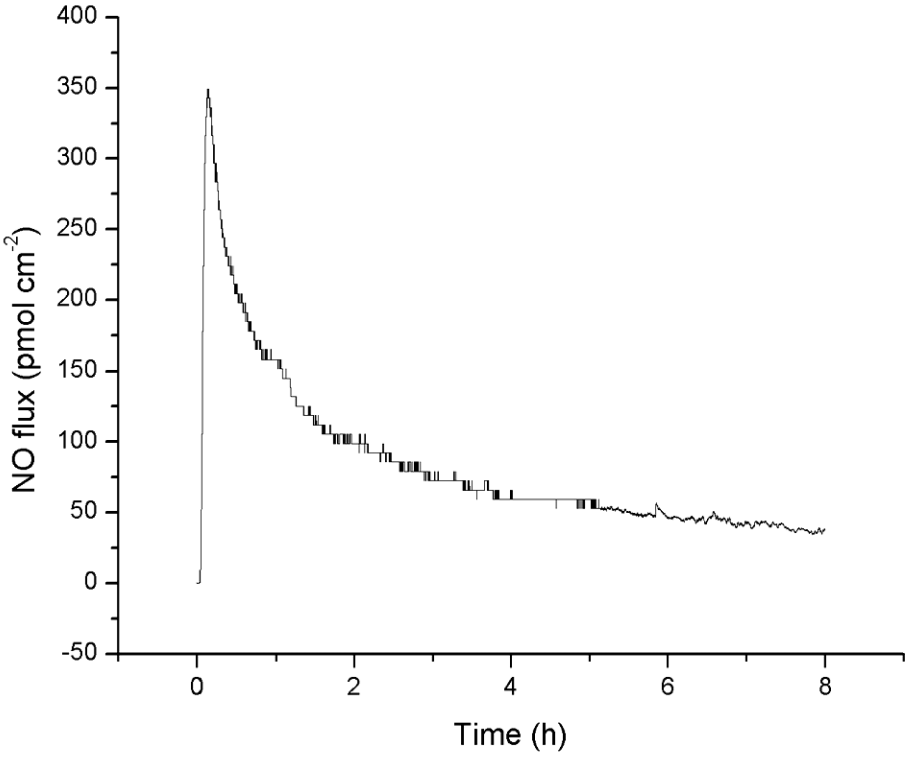

Figure 3.1 Nitric oxide released from a 40% AHAP3/BTMOS xerogel coating in PBS at 37 °C.

Table 3.1 Measured NO released from antibacterial materials

Material	NO delivery	exposure	dose NO[b]	
xerogel	surface flux	2 h	1.32 ± 0.13	(μmol cm^{-2})
		4 h	1.93 ± 0.19	
		6 h	2.39 ± 0.23	
		8 h	2.70 ± 0.27	
PROLI/NO	bolus	70 s	3.4 ± 1.1	(μmol mg^{-1})
		300 s[a]	8.8 ± 2.0	

[a]The majority of NO has been released after this time. The total NO released by 1 mg of PROLI/NO is 10.4 ± 2.1 μmol NO.
[b]Average dose of NO reported with standard deviation

Nitric oxide release from the materials used in this study was measured in deoxygenated PBS per the convention for measuring NO accurately via chemiluminescence. In contrast, the experiments to evaluate the bactericidal effects of these materials were conducted in normal PBS (i.e., not deoxygenated), since the bacteria are aerobic. Nevertheless, control experiments indicated that the NO release from AHAP3/BTMOS xerogels in normal PBS was indistinguishable from measurements made in deoxygenated PBS over 0 – 24 h, the time frame of our experiments (data not shown).

Due to the nature of diazeniumdiolate decomposition to NO (at physiological pH and temperature), bacterial adhesion to NO-releasing xerogel films occurs concurrently with exposure of the bacteria to a local NO flux. Although slower compared to control xerogels, the surface coverage of *P. aeruginosa* to NO-releasing 40% AHAP3/BTMOS xerogels have been shown to reach a steady state at 60 min under static conditions.[27] For these experiments, NO-releasing surfaces were exposed to cell suspensions for 2 h, followed by removal of loose cells and preparation of substrates for imaging (for 2 h time points) or transfer of the substrates to PBS (for extended time points). To apply a similar approach for treatment with antibiotic solutions (i.e., PROLI/NO and amoxicillin), bacteria were allowed to adhere to control xerogel substrates for an hour prior to transfer of the cell-covered substrate to a vial of antibiotic solution. Treating surface-adhered cells with antibacterial agents provided the added benefits of capturing cell damage and debris locally on the surface at the time of treatment while more nearly approximating an infection-causing scenario.

3.3.2 Morphologies of P. aeruginosa and E. coli adhered to control xerogels. Control 40% AHAP3/BTMOS xerogels have been reported to be non-toxic to bacteria adhered at exposure periods > 24 h.[38] Thus, they represent a suitable substrate for the study of normal

morphologies, while providing a consistent sub-stratum for comparison of healthy and antibiotic-treated (solution) cells to those treated via a surface flux of NO. Representative images of untreated *P. aeruginosa* and *E. coli* cells adhered to control xerogels are illustrated in Figure 3.2. *P. aeruginosa* cells are rod-shaped and exhibit regular dimensions (~ 1 x 3 μm) with an inflated appearance and smooth cell exterior. Also rod-shaped, *E. coli* are somewhat larger and more variable in length. On control surfaces, *P. aeruginosa* adhered in well organized patterns that maximized contact along the long axis of the cells while maintaining apparent structural integrity. By comparison, *E. coli* cells tended to maintain some physical separation (i.e., adhering individually or in small groups of 2 to 3 cells). While *P. aeruginosa* are motile via flagella, *E. coli* have a characteristic crown of fimbriae. Healthy cells of both species appeared intact with no visible pores, holes, grooves, or breakages in the cell envelope. To negate any possible effect derived from the presence of proline, *E. coli* and *P. aeruginosa* preadsorbed on control xerogels were incubated for 2 h with 2 and 4 mg mL^{-1} proline, respectively. Physically, the proline exposed cells were indistinguishable from untreated cells. Equivalent cell viability was verified by growing colonies on nutrient agar.

3.3.3 Morphologies of NO-treated P. aeruginosa and E. coli. Sub-bactericidal concentrations such as those used in this study have historically been applied to study antimicrobial effects as they provide 'snapshots' of the organism's morphology between healthy and dead states.[31,34,39] Figure 3.3 illustrates examples of *P. aeruginosa* and *E. coli* bacteria after exposure to NO. A representative collection of images was chosen to demonstrate the full spectrum of related morphologies resulting from NO treatment. Many of the effects of NO exposure (e.g., membrane degradation) were exhibited at multiple doses.

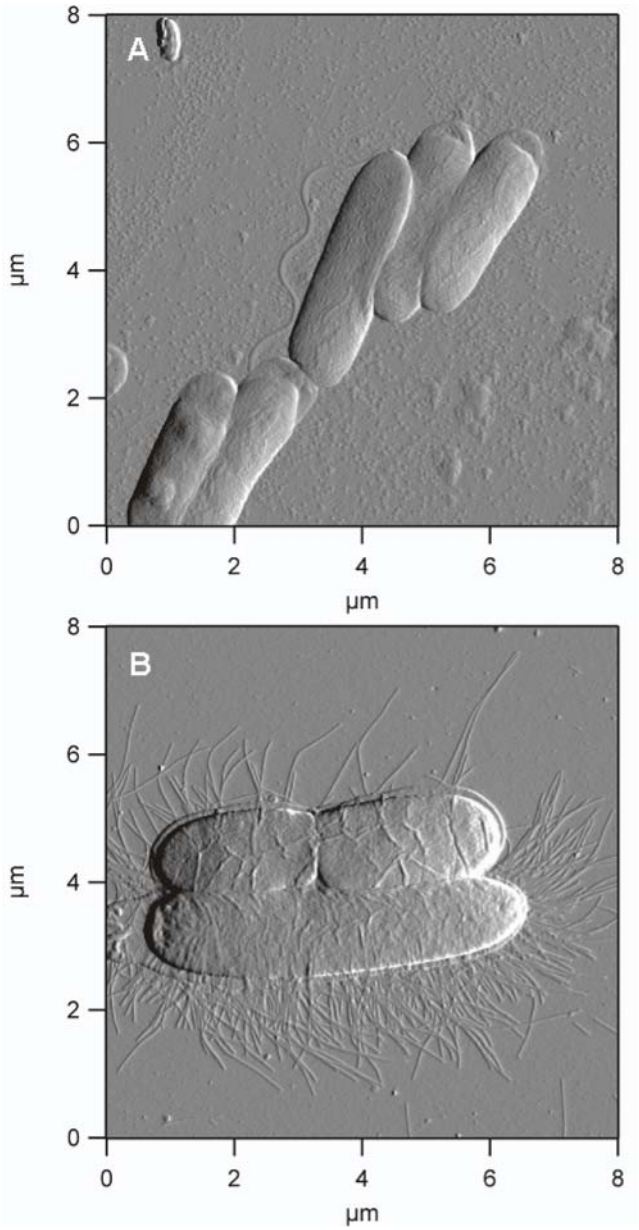

Figure 3.2 Deflection images depict the morphology of healthy (A) *P. aeruginosa*; and (B) *E. coli* bacteria.

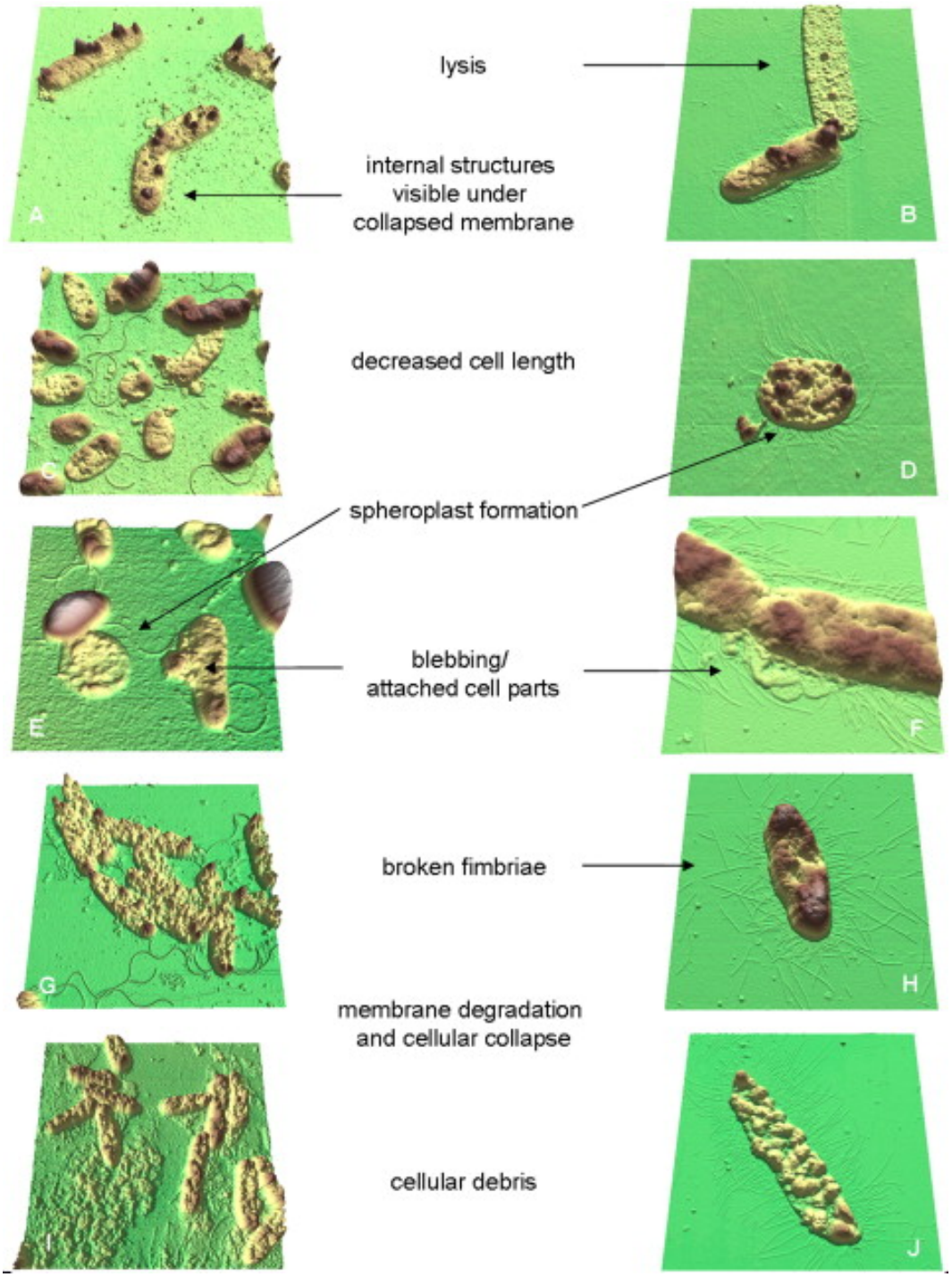

Figure 3.3 Three-dimensional reconstructions of height images illustrate *P. aeruginosa* and *E. coli* morphologies, shown in the left and right columns, respectively. Parts (A-E) depict cells treated by NO flux from 40% AHAP3/BTMOS xerogels for (A, C) 4 h; (B) 6 h; (D, E) 8 h. Parts (F-J) show examples of bacteria treated with sub-bactericidal concentrations of PROLI/NO for 2 h at (F-H) 1 mg mL^{-1}; (I) 4 mg mL^{-1}; and (J) 2 mg mL^{-1}.

A comprehensive list of the morphologies observed after treatment with NO is included in Table 3.2. Many bullets are identical or similar for each species indicating related mechanisms of action against both Gram-negative bacteria. Such features include mild to extensive membrane degradation, debris present on the surface in the vicinity of cells, blebbing or cellular parts abnormally attached to cells, cellular collapse, and lysis. Spheroplast formation and increasingly short cellular length were more infrequent morphologies common to both species, generally observed on xerogels after longer exposures to surfaces fluxes of NO (6 – 8 h, Fig. 3.3D-E). Neither species exhibited population arrangements on NO-releasing xerogels similar to those observed on controls. *P. aeruginosa* adhered in a disorganized array, while *E. coli* cells abandoned their active tendency to maintain spatial separation on a surface. Cells were occasionally observed to adhere across a previously adhered cell, despite a low overall surface coverage.

The collection of morphologies observed indicates cell envelope damage as a visible and significant contributing mechanism to the cytotoxic effect of NO against *P. aeruginosa* and *E. coli*. The morphologies observed in this AFM study closely resemble those reported by Li, et al.[34] who concluded that their antibacterial peptides disrupted, permeabilized, and eventually destroyed the stability of the outer and inner lipid membranes of *P. aeruginosa* and *E. coli*. The single morphology that points strictly to protein damage in this study, the broken fimbriae frequently observed for *E. coli*, also occurred at the cell membrane. Nitric oxide-mediated membrane damage has recently been reported by Hetrick, et al.[28] using confocal fluorescence microscopy. In that study, *P. aeruginosa* membranes became permeable to propidium iodide, a fluorescent dye that may only enter bacterial cells with

Table 3.2 Morphologies exhibited by Gram-negative bacteria after NO treatment

P. aeruginosa	***E. coli***
▪ Cellular debris • Most often concentrated on surface in vicinity of cell • Occasionally cell-associated ▪ Membrane degradation • Increased surface roughness • Layered appearance • Pores and crevices easily visualized ▪ Cell collapse • Lower height (< ~30 nm) • Flatter appearance • Some internal structures visible ▪ Cell lysis ▪ Decreased cell length ▪ Spheroplast formation ▪ Breakage ▪ Blebbing	▪ Cellular debris • Granule-like particles near cell • Occasionally cell-associated ▪ Membrane degradation • Large increases in surface roughness • Bumps and crevices in cell surface ▪ Cell collapse ▪ Cell lysis ▪ Decreased height and length ▪ Spheroplast formation ▪ Damage at apical ends and along sides of cell • Frequent collapse of apical ends • Collapse of specific regions of the cell ◦ Usually along edge of cell ◦ Occasionally in cell interior ▪ Broken fimbriae

compromised membranes, after exposure to NO-releasing silica nanoparticles (maximum NO flux ≈ 21,700 ppb mg^{-1}).

Both delivery routes used in this study released NO exterior to, but in the vicinity of, surface-adhered bacteria. As a broad-spectrum antibiotic, NO exerts both oxidative and nitrosative stress on biomolecules at cell surfaces. Physically, NO and O_2 are lipophilic and membrane permeable leading to the concentration and sequestering of these molecules and their reactive metabolites (e.g., N_2O_3) near lipid bilayers,[21] where membrane-bound and other local proteins become targets of nitrosative stress. The formation of peroxynitrite from the reaction of NO with intracellular O_2^- initiates the radical peroxidation of lipid membranes (oxidative stress), potentially the cause of the observed degradation of these structural components.

3.3.4 Analysis of membrane roughness after NO treatment. To further characterize the effect of NO on the Gram-negative cell, AFM images were obtained of the bacterial membrane. The cell membrane damage by NO was readily observed in representative three-dimensional reconstructions from height images after 2, 4, 6, and 8 h exposures to NO flux from xerogels (Fig. 3.4). The vertical scale is consistent across images (15 nm) to allow comparison between AFM images. Gram-negative cell envelopes are composed of an outer and inner lipid membrane, each about 10 nm thick, separated by a thin, cross-linked peptidoglycan layer. Holes in the outer lipid membrane began forming as early as 2 h (Fig. 3.4B) after exposure to NO surface fluxes. Over time, the degree of membrane degradation continued to increase, with large holes and crevices penetrating into the inner membrane (Fig 3.4C-E). In fact, at exposure times exceeding 4 h the roughness of the membrane exceeded the height scale. The image analysis software was then used to apply light/shadow at

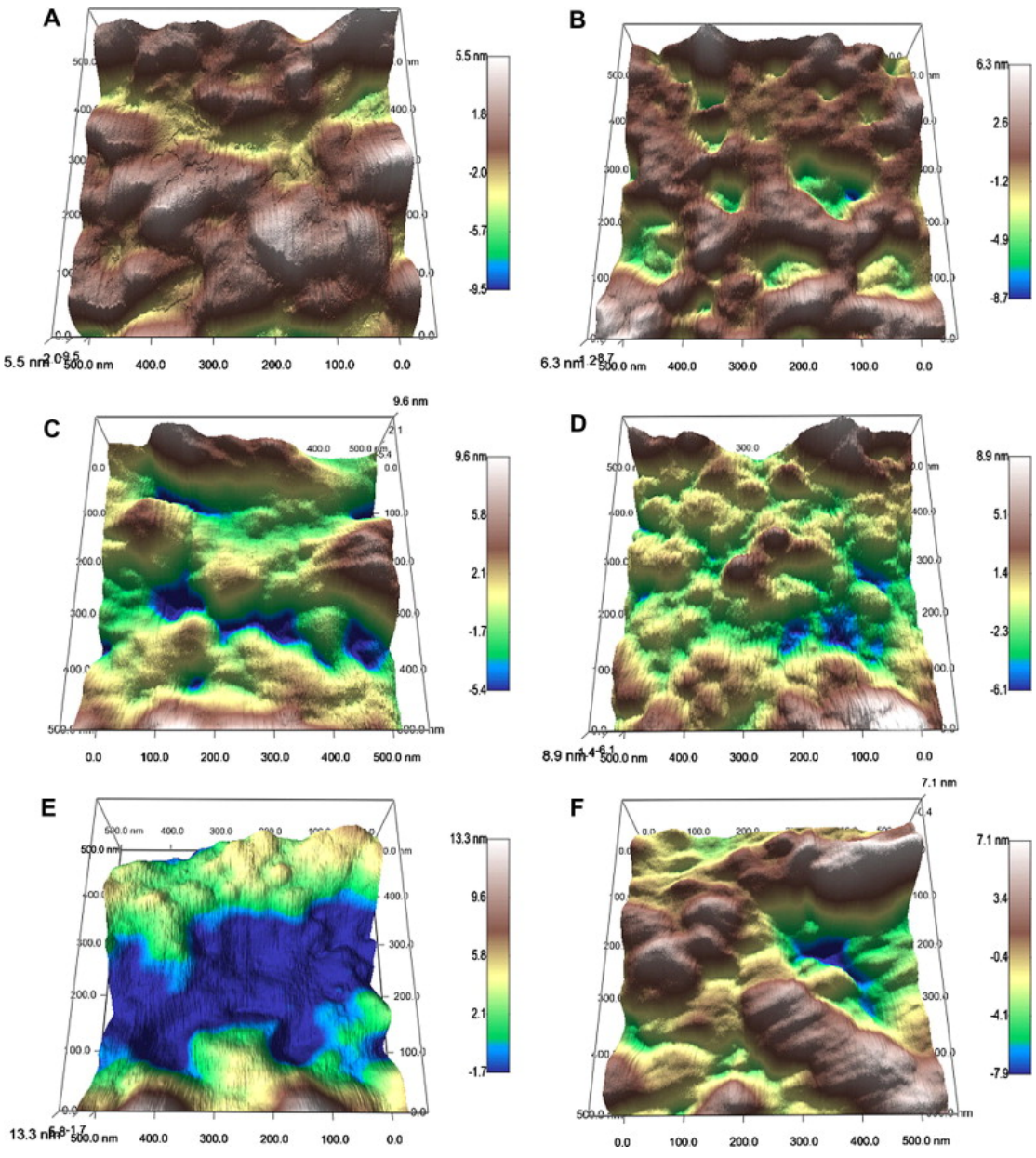

Figure 3.4 *P. aeruginosa* membranes on a control surface (A), and after exposure to NO surface flux for (B) 2 h, (C) 4 h, (D) 6 h, and (E) 8 h from a 40% AHAP3/BTMOS xerogel, and (F) after exposure to 0.07 μM NO in solution (bolus delivery).

identical angles and pitch to add a sense of depth. By comparison, Figure 3.4A depicts the membrane of a healthy *P. aeruginosa* cell adhered to a control xerogel for 24 h. Its morphological analysis confirms that changes in membrane roughness are a function of NO-exposure and not surface residence time.

The quantitative rms roughness of cell membranes as a function of bacteria species and NO exposure time/concentration is given in Table 3.3. As expected, longer exposure to a NO surface flux (40% AHAP3/BTMOS xerogels) correlates with rougher cell membranes ranging from ~1.6 nm for controls to nearly 4 and 12 nm after 8 h NO release for *P. aeruginosa* and *E. coli*, respectively. Similarly, membrane roughness was greater for *E. coli* for cells treated with greater concentrations of PROLI/NO (15.2 ± 4.6 and 28.9 ± 7.9 nm for 1 and 2 mg mL^{-1}, respectively) (Fig. 3.5). Of note, the measured roughness for *P. aeruginosa* was the same at both sub-bactericidal (MBC_{120} of PROLI/NO for *P. aeruginosa* is 8 mg mL^{-1}) concentrations of PROLI/NO (2 and 4 mg mL^{-1}), and approximately double that measured for the longest exposure to NO-releasing xerogels. If the deterioration of the lipid bilayer leads to increased surface roughness, this may be indirect evidence that protein and/or DNA damage contributes significantly to the cytotoxic effect of PROLI/NO against this species.

3.3.5 Comparison of morphologies resulting from NO and amoxicillin treatment. Amoxicillin, a β-lactam antibiotic, functions by inhibiting enzymes that cross-link chains in the peptidoglycan layer. Treatment of *E. coli* with a sub-bactericidal concentration of amoxicillin was therefore expected to generate morphologies typical of cell wall degradation. (*P. aeruginosa* was not treated with amoxicillin as it has demonstrated resistance to the effects of this β-lactam.) The most common morphologies observed by imaging amoxicillin-

Table 3.3 Root-mean-square (rms) roughness of cell membranes

species	material	exposure	average (nm)[a]
P. aeruginosa	xerogel	control	1.61 ± 0.27
		2 h	2.13 ± 0.09
		4 h	2.25 ± 0.30
		6 h	3.20 ± 0.31
		8 h	3.84 ± 0.76
	PROLI/NO	2 mg mL^{-1}	7.15 ± 1.52
		4 mg mL^{-1}	7.10 ± 0.86
	NO solution	0.07 μM	3.16 ± 0.61
E. coli	xerogel	control	1.55 ± 0.21
		2 h	2.66 ± 0.66
		4 h	3.24 ± 0.45
		6 h	4.33 ± 0.55
		8 h	11.7 ± 1.9
	PROLI/NO	1 mg mL^{-1}	15.2 ± 4.6
		2 mg mL^{-1}	28.9 ± 7.9

[a]Average rms roughness reported with standard deviation

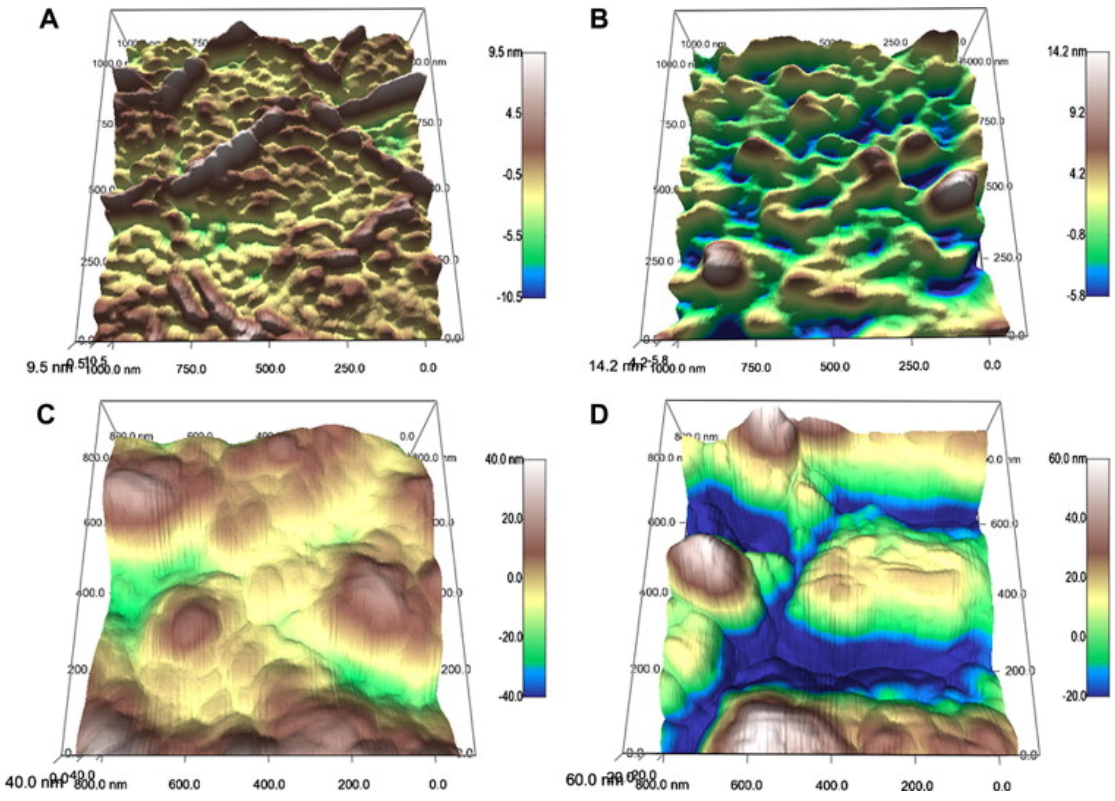

Figure 3.5 Three-dimensional reconstructions of *E. coli* membranes compare (A) untreated relative to (B) the degradation sustained after 6 h NO-release from a xerogel surface. Treatment with sub-bactericidal PROLI/NO concentrations of (C) 1 mg mL^{-1} and (D) 2 mg mL^{-1} show more extensive damage only 2 h after exposure. Note the difference in scale range.

treated *E. coli* were perforations in the cell surface (pore formation) and regions of collapsed cell wall, both concentrated (but not restricted to) the apical ends of the cells (Fig. 3.6C, D). These observations are in agreement with a study that used AFM to compare the morphological changes sustained by *E. coli* after treatment with amoxicillin and its parent molecule, the natural product penicillin.[37] Both *E. coli* (Fig. 3.6A) and *P. aeruginosa* (Fig. 3.6B) exhibited analogous morphologies to the amoxicillin-treated cells when treated with low levels of NO. In fact, these morphologies were only visualized on NO-releasing xerogels at 2 h time points, and thus at the lowest concentrations of NO treatment used in this study. At greater NO doses, these morphologies were obscured as the extent of membrane damage increased and the incidence of localized effects decreased. Interestingly, the morphologies observed for treatment of *E. coli* with penicillin, described by Yang, et al.[37] as randomly distributed grooves and holes, strongly resemble the morphological changes sustained by both *E. coli* and *P. aeruginosa* at greater NO doses. The similarity of morphologies observed after treatment with amoxicillin, which functions by a known mechanism of action, to those after exposure to NO offers additional support to the conclusion that exposure to NO results in the deterioration of the cell envelope of Gram-negative bacteria.

3.3.6 Comparison of NO delivery methods. Comparing NO-delivery methods proved less straightforward than varying exposure time or concentration for a single delivery method. Both the NO-release kinetics (slow versus fast) and manner of delivery (surface flux versus burst of NO release) differ for 40% AHAP3/BTMOS xerogels and PROLI/NO. While treatment with PROLI/NO resulted in rougher, more highly deteriorated cells than exposure to a sustained surface flux as visualized qualitatively (Fig. 3.3) and measured quantitatively

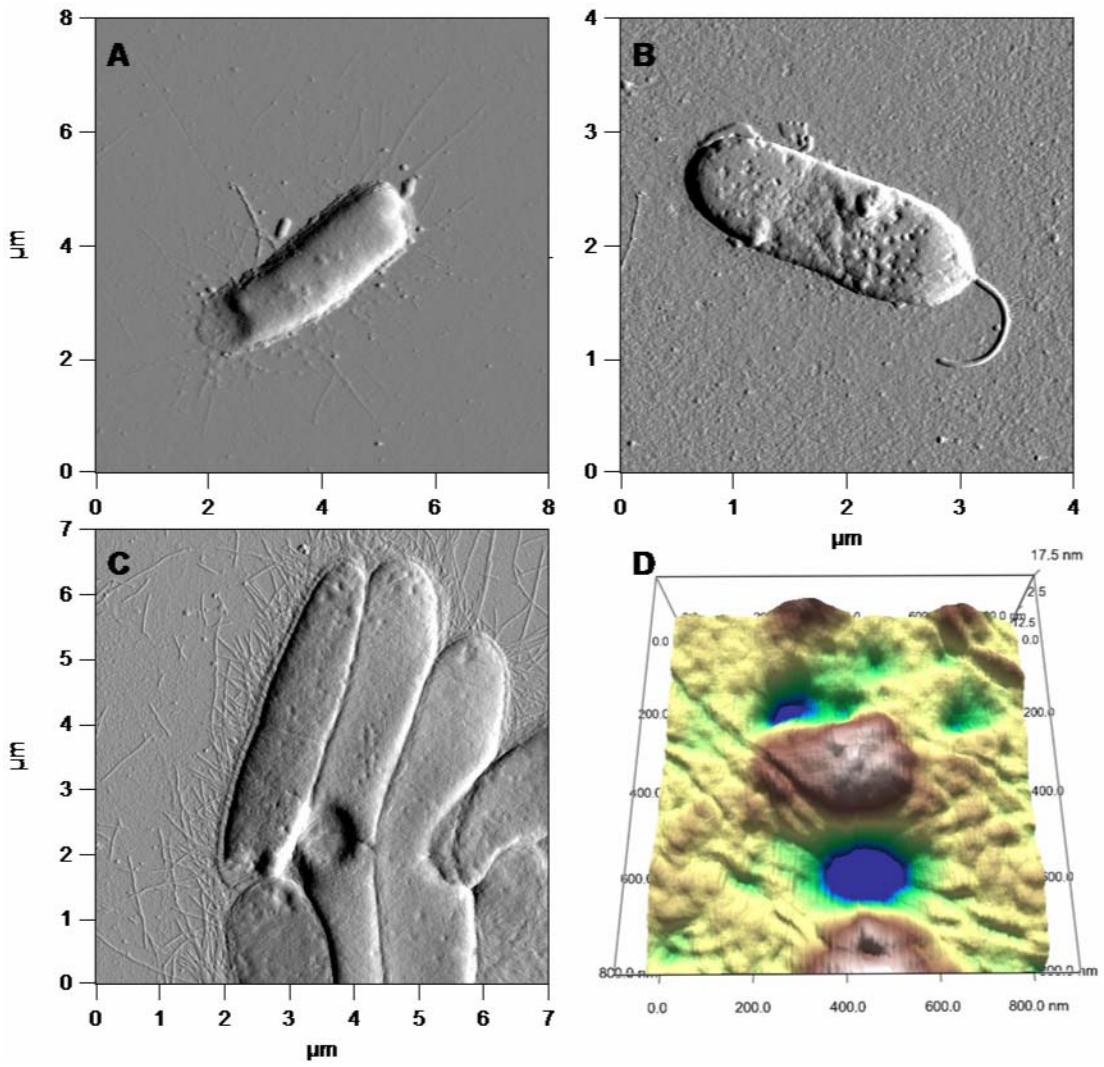

Figure 3.6 Comparison of the morphological effects caused by treatment with NO on (A) *E. coli* and (B) *P. aeruginosa* strongly resemble the morphologies demonstrated by *E. coli* after treatment with (C) amoxicillin, a β-lactam that inhibits cell wall synthesis. Furthermore, the three-dimensional rendering of (D) the compromised cell wall after treatment with amoxicillin resembles the holes and crevices exhibited by *P. aeruginosa* and *E. coli* after NO treatment, which is indicative of membrane damage.

(Table 3.3), the total amount of NO released as a bolus from sub-bactericidal concentrations of PROLI/NO exceeded that delivered by sub-bactericidal fluxes of NO from 40%AHAP3/BTMOS. As the molecules of NO released from PROLI/NO were dispersed throughout the solution rather than being concentrated at the location of bacterial adhesion (i.e., at the surface), this may explain the significantly greater quantities of NO necessary induce a bactericidal effect.

To deconvolute the efficacy of the delivery routes, *P. aeruginosa* cells were treated with a bolus of NO slightly less than that delivered by a 40% AHAP3/BTMOS xerogel over 2 h. Xerogel-adhered *P. aeruginosa* cells were immediately added to a 0.07 μM solution of NO in 5 mL of PBS (prepared from a saturated NO solution) and incubated for 2 h under conditions identical to the PROLI/NO experiments. The membrane roughness remained greater when cells were treated by a bolus compared to surface flux from an NO-releasing 40% AHAP3/BTMOS xerogel (3.2 ± 0.6 nm vs. 2.1 ± 0.1 nm, respectively) (Table 3.3), and a comparison of the *P. aeruginosa* membrane after treatment with an NO solution (Fig. 3.4F) to that after 2 h exposure to surface flux (Fig. 3.4B) clearly demonstrates larger pores and crevices in the former.

Bacterial species have evolved strategies to protect against the harmful effects of NO.[40] For example, specific transcription factors (e.g., SoxR, OxyR) identified in *E. coli* are capable of sensing NO released from macrophages and respond by up-regulating gene expression to combat toxic effects.[41,42] Once detected in vivo, these proteins convert NO to less toxic by-products such as nitrate.[43] Although the molecules of NO released from PROLI/NO are dispersed throughout the medium, the total concentrations of NO and RNS available to react with the adhered cells are greater during the initial period of incubation

when they are released via a bolus. Delivered in a highly concentrated burst, NO may devastate bacterial cells before they are capable of mounting a defense. As an extension of this hypothesis, future studies should investigate the behaviour of bacteria selected after exposure to increasing concentrations of NO in an attempt to foster tolerance and probe the upper limit of resistance to NO.

3.4 Conclusions

The morphologies of two Gram-negative species of bacteria were observed using AFM after treatment with the antimicrobial agent NO. Quantitative measurements of surface roughness and qualitative observation of increased surface debris and changes in cell shape (e.g., blebbing) and adhesion patterns indicate that membrane degradation is a significant contributing factor to NO's bacterial cytotoxicity. Comparison of morphological effects perpetrated via a single, known mechanism (i.e., inhibition of cell wall synthesis by amoxicillin) to those observed from treatment of NO aids in confirming the antimicrobial mechanism of the latter. By evaluating NO sources with different NO-release kinetics, we conclude that greater levels of NO released over short durations are more damaging to Gram-negative bacteria than sustained, lower-level surface fluxes. The double lipid bilayer of Gram-negative bateria typically acts as a permeability barrier to antibiotics that function within the cell. Ironically, it is this same structural characteristic that renders these cells particularly susceptible to NO-induced membrane damage. As degradation of the cell envelope leads to an increase in permeability, treatment with NO may elicit synergistic effects when used in concert with antibiotics.

3.5 References

(1) Lowenstein, C. J.; Dinerman, J. L.; Snyder, S. H. Nitric oxide: A physiologic messenger. *Ann. Intern. Med.* **1994**, *120*, 227-237.

(2) Bogdan, C. Nitric oxide and the immune response. *Nat. Immunol.* **2001**, *2*, 907-916.

(3) Bonavida, B.; Khineche, S.; Huerta-Yepez, S.; Garbán, H. Therapeutic potential of nitric oxide in cancer. *Drug Resistance Updates* **2006**, *9*, 157-173.

(4) Buga, G. M.; Ignarro, J. L. Nitric Oxide and Cancer. *Biology and Pathobiology*; Academic Press: San Diego, 2000; pp 895-920.

(5) Hetrick, E. M.; Prichard, H. L.; Klitzman, B.; Schoenfisch, M. H. Reduced foreign body response at nitric oxide-releasing subcutaneous implants. *Biomaterials* **2007**, *28*, 4571-4580.

(6) Keefer, L. K. Progress Toward Clinical Application of the Nitric Oxide-Releasing Diazeniumdiolates. *Annu. Rev. Pharmacol. Toxicol.* **2003**, *43*, 585-607.

(7) Napoli, C.; Ignarro, L. J. Nitric oxide-releasing drugs. *Annu. Rev. Pharmacol. Toxicol.* **2003**, *43*, 97-123.

(8) Smith, D. J.; Chakravarthy, D.; Pulfer, S.; Simmons, M. L.; Saavedra, J. E. et al. Nitric oxide-releasing polymers containing the [N(O)NO]- group. *J. Med. Chem.* **1996**, *39*, 1148-1156.

(9) Lyn, D.; Williams, H. The chemistry of *S*-nitrosothiols. *Acc. Chem. Res.* **1999**, *32*, 869-876.

(10) Butler, A. R.; Rhodes, P. Chemistry, analysis, and biological rolse of *S*-nitrosothiols. *Anal. Biochem.* **1997**, *249*, 1-9.

(11) Shin, J. H.; Metzger, S. K.; Schoenfisch, M. H. Synthesis of nitric oxide-releasing silica nanoparticles. *J. Am. Chem. Soc.* **2007**, *129*, 4612-4619.

(12) Shin, J. H.; Schoenfisch, M. H. Inorganic/organic hybrid silica nanoparticles as a nitric oxide delivery scaffold. *Chem. Mater.* **2008**, *20*, 239-249.

(13) Marxer, S. M.; Rothrock, A. R.; Nablo, B. J.; Robbins, M. E.; Schoenfisch, M. H. Preparation of nitric oxide (NO)-releasing sol-gels for biomaterial applications. *Chem. Mater.* **2003**, *15*, 4193-4199.

(14) Robbins, M. E.; Hopper, E. D.; Schoenfisch, M. H. Synthesis and characterization of nitric oxide-releasing sol-gel microarrays. *Langmuir* **2004**, *20*, 10296-10302.

(15) Hrabie, J. A.; Klose, J. R.; Wink, D. A.; Keefer, L. K. New nitric oxide-releasing zwitterions derived from polyamines. *J. Org. Chem.* **1993**, *58*, 1472-1476.

(16) Saavedra, J. E.; Southan, G. J.; Davies, K. M.; Lundell, A.; Markou, C. et al. Localizing antithrombotic and vasodilatory activity with a novel, ultrafast nitric oxide donor. *J. Med. Chem.* **1996**, *39*, 4361-4365.

(17) Foley, E.; O'Farrell, P. H. Nitric oxide contributes to induction of innate immune responses to Gram-negative bacteria in Drosophila. *Genes Dev.* **2003**, *17*, 115-125.

(18) MacMicking, J.; Xie, Q. W.; Nathan, C. Nitric oxide and macrophage function. *Annu. Rev. Immunol.* **1997**, *15*, 323-350.

(19) Wink, D. A.; Mitchell, J. B. Chemical biology of nitric oxide: Insights into regulatory, cytotoxic, and cytoprotective mechanisms of nitric oxide. *Free Radic. Biol. Med.* **1998**, *25*, 434-456.

(20) Fang, F. C. Mechanisms of nitric oxide-related antimicrobial activity. *J. Clin. Invest.* **1997**, *99*, 2818-2825.

(21) Moller, M. N.; Li, Q.; Lancaster, J. R. J.; Denicola, A. Acceleration of nitric oxide autooxidation and nitrosation by membranes. *Life* **2007**, *59*, 243-248.

(22) Zaki, M. H.; Akuta, T.; Akaike, T. Nitric oxide-induced nitrative stress involved in microbial pathogenesis. *J. Pharmacol. Sci.* **2005**, *98*, 117-129.

(23) Ghaffari, A.; Miller, C. C.; McMullin, B.; Ghahary, A. Potential application of gaseous nitric oxide as a topical antimicrobial agent. *Nitric Oxide* **2006**, *14*, 21-29.

(24) Nablo, B. J.; Chen, T.-Y.; Schoenfisch, M. H. Sol-gel derived nitric-oxide releasing materials that reduce bacterial adhesion. *J. Am. Chem. Soc.* **2001**, *123*, 9712-9713.

(25) Nablo, B. J.; Rothrock, A. R.; Schoenfisch, M. H. Nitric oxide-releasing sol-gels as antibacterial coatings for orthopedic implants. *Biomaterials* **2005**, *26*, 917-924.

(26) Nablo, B. J.; Schoenfisch, M. H. Antibacterial properties of nitric oxide-releasing sol-gels. *J. Biomed. Mater. Res.* **2003**, *67A*, 1276-1283.

(27) Hetrick, E. M.; Schoenfisch, M. H. Antibacterial nitric oxide-releasing xerogels: Cell viability and parallel plate flow cell adhesion studies. *Biomaterials* **2007**, *28*, 1948-1956.

(28) Hetrick, E. M.; Shin, J. H.; Stasko, N. A.; Johnson, B. A.; Wespe, D. A. et al. Bactericidal efficacy of nitric oxide-releasing silica nanoparticles. *ACS Nano* **2007**, *2*.

(29) Waisbren, S. J.; Hurley, D. J.; Waisbren, B. A. Morphological expression of antibiotic synergism against *Pseudomonas aeruginosa* as observed by scanning electron microscopy. *Antimicrob. Agents Chemother.* **1980**, *18*, 969-975.

(30) Klainer, A. S.; Russell, R. R. B. Effect of the inhibition of protein synthesis on the *Escherichia coli* cell envelope. *Antimicrob. Agents Chemother.* **1974**, *6*, 216-224.

(31) Iida, K.; Koike, M. Cell wall alterations of Gram-negative bacteria by aminoglycoside antibiotics. *Antimicrob. Agents Chemother.* **1974**, *5*, 95-97.

(32) Da Silva, A.; Teschke, O. Effects of the antimicrobial peptide PGLa on live *Escherichia coli*. *Biochim. Biophys. Acta* **2003**, *1643*, 95-103.

(33) Eaton, P.; Fernandes, J. C.; Pereira, E.; Pintado, M. E.; Malcata, F. X. Atomic force microscopy study of the antibacterial effects of chitosans on *Escherichia coli* and *Staphylococcus aureus*. *Ultramicroscopy* **2008**, *108*, 1128-1134.

(34) Li, A.; Lee, P. Y.; Ho, B.; Ding, J. L.; Lim, C. T. Atomic force microscopy study of the antimicrobial action of Sushi peptides on Gram-negative bacteria. *Biochim. Biophys. Acta* **2007**, *1768*, 411-418.

(35) Lu, Z.; Li, C. M.; Bao, H.; Qiao, Y.; Toh, Y. et al. Mechanism of antimicrobial activity of CdTe quantum dots. *Langmuir* **2008**, *24*, 5445-5452.

(36) Meincken, M.; Holroyd, D. L.; Rautenbach, M. Atomic force microscopy study of the effect of antimicrobial peptides on the cell envelope of *Escherichia coli*. *Antimicrob. Agents Chemother.* **2005**, *49*, 4085-4092.

(37) Yang, L.; Wang, K.; Tan, W.; He, X.; Jin, R. et al. Atomic force microscopy study of different effects of natural and semisynthetic β-lactam on the cell envelope of *Escherichia coli*. *Anal. Chem.* **2006**, *78*, 7341-7345.

(38) Deupree, S. M.; Schoenfisch, M. H. Quantitative method for determining the lateral strength of bacterial adhesion and application for characterizing adhesion kinetics. *Langmuir* **2008**, *24*, 4700-4707.

(39) Hayami, H.; Goto, T.; Kawahara, M.; Ohi, Y. Activities of β-lactams, fluoroquinolones, amikacin, and fosfomycin alone and in combination against *Pseudomonas aeruginosa* isolated from complicated urinary tract infections. *J. Infect. Chemother.* **1999**, *5*, 130-138.

(40) Crawford, M. J.; Goldberg, D. E. Role for the *Salmonella* flavohemoglobin in protection from nitric oxide. *J. Biol. Chem.* **1998**, *273*, 12543-12547.

(41) Nunoshiba, T.; de Rojas-Walker, T.; Wishnok, J. S.; Tannenbaum, S. R.; Demple, B. Activation by nitric oxide of an oxidative-stress response that defends *Escherichia coli* against activated macrophages. *Proc. Natl. Acad. Sci. USA* **1993**, *90*, 9993-9997.

(42) Hausladen, A.; Privalle, C. T.; Keng, T.; DeAngelo, J.; Stamler, J. S. Nitrosative stress: Activation of the transcription factor OxyR. *Cell* **1996**, *86*, 719-729.

(43) Hausladen, A.; Gow, A. J.; Stamler, J. S. Nitrosative stress: Metabolic pathway involving the flavohemoglobin. *Proc. Natl. Acad. Sci. USA* **1998**, *95*, 14100-14105.

Chapter 4:

Synergy of nitric oxide and silver sulfadiazine against Gram-negative, -positive, and antibiotic-resistant bacteria

4.1 Introduction

The antimicrobial properties of silver or more specifically ionic silver (Ag^+) have been recognized and utilized for millennia. Nano- to micromolar concentrations of Ag^+ exhibit broad-spectrum bactericidal (including Gram-negative and Gram-positive species), fungicidal, viricidal, and protozoicidal activity,[1] bonding covalently to electron-donating groups (e.g., the sulfhydryl of cysteine) or electrostatically to negatively charged molecules (e.g., DNA). Most bacterial sites targeted by Ag^+ are proteinaceous, where alterations in amino acid residues lead to structural damage and disruption of replicative and metabolic processes resulting in cell death.[1-6] Evidence suggests that interactions with DNA also play an important role in the antimicrobial efficacy of Ag^+.[4,5] In wound treatment, Ag^+ is generally delivered via silver compounds such as silver (I) sulfadiazine (AgSD).[7] Most causative pathogens related to burns and chronic wound infections are susceptible to the levels of AgSD attainable topically.[8,9] Fortunately, exposure to clinical levels of Ag^+ generally does not pose a threat to human health, despite the broad range of reactivity.[1,7]

The endogenous expression of nitric oxide (NO) has been conserved throughout higher organisms as the immune system's first-line defense against infection.[10-13] Like Ag^+, NO is a broad-spectrum antimicrobial agent that targets a number of reactive sites. Although NO can

modify proteins and other biological macromolecules directly,[14] it is a highly reactive radical and frequently combines with locally abundant small molecules such as oxygen (O_2) and superoxide (O_2^-) creating an arsenal of reactive byproducts that include dinitrogen trioxide (N_2O_3) and peroxynitrite ($ONOO^-$).[11,15] Collectively these reactive species evoke potent antibacterial effects by rendering nitrosative and oxidative stresses to bacteria.[11,15-19] In vitro, NO administered from both a gas cylinder and via soluble, small-molecule diazeniumdiolate NO donors has been shown to kill a range of pathogens.[20-22] Furthermore, our group has demonstrated the bactericidal activity of NO-releasing xerogel coatings that simultaneously reduce the incidence of bacterial adhesion.[23-25] These studies suggest that site-directed NO delivery is a promising strategy for treatment of infection.

Although the appropriate use of antimicrobials to treat infection is a beneficial practice, artificial pressures resulting from over use, patient non-compliance, and widespread application have promoted the unnatural selection of inherently resistant microbes.[26] Even resistance to broad-spectrum agents has been observed.[7,27] To complicate matters, methods of gene sharing employed by bacteria promote the localized collection of resistance determinants, often on transferable plasmids, leading to the emergence of multi-drug resistant (MDR) and extensively drug resistant (XDR) species.[28,29] In recent years, a dramatic rise in the incidence of 'super bugs,' or bacteria that are resistant to those antibiotics generally reserved as a last resort treatment option, has become prevalent.[30,31] Unfortunately, the discovery of new antimicrobials progresses slowly while resistance to all clinically employed antimicrobial agents rapidly continues to emerge,[26] highlighting the critical need for alternative approaches to treating infection.

Combination therapy is one strategy for stemming the emergence of resistant species.[32-34] The concerted use of two or more biocides with different mechanisms of action decreases the likelihood that an organism will possess all the traits necessary to ensure its selection and survival. Agents possessing a broad spectrum of antimicrobial action may both lower the probability of developing resistance and manage the polymicrobial burden typically found in topical infections.[33,34] As smaller quantities of each drug are generally required in the application of combination therapy, dose-related toxicity experienced to a particular biocide may also be reduced.[33,34] Finally, the combination of certain antimicrobials may result in synergistic effects.[33,34] Synergistic combinations are more potent than equivalent doses administered individually, further reducing potential toxicity to the patient and cost of treatment. Herein, NO generated from diazeniumdiolate-modified proline (PROLI/NO) and AgSD were evaluated alone and in combination using acute (2 h) viability assays to determine in vitro efficacy against two Gram-negative and four Gram-positive pathogenic strains of bacteria, including two antibiotic-resistant 'super bugs'.

4.2 Experimental

4.2.1 Materials. L-proline, sulfadiazine (SD), and AgSD were obtained from Sigma-Aldrich (St. Louis, MO). Tryptic soy broth (TSB) and tryptic soy agar (TSA) were manufactured by BD (Franklin Lakes, NJ) and purchased from Fisher Scientific (Pittsburgh, PA). Sodium chloride, potassium chloride, and sodium phosphate monobasic obtained from Fisher and sodium phosphate dibasic obtained from Sigma-Aldrich were used to prepare phosphate buffered saline (PBS, I_c = 0.16 M, pH = 7.4). Distilled water was purified using the Millipore Milli-Q UV Gradient A-10 system (Bedford, MA) to a resistivity of 18.2 MΩ

cm and used to prepare the reagents for bactericidal assays. Materials used for growing bacteria and/or evaluating bactericidal activity were exposed to UV radiation or sanitized in an autoclave prior to use, unless purchased sterile. Argon, NO, nitrogen (N_2), and a NO standard (25.7 ppm in N_2) were purchased from National Welders (Raleigh, NC).

4.2.2 Cell culture. The strains of bacteria used in this study were obtained from American Type Culture Collection (ATCC, Manassas, VA). The ATCC identification number for each strain was as follows: *E. coli* (53323), vancomycin-susceptible *E. faecalis* (VSEF) (29212), vancomycin-resistant *E. faecalis* (VREF) (51299), *P. aeruginosa* (19143), methacillin-susceptible *S. aureus* (MSSA) (29213), methacillin-resistant *S. aureus* (MRSA) (33591). Experiments requiring transfer of biohazardous materials were conducted in a dedicated laminar flow hood equipped with UV lamp. Lyophilized bacteria were reconstituted in TSB and cultured overnight at 37 °C. A 1-mL aliquot of culture was grown in 100 mL of TSB for 2-4 h until reaching an optical density at 600 nm (OD_{600}) ~ 0.15-0.3. The resulting culture was stored at -80 °C in 1-mL aliquots. For daily experiments, 1 mL of bacteria culture was grown in 100 mL of TSB overnight at 37 °C. Re-cultured in fresh TSB the next day, the bacteria were then grown to mid-exponential phase, as determined by OD_{600} measurements. The relationship between the OD_{600} and the concentration of bacteria in the culture suspension was calibrated for each strain using a Spectronic 301 spectrophotometer (Milton Roy, Ivyland, PA) and enumeration of cfu from culture dilutions grown on TSA plates.

4.2.3 Synthesis and characterization of PROLI/NO. The synthesis protocol reported by Saavedra, et al. was used in the preparation of PROLI/NO.[35] Briefly, 10 g of L-proline was dissolved in 39 mL of 25% sodium methoxide in methanol. An additional 20 mL of

methanol was added, and the solution was placed into a custom NO reaction bomb, which was then purged with Ar. The proline solution was then exposed to 5 atm of NO for 3 d to form PROLI/NO as a white precipitate in the methanol. After purging the bomb with Ar, the precipitate was isolated by vacuum filtration, washed with ether, and dried under vacuum. The white solid (PROLI/NO) was divided into small aliquots (< 1 g) and stored over dessicant at -20 °C.

Nitric oxide release from PROLI/NO was characterized using a chemiluminescent NO analyzer (Sievers Model 280, Boulder, CO). Briefly, a known quantity of PROLI/NO was inserted into a glass flask containing PBS at 37 °C. Nitric oxide generated into solution via diazeniumdiolate NO donor decomposition was carried to the analyzer by N_2 bubbling through the solution at a flow rate of 80 mL min^{-1}. The NO analyzer was calibrated using an atmospheric sample passed through an NO zero filter and a 25.7 ppm NO standard. The NO release from PROLI/NO was measured periodically to ensure no significant decomposition of the NO donor over the duration of the study.

4.2.4 Single-agent bactericidal assays. The bactericidal efficacy of single agents (e.g., AgSD, PROLI/NO) was evaluated against each pathogenic strain of bacteria using a technique adapted from the standard microdilution broth procedure as described below.[36] The minimum bactericidal concentration at 120 min (MBC_{120}) was defined as the concentration of AgSD or PROLI/NO that resulted in a 3-log reduction in viability for a particular bacteria species over 120 min. Each strain of bacteria was tested against 5 concentrations each of AgSD and PROLI/NO. The antimicrobial concentrations tested were adjusted such that at least one concentration bracketed the MBC_{120} at low and high levels, and the results were verified in independent replicates (n = 3). To prevent thermal

decomposition of the NO donor moiety, PROLI/NO was pre-weighed into chilled vials, and the appropriate volume of cell suspensions was added to obtain the target PROLI/NO concentration. The bactericidal assays were conducted at 37 °C with shaking, and cell viability was assessed at 0, 60, and 120 min by plating aliquots of the treated bacteria diluted in PBS on TSA plates. The toxicity of SD and proline were evaluated at the concentrations equivalent to and via the protocols used for determining the MBC_{120} of AgSD and PROLI/NO, respectively.

4.2.5 AFM imaging. Atomic force microscopy was employed to visualize the membrane degradation rendered to *E. coli* by treatment with sub-bactericidal concentrations of PROLI/NO. Bacteria were adhered to a non-toxic substrate as described previously[37] and treated with sub-bactericidal concentrations of PROLI/NO (1 and 2 mg mL^{-1}) for 2 h. Control (untreated) and NO-treated cells were imaged in air using AC mode with Olympus AC240TS silicon beam cantilevers (Center Valley, PA) possessing a spring constant of 2 N m^{-1} and resonant frequency of 70 kHz. Simultaneous height, amplitude, and phase images were acquired at a resolution of 512 x 512 pixels and a scan speed of 1 Hz.

4.2.6 Checkerboard assay. The checkerboard method[33] was employed to determine the efficacy of AgSD and PROLI/NO in combination. Modifications analogous to those used in the single-agent bactericidal assays were adopted as described below. Briefly, bacteria were incubated with an array of antimicrobial combinations of AgSD and PROLI/NO for 2 h at 37 °C. The highest concentration for each antimicrobial (arbitrarily termed agent A and B) initially tested was chosen at half its MBC_{120}, as determined in the single-agent assay. Three additional dosages at stepwise, two-fold reductions in concentration were evaluated, resulting in 16 total combinations of AgSD and PROLI/NO tested against each strain of bacteria. For

strains that were particularly susceptible to the combination (i.e., MSSA, VSEF, VREF), lower concentrations of each agent were selected to probe the synergistic limit. Again, viable cells were enumerated at 0, 60, and 120 min. The fractional bactericidal concentration index at 120 min (FBC_{120}) was calculated using Equation 4.1:

$$FBC_{120} = \frac{MBC_{120AB}}{MBC_{120A}} + \frac{MBC_{120BA}}{MBC_{120B}} \qquad \text{Eq. (4.1)}$$

adapted from the fractional inhibitory concentration index (FIC) reported by Elion et al.,[38] where MBC_{120A} and MBC_{120B} are the values determined for agent A and B, respectively, in the single-agent assay; and, MBC_{120AB} and MBC_{120BA} are the concentrations of agent A and B that constituted the most effective bactericidal combination as determined by a 3-log reduction of viability. Synergy assays were conducted in three independent experiments for each strain of bacteria. A $FBC_{120} < 0.5$ was defined as synergistic, while a $FBC_{120} < 0.25$ was considered highly synergistic.

4.3 Results

4.3.1 Bactericidal activity of AgSD and PROLI/NO independently. The MBC_{120} values for AgSD and PROLI/NO were evaluated against two Gram-negative (*P. aeruginosa* and *E. coli*) and four Gram-positive (VSEF, VREF, MSSA, and MRSA) pathogenic species of bacteria, including two antibiotic-resistant 'super bugs'. The MBC_{120} was assigned as the integer concentration that was repeatedly identified as producing a 3-log reduction in viability. Broth microdilution experiments indicated an extensive bactericidal range for AgSD spanning 3 orders of magnitude (Table 4.1). *P. aeruginosa* exhibited levels of

Table 4.1 Bactericidal activity of AgSD and PROLI/NO independently and in combination.

Species	Gram class	MBC_{120} AgSD (mg L^{-1})	MBC_{120} AgSD (mmol L^{-1})	MBC_{120} PROLI/NO (g L^{-1})	MBC_{120} total NO (mmol L^{-1})	FBC_{120}
P. aeruginosa	-	5	0.014	8	83	0.58 ± 0.04
E. coli	-	50	0.14	4	42	0.34 ± 0.04
S. aureus	+	50	0.14	12	130	0.23 ± 0.07
E. faecalis	+	2000	5.60	18	190	0.07 ± 0.01
MRSA	+	200	0.56	18	190	0.52 ± 0.08
VREF	+	2000	5.60	30	310	0.15 ± 0.03

susceptibility in the low micromolar range (14 μM, 5 mg L^{-1}) comparable to previous reports.[4,39] The bactericidal concentrations for *E. coli* and MSSA were a full order of magnitude greater (140 μM, 50 mg L^{-1}) than *P. aeruginosa*, while MRSA required a four-fold greater dose (560 μM , 200 mg L^{-1}) than the MSSA strain. Both *Enterococcus* strains required a ten-fold greater dose to achieve a 3-log reduction in viability (5600 μM, 2000 mg L^{-1}) compared to MRSA.

Bactericidal concentrations of PROLI/NO also varied significantly between pathogens. The Gram-negative species *E. coli* and *P. aeruginosa* required the lowest PROLI/NO doses at 4 g L^{-1} (42 mmol L^{-1} NO) and 8 g L^{-1} (83 mmol L^{-1} NO), respectively. The most susceptible Gram-positive strain was MSSA, with an MBC_{120} of 12 g L^{-1} (130 mmol L^{-1} NO), followed by VSEF and MRSA, both requiring 18 g L^{-1} (190 mmol L^{-1} NO). VREF exhibited the greatest resistance to NO, tolerating concentrations of PROLI/NO up to 30 g L^{-1} (310 mmol L^{-1} NO).

To verify that dissociated SD or regenerated proline did not contribute to observed cytotoxicity, we examined the bactericidal activity of these compounds with similar testing protocols. Molar concentrations of SD equaling the MBC_{120} for AgSD against each of the 6 pathogens studied proved overwhelmingly non-toxic to the bacteria, having neither a bacteriostatic nor bactericidal effect. In all cases the bacteria continued to multiply during treatment, such that populations increased between 2- to 10-fold over 2 h. Proline exhibited a similar non-toxic effect at concentrations equaling the MBC_{120} of PROLI/NO for each species. Thus, the bactericidal activity of AgSD and PROLI/NO as single agents can be ascribed to Ag^{+} and NO, respectively, under the experimental protocol adopted against these pathogens in this study.

The Gram-positive species studied generally exhibited superior tolerance to the single agents, Ag^+ and NO, than the Gram-negative species. Indeed, the two strains of *E. faecalis* indicated the greatest tolerance to both PROLI/NO and AgSD. The resilience of these strains mirrors a report on the efficacy of dilute honey, another broad-spectrum antimicrobial, against a variety of bacterial species, where *E. faecalis* again displayed exceptional fortitude.[40] Among the Gram-positive species examined in our study, the antibiotic-resistant strains tended to demonstrate greater tolerance to each biocide than their antibiotic-susceptible congeners. We observed that MRSA exhibited significantly greater tolerance to both Ag^+ and NO than its methicillin-susceptible counterpart. Similarly, VREF required nearly twice the dose of PROLI/NO than the vancomycin-susceptible strain. The phenomenon that resistant bacteria selected by exposure to one antimicrobial frequently demonstrate resistance to other agents has been documented repeatedly.[41-43]

By determining cell viability at one or more intermediate time points, the dose-response of bacteria to a drug may be monitored over time, circumventing the all-or-none result typically obtained from inhibition or endpoint-only bactericidal assays. Figure 4.1 depicts cell viability for each species treated with MBC_{120} concentrations of AgSD and PROLI/NO at 0, 1, and 2 h. Most bacteria have already undergone a full log reduction in viability by the first 60 min, indicating swift bactericidal action. The Gram negative strains suffered a less drastic decrease in viability in the first hour after treatment with AgSD than Gram-positive bacteria.

4.3.2 Synergistic activity of AgSD and PROLI/NO in combination. Using the checkerboard technique and Eq. 4.1, FBC_{120} values were determined to evaluate the combined efficacy of AgSD and PROLI/NO against *P. aeruginosa*, *E. coli*, VSEF, VREF,

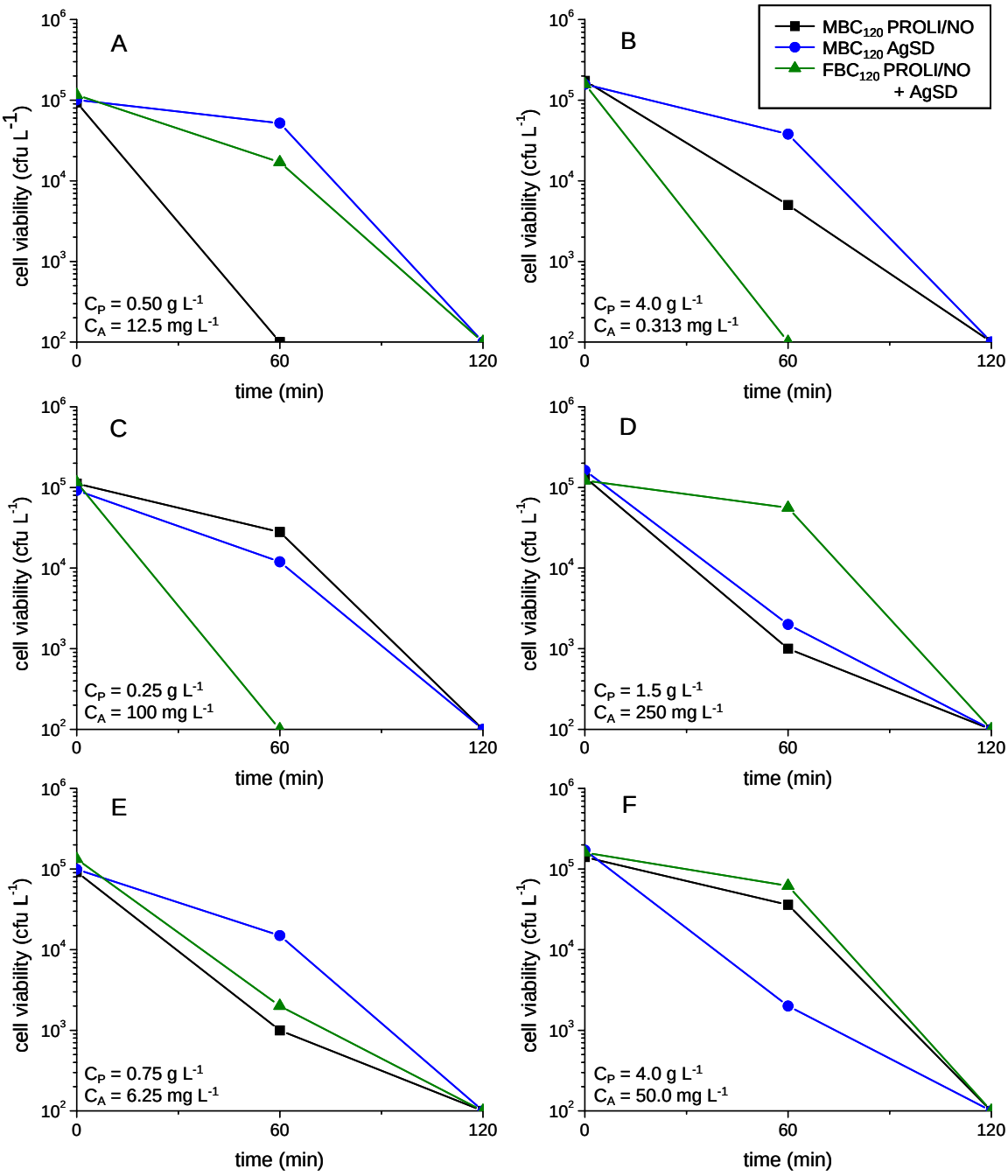

Figure 4.1 Bacteria viability over 120 min obtained using assays to evaluate the efficacy of PROLI/NO and AgSD independently and in combination. Curves indicate representative data obtained at MBC_{120} and FBC_{120} levels for (A) *E. coli*, (B) *P. aeruginosa*, (C) VSEF, (D) VREF, (E) MSSA, and (F) MRSA. Each inset lists the concentration of PROLI/NO (C_P) and the concentration of AgSD (C_A) used to obtain the FBC_{120} curve.

MSSA, and MRSA. The FBC_{120} values provided in Table 4.1 were averaged from 3 independent checkerboard arrays. Bactericidal synergism ($FBC_{120} < 0.5$) was evident for 4 out of 6 species tested, including VREF. Two species (*P. aeruginosa* and MRSA) exhibited FBC_{120} values near 0.5 and, under the acute treatment duration, may have experienced a borderline synergistic effect. Two species (*P. aeruginosa* and MRSA) exhibited FBC_{120} values near 0.5 and, considering the acute treatment duration, may have experienced a borderline synergistic effect. While Gram-positive bacteria were least susceptible to both AgSD and PROLI/NO as individual antimicrobial agents, the combination of AgSD and PROLI/NO was most synergistic against these same species. A highly synergistic effect ($FBC_{120} < 0.25$) was observed for half of the strains tested, all of which were Gram-positive species. Both *E. faecalis* strains demonstrated the greatest tolerance to each agent individually, but suffered the highest degree of susceptibility to the combination of AgSD and PROLI/NO, with FBC_{120} values of 0.15 and 0.07, respectively. The MSSA strain also exhibited a high degree of susceptibility to this combination ($FBC_{120} = 0.23$), although MRSA was affected to a lesser degree ($FBC_{120} = 0.52$). The lowest degree of cooperativity was observed for *P. aeruginosa* ($FBC_{120} = 0.58$). Notably, this species was the most susceptible, by an order of magnitude, to AgSD alone. *E. coli*, the other Gram-negative species studied, exhibited an FBC_{120} of 0.34. Representative cell viability data for all species at synergistic levels of AgSD and PROLI/NO are shown in Figure 4.1. The synergistic combinations, like the bactericidal concentrations for single agents, also show a high efficacy in the first hour, as cell viability was again reduced by a full log in all cases except the antibiotic resistant strains.

4.4 Discussion

4.4.1 Bactericidal efficacy of PROLI/NO and AgSD. To understand the synergism observed in this study, it is first necessary to parse out the mechanisms of AgSD and PROLI/NO action. The various roles of NO in killing bacteria have been reviewed previously.[11,14,17,44] As an indiscriminate and short-lived reactant, the target sites available in the immediate vicinity of NO play a key role in determining the type of antimicrobial action rendered. Nitric oxide may react directly with the thiols, amines, and transition-metal centers of proteins. It may also react with local small molecules, forming reactive intermediates that elicit effects through nitrosative and oxidative interactions with biological molecules. The NO donor used in our study (PROLI/NO) releases NO rapidly upon exposure to aqueous solution ($t_{1/2}$ = 100 s),[35,37] where NO and its reactive intermediates likely modify biomolecules on the exterior of bacteria, such as membrane-bound proteins and lipids. Reaction with O_2^- forms $ONOO^-$, a strong oxidant that can degrade membranes through lipid peroxidation and oxidize nearby proteins, compromising cellular integrity. Additionally, NO is a lipophilic, uncharged, diatomic molecule that readily diffuses across lipid membranes. Upon gaining access to the cytoplasm, NO and its congeners may react with numerous intracellular proteins and DNA, disrupting crucial cellular processes. Thus, NO is both an extra- and intra-cellular threat to bacteria. Although the bactericidal effects have been demonstrated frequently, little progress has been achieved in identifying specific critical targets of NO and its by-products,[19,45] likely due to these multi-faceted mechanisms.

Despite its long-term application for treating chronic and burn wounds topically, AgSD's mechanism(s) of action also remains uncertain. In aqueous media, AgSD gradually dissociates into Ag^+ and SD. Ionic silver reacts directly with thiol-containing amino acids.[46]

Mechanistic studies have shown that treatment with Ag^+ affects DNA replication and cellular respiration, among other functions.[1-6] A member of the sulfonamide family of semisynthetic antibacterial agents, SD is a biocide in its own right. Sulfonamides are structural analogues of *p*-aminobenzoate characterized by their ability to interfere with folate synthesis by competitively binding the enzyme dihydropteroate synthase within the cytoplasm of bacteria. This process is specifically detrimental to bacteria, as higher organisms obtain this metabolite through dietary ingestion. At physiological pH ~ 7 SD is negatively charged ($pK_a = 6.48$)[47] and less likely to diffuse across biological membranes to access its intracellular target.[48] Despite the potential antimicrobial activity of SD, it is generally believed that Ag^+ serves as the primary biocide upon AgSD dissociation, at least for topical applications.[49] This phenomenon was verified in our experiments by showing that treatment with SD alone was non-toxic to the 6 strains of bacteria studied.

As evidenced by the ineffectiveness of SD, the ability of a biocide to access target sites is imperative for antimicrobial efficacy. The outer membrane characteristic of Gram-negative species acts as a particularly efficient permeability barrier, conferring intrinsic resistance to host defense mechanisms, bile salts and digestive enzymes, and many biocides that are effective against other types of bacteria.[50] Thus, Gram-negative bacteria are generally more tolerant than Gram-positive species of antimicrobial agents.[51] Hence, the greater efficacy of Ag^+ and NO (individually) observed against Gram-negative species may indicate that important targets of these biocides reside on the exterior of the bacteria where the rate of passive diffusion is less important. When considering the reactivity of Ag^+, NO, and NO-derived by-products, this is not entirely surprising. Empirical evidence drawn from morphological observation supports this hypothesis. For example Feng et al. used TEM to

visualize cell wall damage for *E. coli* and *S. aureus* bacteria induced by silver nitrate, with the Gram-negative *E. coli* exhibiting a more pronounced detrimental effect.[5] Similarly, electron micrographs of AgSD-treated *P. aeruginosa* and *Enterobacter cloacae* have indicated altered cell wall morphology, while resistant species did not show any changes.[52,53] As previously discussed, NO may function by degrading the lipid membrane itself. Confocal microscopy and atomic force microscopy studies of bacteria after treatment with NO have demonstrated increased permeability of the cell wall to dye compounds and deterioration of the cell envelope.[24,37] Figure 4.2 depicts representative AFM images of *E. coli* before and after treatment with PROLI/NO that both demonstrate degradation of the cell membrane after treatment with NO and a positive correlation between dosage and degree of damage.

4.4.2 Proposed mechanisms for the synergistic action of PROLI/NO and AgSD. Two possible cooperative mechanisms seem plausible based on the cumulative knowledge of Ag^+ and NO activity, neither of which are mutually exclusive. Agents that act by disrupting the structure of the lipid bilayer or otherwise compromising the cell wall, independent of the level of bactericidal activity possessed alone, should in principle work synergistically when combined with a second agent whose activity is frustrated by low levels of permeability. Such a mechanism was previously demonstrated for the efficacy of streptomycin against *E. faecalis* where the use of cell wall-active agents such as penicillin and vancomycin improved the intracellular permeability of the antibiotic.[54,55] A similar phenomenon has been demonstrated against other Gram-negative and -positive species.[34] We hypothesize that such synergism may occur if cell wall or membrane damage elicited by Ag^+ and/or NO significantly increases the permeability of bacteria. Both of the antimicrobial agents evaluated in our study have intracellular activity that would be expected to be enhanced by a

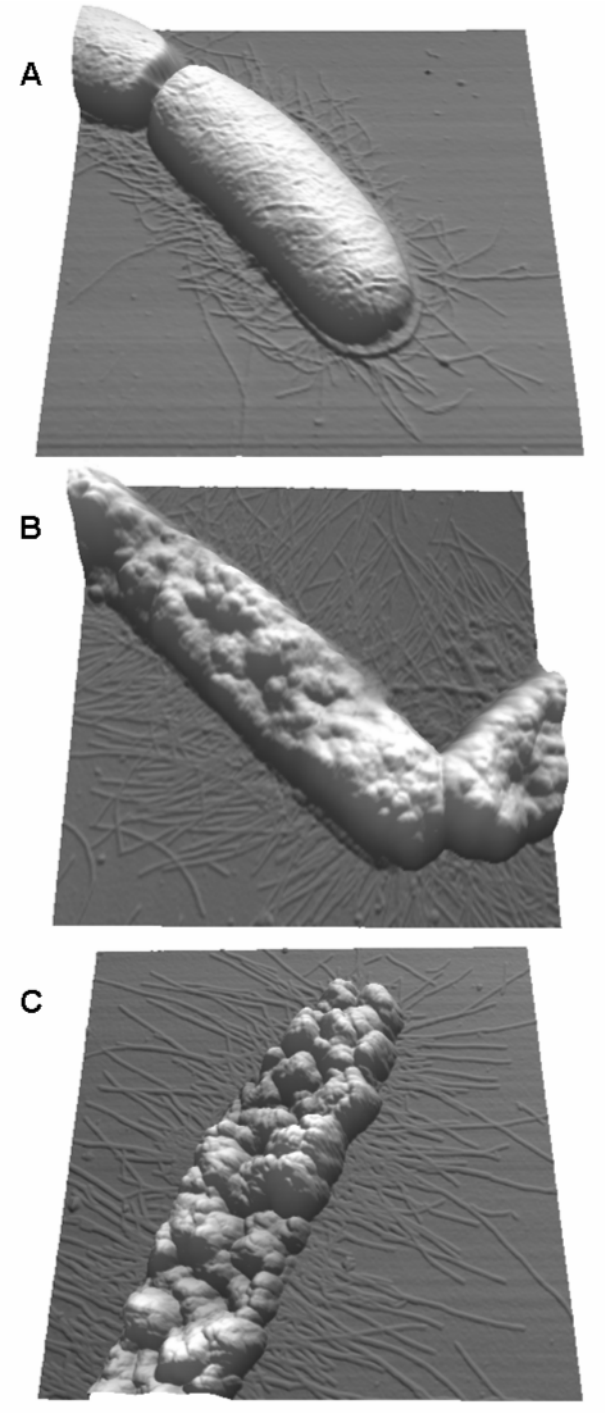

Figure 4.2 Representative AFM images of *E. coli* cells 120 min after treatment with (A) 0 g L^{-1}, (B) 1 g L^{-1}, and (C) 2 g L^{-1} PROLI/NO. Membrane damage sustained after exposure to NO trend with increasing PROLI/NO concentrations.

faster rate of entry into the bacteria. Furthermore, increased permeability of the lipid membrane could also allow intracellular access to the anionic SD inhibiting folate synthesis in the cytoplasm of bacteria.

To evaluate this hypothesis, representative Gram-negative (*P. aeruginosa*) and -positive (*S. aureus*) bacteria were treated with a range of SD concentrations in combination with doses of PROLI/NO at one half and one quarter of the respective bactericidal levels. The concentrations of SD tested included the molar bactericidal concentration of AgSD, and solutions two- and four-fold greater and less than this concentration. As SD was found to be non-toxic to all the species tested in this study, typical FBC_{120} indices were unobtainable. No synergistic effect was observed against *S. aureus*, as the bacterial viability at all combinations was indistinguishable from treatment with PROLI/NO alone (Fig. 4.3A-B). *P. aeruginosa* suffered a slight decrease in viablility at the highest concentration of PROLI/NO (4 g L^{-1}) but no obvious synergism was observed at the lower PROLI/NO concentration (2 g L^{-1}) (Fig. 4.3C-D). Thus, although some synergism was observed for *P. aeruginosa*, the effect was lower than what would be expected if this were the primary synergistic mechanism. Even the lowest concentration of SD evaluated (0.875 mg L^{-1}) was almost three-fold greater than the concentration of AgSD required for synergy against *P. aeruginosa* (0.31 mg L^{-1}) with a 4 g L^{-1} dose of PROLI/NO. These results indicate that combination treatment with NO and SD was not particularly effective against *P. aeruginosa* or *S. aureus* over a 2 h time frame. Some enhanced effect may occur at extended periods once endogenous folate reserves are depleted and cellular activity decreases due to starvation, but the primary mechanism of the acute synergy observed involves both NO and Ag^{+}.

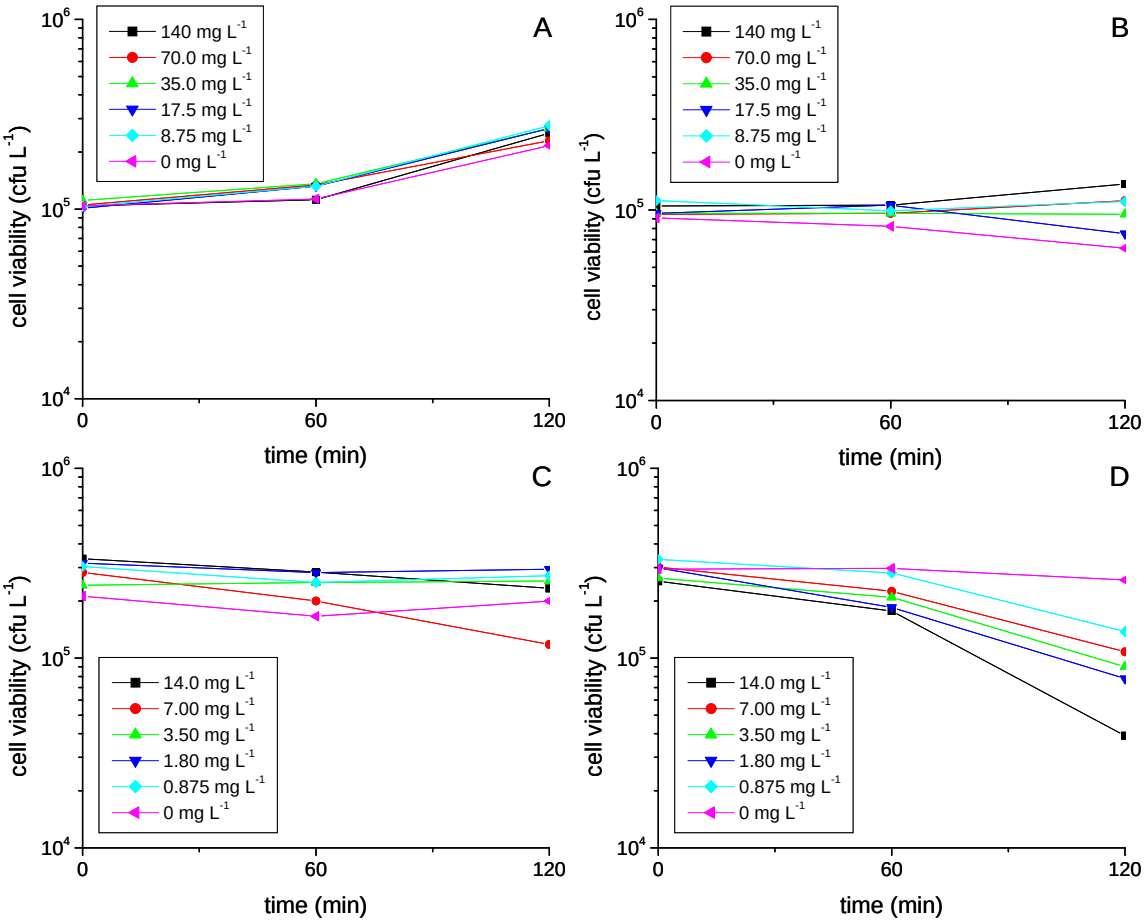

Figure 4.3 Bacteria viability over 120 min obtained using efficacy assays to evaluate synergy between PROLI/NO and SD. *S. aureus* (MSSA) viability was determined using the listed range of SD concentrations in combination with (A) 3 g L^{-1} and (B) 6 g L^{-1} PROLI/NO. Similarly, the viability of *P. aeruginosa* was evaluated using the SD concentrations listed in combination with (C) 2 g L^{-1} and (D) 4 g L^{-1} PROLI/NO.

Such a mechanism was discussed by Fang,[11] who suggested a possible synergistic effect in bactericidal efficacy for NO when present during bursts of bacterial respiratory activity. Among other bactericidal mechanisms, Ag^+ has been implicated in disruption of cellular respiration. Uncoupling of the respiratory chain initially results in stimulated respiration as bacteria attempt to regenerate the proton gradient across the membrane. Dibrov et al. demonstrated that the interaction of Ag^+ with reconstituted membrane vesicles of *Vibrio cholerae* resulted in the collapse of the proton motive force and dissipation of the proton gradient across the bacterial membrane.[3] Holt and Bard showed that $AgNO_3$ inhibited the respiratory chain by preventing the transport of protons outside of the cell.[6] One important implication of their study was the probable accumulation of reactive oxygen species such as O_2^- and OH^- at the membrane. The bactericidal efficacy of NO would increase with the number of reactive by-products it produces. For example, if a high concentration of O_2^- is generated upon treatment with Ag^+, the resulting increase in $ONOO^-$ formation in the presence of NO would result in a more rapid rate of oxidative membrane and protein damage. Thus, the generation of large quantities of reactive nitrogen and oxygen species following the Ag^+-induced collapse of the proton gradient across the cell membrane may explain the synergistic activity of combined AgSD and PROLI/NO treatment.

To evaluate this mechanism, both direct and indirect experiments are planned. The production of NO, O_2^-, and $ONOO^-$ may be monitored using metabolite-sensitive fluorescent dyes. Using confocal fluorescent microscopy, co-localization of these reactants with bacterial cells may be verified. Furthermore, the synergistic mechanism may be indirectly probed by adjusting the sequence of addition. If the build-up of O_2^-results in increased $ONOO^-$ formation and greater bactericidal efficacy, cellular respiration must still first be

inhibited by Ag^+. Hence, synergistic effects observed by varying the order of antimicrobial addition may prove useful for verifying the mechanism of action.

4.5 Conclusions

The combination of AgSD and PROLI/NO is synergistic across a wide range of bacteria types, including Gram-positive, Gram-negative, and antibiotic-resistant 'super bugs'. Possible explanations for the synergy include increased access to the cytoplasm due to compromised cell envelope and/or an abundance of reactive species resulting from uncoupling of cellular respiration. While it is not clear why the combination of AgSD and PROLI/NO is so effective against Gram-positive species, particularly *E. faecalis*, this trend is clear. The evidence presented herein provides an impetus to further investigate the clinical uses of NO in combination with AgSD and other antibiotics. Possessing the ability to efficiently eradicate a wide range of bacterial species, such combinations may be particularly useful in topical wound treatment due to the potential for treating polymicrobial and antibiotic-resistant infections without fostering selection for resistant species. Further mechanistic studies aimed at elucidating the synergistic action of AgSD and NO would provide a strong foundation for developing and improving additional combination therapies.

4.6 References

(1) Russell, A. D.; Hugo, W. B. Antimicrobial activity and action of silver. *Prog. Med. Chem.* **1994**, *31*, 351-371.

(2) Bragg, P. D.; Rainne, D. G. The effect of silver ions on the respiratory chain of *Escherichia coli*. *Can. J. Microbiol.* **1974**, *20*, 883-889.

(3) Dibrov, P.; Dzioba, J.; Gosink, K. K.; Häse, C. C. Chemiosmotic mechanism of antimicrobial activity of Ag^+ in *Vibrio cholerae*. *Antimicrob. Agents Chemother.* **2002**, *46*, 2668-2670.

(4) Modak, S. M.; Fox, J., C. L. Binding of silver sulfadiazine to the cellular components of *Pseudomonas aeruginosa*. *Biochem. Pharmacol.* **1973**, *22*, 2391-2404.

(5) Feng, Q. L.; Wu, J.; Chen, G. Q.; Cui, F. Z.; Kim, T. N. et al. A mechanistic study of the antibacterial effect of silver ions on *Escherichia coli* and *Staphylococcus aureus*. *J. Biomed. Mater. Res.* **2000**, *52*, 662-668.

(6) Holt, K. B.; Bard, A. J. Interaction of silver (I) ions with the respiratory chain of *Escherichia coli*: An electrochemical and scanning electrochemical microscopy study of the antimicrobial mechanism of micromolar Ag^+. *Biochemistry* **2005**, *44*, 13214-13223.

(7) Silver, S.; Phung, L. T.; Silver, G. Silver as biocides in burn and wound dressings and bacterial resistance to silver compounds. *J. Ind. Microbiol. Biotechnol.* **2006**, *33*, 627-634.

(8) Carr, H. S.; Wlodkowski, T. J.; Rosenkranz, H. S. Silver sulfadiazine: in vitro antibacterial activity. *Antimicrob. Agents Chemother.* **1973**, *4*, 585-587.

(9) Wlodkowski, T. J.; Rosenkranz, H. S. Antifungal activity of silver sulphadiazine. *Lancet* **1973**, *ii*, 739-740.

(10) Bogdan, C. Nitric oxide and the immune response. *Nat. Immunol.* **2001**, *2*, 907-916.

(11) Fang, F. C. Host/pathogen interactions: Mechanisms of nitric oxide-related antimicrobial activity. *J. Clin. Invest.* **1997**, *99*, 2818-2825.

(12) Foley, E.; O'Farrell, P. H. Nitric oxide contributes to induction of innate immune responses to Gram-negative bacteria in Drosophila. *Genes Dev.* **2003**, *17*, 115-125.

(13) MacMicking, J.; Xie, Q. W.; Nathan, C. Nitric oxide and macrophage function. *Annu. Rev. Immunol.* **1997**, *15*, 323-350.

(14) Mannick, J. B. Immunoregulatory and antimicrobial effects of nitrogen oxides. *Proc. Am. Thorac. Soc.* **2006**, *3*, 161-165.

(15) Wink, D. A.; Mitchell, J. B. Chemical biology of nitric oxide: Insights into regulatory, cytotoxic, and cytoprotective mechanisms of nitric oxide. *Free Radic. Biol. Med.* **1998**, *25*, 434-456.

(16) Moller, M. N.; Li, Q.; Lancaster, J. R. J.; Denicola, A. Acceleration of nitric oxide autooxidation and nitrosation by membranes. *Life* **2007**, *59*, 243-248.

(17) Zaki, M. H.; Akuta, T.; Akaike, T. Nitric oxide-induced nitrative stress involved in microbial pathogenesis. *J. Pharmacol. Sci.* **2005**, *98*, 117-129.

(18) Wink, D. A.; Kasprzak, K. S.; Maragos, C. M.; Elespuru, R. K.; Misra, M. et al. DNA deaminating ability and genotoxicity of nitric oxide and its progenitors. *Science* **1991**, *254*, 1001-1003.

(19) Schapiro, J. M.; Libby, S. J.; Fang, F. C. Inhibition of bacterial DNA replication by zinc mobilization during nitrosative stress. *Proc. Natl. Acad. Sci. USA* **2003**, *100*, 8496-8501.

(20) Ghaffari, A.; Miller, C. C.; McMullin, B.; Ghahary, A. Potential application of gaseous nitric oxide as a topical antimicrobial agent. *Nitric Oxide* **2006**, *14*, 21-29.

(21) Raulli, R.; McElhaney-Feser, G.; Hrabie, J. A.; Cihlar, R. L. Antimicrobial properties of nitric oxide using diazeniumdiolates as the nitric oxide donor. *Rec. Res. Devel. Microbiology* **2002**, *6*, 177-183.

(22) Keefer, L. K. Progress toward clinical application of the nitric oxide-releasing diazeniumdiolates. *Annu. Rev. Pharmacol. Toxicol.* **2003**, *43*, 585-607.

(23) Hetrick, E. M.; Schoenfisch, M. H. Antibacterial nitric oxide-releasing xerogels: Cell viability and parallel plate flow cell adhesion studies. *Biomaterials* **2007**, *28*, 1948-1956.

(24) Hetrick, E. M.; Shin, J. H.; Stasko, N. A.; Johnson, B. A.; Wespe, D. A. et al. Bactericidal efficacy of nitric oxide-releasing silica nanoparticles. *ACS Nano* **2007**, *2*.

(25) Nablo, B. J.; Rothrock, A. R.; Schoenfisch, M. H. Nitric oxide-releasing sol-gels as antibacterial coatings for orthopedic implants. *Biomaterials* **2005**, *26*, 917-924.

(26) Levy, S. B. *The Antibiotic Paradox*; 2nd ed.; Perseus: Cambridge, 2002.

(27) Kliebe, C.; Nies, B. A.; Meyer, J. F.; Tolxdorff-Neutzling, R. M.; Wiedemann, B. Evolution of plasmid-encoded resistance to broad-spectrum cephalosporins. *Antimicrob. Agents Chemother.* **1985**, *28*, 302-307.

(28) Hall, R. M.; Collins, C. M. Mobile gene cassettes and integrons: capture and spread of genes by site-specific recombination. *Mol. Microbiol.* **1995**, *15*, 593-600.

(29) Levy, S. B. Multidrug resistance: a sign of the times. *New Eng. J. Med.* **1998**, *338*, 1376-1378.

(30) Hiramatsu, K. Vancomycin resistance in *Staphylococci*. *Drug Res. Updates* **1998**, *1*, 135-150.

(31) Michel, M.; Gutmann, L. Methicillin-resistant *Staphylococcus aureus* and vancomycin-resistant *Enterococci*: Therapeutic realities and possibilities. *Lancet* **1997**, *349*, 1901-1906.

(32) Cottarel, G.; Wierzbowski, J. Combination drugs, an emerging option for antibacterial therapy. *Trends Biotechnol.* **2007**, *25*, 547-555.

(33) Eliopoulos, G. M.; Moellering, J., R. C. Antimicrobial Combinations. *Antibiotics in Laboratory Medicine*; 4th ed.; Williams & Wilkins: Baltimore, 1996; pp 330-396.

(34) Eliopoulos, G. M.; Eliopoulos, C. T. Antibiotic combinations: Should they be tested? *Clin. Microbiol. Rev.* **1988**, *1*, 139-156.

(35) Saavedra, J. E.; Southan, G. J.; Davies, K. M.; Lundell, A.; Markou, C. et al. Localizing antithrombotic and vasodilatory activity with a novel, ultrafast nitric oxide donor. *J. Med. Chem.* **1996**, *39*, 4361-4365.

(36) Amsterdam, D. Susceptibility Testing of Antimicrobials in Liquid Media. *Antibiotics in Laboratory Medicine*; 4th ed.; Williams & Wilkins: Baltimore, 1996; pp 52-111.

(37) Deupree, S. M.; Schoenfisch, M. H. Morphological analysis of the antimicrobial action of nitric oxide on Gram-negative pathogens using atomic force microscopy. *Acta Biomater.* **2009**, *(in press)*.

(38) Elion, G. B.; Singer, S.; Hitchings, C. H. Antagonists of nucleic acid derivitives. VIII. Synergism in combinations of biochemically related antimetabolites. *J. Biol. Chem.* **1954**, *208*, 477-488.

(39) Rosenkranz, H. S.; Carr, H. S. Silver sulfadiazine: Effect on the growth and metabolism of bacteria. *Antimicrob. Agents Chemother.* **1972**, *2*, 367-372.

(40) Kwakman, P. H. S.; Van den Akker, J. P. C.; Güçlü, A.; Aslami, H.; Binnekade, J. M. et al. Medical-grade honey kills antibiotic-resistant bacteria in vitro and eradicates skin colonization. *Clin. Infect. Dis.* **2008**, *46*, 1677-1682.

(41) Akimitsu, N.; Hamamoto, H.; Inoue, R.; Shoji, M.; Akamine, A. et al. Increase in resistance of methicillin-resistant *Staphylococcus aureus* to β-lactams caused by mutations conferring resistance to benzalkonium chloride, a disinfectant widely used in hospitals. *Antimicrob. Agents Chemother.* **1999**, *43*, 3042-3043.

(42) Datta, N.; Faiers, M. C.; Reeves, D. S.; Brumfitt, W.; Orskov, F. et al. R factors in *Escherichia coli* in faeces after oral chemotherapy in general practice. *Lancet* **1971**, *1*, 312-315.

(43) Levy, S. B.; Marshall, B.; Schluederberg, S.; Rowse, D.; Davis, J. High frequency of antimicrobial resistance in human fecal flora. *Antimicrob. Agents Chemother.* **1988**, *32*, 1801-1806.

(44) De Groote, M. A.; Fang, F. C. NO inhibitions: Antimicrobial properties of nitric oxide. *Clin. Infect. Dis.* **1995**, *21 (Suppl 2)*, S162-S165.

(45) Brandes, N.; Rinck, A.; Leichert, L. I.; Jakob, U. Nitrosative stress treatment of *E. coli* targets distinct set of thiol-containing proteins. *Mol. Microbiol.* **2007**, *66*, 901-914.

(46) Liau, S. Y.; Read, D. C.; Pugh, W. J.; Furr, J. R.; Russell, A. D. Interaction of silver nitrate with readily identifiable groups: Relationship to the antibacterial action of silver ions. *Lett. Appl. Microbiol.* **1997**, *25*, 279-283.

(47) Sakurai, H.; Ishimitsu, T. Microionization constants of sulphonamides. *Talanta* **1980**, *27*, 293-298.

(48) Zarfl, C.; Matthies, M.; Klasmeier, J. A mechanistical model for the uptake of sulfonamides by bacteria. *Chemosphere* **2008**, *70*, 753-760.

(49) Klasen, H. J. Historical review of the use of silver in the treatment of burns. I. Early uses. *Burns* **2000**, *26*, 117-130.

(50) Nikaido, H.; Vaara, M. Molecular basis of bacterial outer membrane permeability. *Microbiol. Rev.* **1985**, *49*, 1-32.

(51) Maillard, J.-Y. Bacterial target sites for biocide action. *J. Appl. Microbiol.* **2002**, *92*, 16S-27S.

(52) Rosenkranz, H. S.; Coward, J. E.; Wlodkowski, T. J.; Carr, H. S. Properties of silver sulfadiazine-resistant *Enterobacter cloacae*. *Antimicrob. Agents Chemother.* **1973**, *5*, 199-201.

(53) Coward, J. E.; Carr, H. S.; Rosenkranz, H. S. Silver sulfadiazine: Effect on the ultrastructure of *Pseudomonas aeruginosa*. *Antimicrob. Agents Chemother.* **1973**, *3*, 621-624.

(54) Moellering, J., R. C.; Weinberg, A. N. Studies on antibiotic synergism against enterococci. II. Effect of various antibiotics on the uptake of 14C-labeled streptomycin by enterococci. *J. Clin. Invest.* **1971**, *50*, 2580-2584.

(55) Moellering, J., R. C.; Wennersten, C.; Weinberg, A. N. Studies on antibiotic synergism against enterococci. I. Bacteriologic studies. *J. Lab. Clin. Med.* **1971**, *77*, 821-828.

Chapter 5:

Summary and future research directions

5.1 Summary of research

The overall goal of my dissertation research has been to contribute to the current knowledge of the process of infection and the development and evaluation of novel treatment options. Chapter 2 described the development of a technique for using AFM to measure the force required to detach bacteria adhered to a surface using an AFM probe to apply a lateral force sufficient to break the adhesive bacteria-surface interactions during a normal contact-based imaging mode. Large scan sizes (40 μm^2) allowed for concerted acquisition of detachment forces for multiple bacteria. In addition, the total compression of the cantilever was determined for each cell detachment event using deflection image analysis. The resulting methodology enabled a more accurate and high-throughput measurement of the forces necessary to remove individual cells compared to previous reports. This technique was then applied to measuring Phase II adhesion kinetics (>18 h after initial attachment) of two representative pathogens, *P. aeruginosa* and *S. aureus*, on a bare substrate. *P. aeruginosa* reinforced its adhesion to the surface at a rate 7-fold faster than *S. aureus*, while the overall adhesion strength of *P. aeruginosa* was larger than *S. aureus*. Furthermore, it was observed that changes in adhesion strength did not proceed uniformly across a population of the same species.

As discussed in Chapter 3, AFM was also employed conduct an analysis of the morphological changes undergone by two pathogenic Gram-negative species, *E. coli* and *P. aeruginosa*, subsequent to NO-treatment. The Schoenfisch lab has developed and characterized numerous NO-releasing scaffolds with bactericidal properties. Two materials embodying different NO-delivery routes were used in this study, namely a polymer coating that released NO as a sustained surface flux and a small-molecule donor that delivered its payload of NO as a short-duration bolus. In a qualitative sense, changes in cell morphologies subsequent to exposure to NO demonstrated a considerable increase in cellular debris and deterioration of the cell wall relative to control cells, while similarities to the morphologies exhibited after treatment with the β-lactam amoxicillin also suggested that deterioration of the cell envelope is one visible effect of NO-treatment. From a quantitative standpoint, measurements of cell surface roughness were obtained to study the membrane degradation induced by NO as a function of time, concentration, and NO-delivery route. A positive correlation was observed between membrane roughness and dose of NO, while NO delivered quickly in a bolus induced more damage than a comparable amount of NO delivered via a sustained surface flux.

Chapter 4 introduced modified viability assays that were designed to further explore the antimicrobial properties of NO, specifically in combination with a second drug AgSD. As NO is a cell wall-active agent that should increase bacterial permeability, it was hypothesized that the combination of NO with a drug whose bactericidal mechanism functions intracellularly would elicit a synergistic bactericidal effect. Previous studies have implicated dissociated Ag^+ as the primary biocide responsible for antimicrobial action. As a member of the sulfonamide family of synthetic antibiotics (inhibitors of folic acid synthesis), SD has

potential intracellular antimicrobial action. However, it is thought to be inert in topical applications as the active, charged species has very low membrane permeability. Thus, a synergistic effect was postulated upon combination of PROLI/NO and AgSD, as membrane damage rendered during a burst of NO release should allow SD access to the interior of the cell where it can fulfill its antibiotic potential without inhibiting the function of Ag^+.

Standard microdilution and checkerboard viability assays were modified to require bactericidal efficacy over a short-duration treatment window (2 h) and conducted to evaluate the activity of PROLI/NO and AgSD both individually and in combination. Synergistic activity was demonstrated against both Gram-negative and -positive bacteria. A highly synergistic reaction was seen against three of four Gram-positive species tested, including vancomycin-resistant *E. faecalis*. Two species (*P. aeruginosa* and MRSA) exhibited FBC_{120} values near 0.5 (the standard upper limit for indication of synergy). Although not technically synergistic by traditional standards, it is possible that some synergistic action was observed since the duration of exposure used in this study was very short relative to the standard synergy determinations for which the FIC and FBC indices were developed.

5.2 Future directions

5.2.1 Applications of lateral force measurements using AFM to evaluate bacterial adhesion. As presented in Chapter 2, an AFM technique was developed for applying a lateral force to detach adhered bacteria. This method was specifically designed to probe late-stage (Phase II) adhesion forces, which may be characterized by both specific and non-specific interactions (see Section 1.1.3 and Fig. 1.2). While the application described in Chapter 2 investigates non-specific interactions developed by *S. aureus* and *P. aeruginosa* on

bare substrates, a second evident research direction would involve the study of specific protein-bacteria interactions. Specific interactions, characterized by molecular recognition and (frequently) high-affinity, often confer greater resistance to detachment than non-specific interactions.[1,2] Some types of specific interactions, termed catch-bonds, are actually strengthened in high shear environments.[3,4] *S. aureus*, in particular, has been shown to specifically recognize and bind to numerous proteins, including fibrinogen, fibronectin, and collagen.[2,5-7] Strong interactions with these proteins, present as a conditioning layer on implanted material surfaces, are thought to be responsible for the high percentage of *S. aureus*-produced device-related infections.[8,9]

Some important variables in experimental design must be optimized. Surface-bound protein may be simply adsorbed or covalently attached to the surface. Relying on adsorption is preferable as it mimics in vivo conditions, while covalent modification may alter protein structure, thereby reducing incidence or degree of specific recognition and binding. Conversely, it is important to ensure that interactions are breaking between the bacterium and the protein, not between the protein and the surface. In addition, for the investigation of non-specific interactions, an intermediate drying step proved necessary for achieving measurable adhesive forces.[10] While this appropriately mimics contamination of a material surface ex vivo, it is uncertain how this dehydration step would affect the specific interactions formed between bacteria and protein that typically occur in vivo. Maintaining a hydrated surface would be preferable as this would most closely simulate the situation where a bacterium such as *S. aureus* would come into contact with a protein-coated biomaterial.

Preliminary experiments were undertaken to evaluate the adhesion of *S. aureus* to collagen-coated polyurethane (PU). Using a polydimethylsiloxane (PDMS) stamp, collagen

was patterned onto a PU surface. Sandwiching the protein between areas of bare substrate allows for intra-experiment controls to evaluate both preference and strength of adhesion. Protein adsorption was verified, as collagen patterns (e.g., 10 μm stripes) were visualized using AFM deflection images, while the stamped region became increasingly hydrophobic on the macroscopic scale. Although sub-monolayer coverage was obtained within the patterned regions, *S. aureus* was seen to preferentially adhere to the protein-patterned regions after 1 h incubation. To more closely mimic an in vivo situation, a closed fluid cell (CFC) that would house the cantilever and substrate within a buffered, hydrated environment was coupled to the AFM. A 5-mL suspension of *S. aureus* was introduced into the CFC for 1 h. The system was flushed with 15 mL of PBS and then imaged in PBS using contact mode. The overall surface coverage of detected cells was low, indicating some unknown variable that either discouraged attachment or prevented measurable adhesion forces (i.e., bacteria were dislodged at undetectable forces). Although further optimization is needed, measurement of bacterial adhesion to protein-coated materials represents an important line of study for understanding both fundamental adhesive interactions and how bacteria adhered to tissue or implanted medical devices behave within shearing environments.

There is no doubt that *S. aureus* is a troublesome pathogen, expressing not only a variety of specific adhesins but also developing resistance mechanisms (e.g., methacillin resistance) that are subsequently propagated to future generations and even shared between near relatives (e.g., *Enterococcus* subspecies).[11] Our previous study (Chapter 2), however, indicated that *S. aureus* exhibited relatively low adhesion rates to bare xerogel materials compared to *P. aeruginosa*. This may indicate that materials that resist protein adsorption may inhibit the success of *S. aureus* adhesion events and, subsequently, colonization and

infection. Therefore a second potential application of lateral force measurements would entail screening promising materials for their anti-adhesive properties.

5.2.2 Induction of NO-resistance in bacteria. Nitric oxide is ubiquitously produced in all living systems as a signaling molecule, while in higher organisms it also functions in the immune response to infection. One pressing question that must be asked of any promising clinical antibacterial is the potential prevalence for resistance to develop. Given the conserved nature of NO as an endogenous antibacterial (natural selection), it would be expected that many pathogenic bacteria would have already evolved resistance mechanisms to NO. To a certain extent this is true, as some bacteria produce low molecular weight scavengers and/or up-regulate the expression of certain proteins when exposed to low levels of NO.[12-16] But, unlike the efflux pumps that efficiently remove large quantities of an antibiotic from bacteria, the mechanisms identified for deactivating NO function on a molecule-to-molecule basis. In other words, one protein can effectively neutralize only a single molecule of NO. In fact, this is not surprising as the inherently reactive, broad-spectrum nature of NO would render most typical means of resistance ineffective. Thus, known NO-resistance mechanisms require a large input of energy, and would likely prove insufficient to handle levels of NO-exposure exceeding endogenous concentrations.

Hence, we hypothesized that the development of resistance to high levels of NO would be unlikely. To probe the upper limit of tolerance, we are attempting to induce bacterial resistance to NO. Cultures of *E. coli* are treated for 2 h with concentrations of PROLI/NO at half the MBC_{120}. Aliquots of the treated cells are plated on agar, and colonies that grow (NO-survivors) are re-cultured in nutrient broth and cycled through another treatment process. Such step-wise selection procedures have proven successful in isolating bacteria

resistant to Ag^{+}.[17] Through 6 cycles completed thus far, we have been unable to induce a tolerance to NO. While the continuation of negative results only indicates that NO-resistant species have not yet emerged, the greater number of consecutive generations exposed to this type of treatment can speak for the unlikelihood of resistance developing. This series of experiments is currently under investigation.

5.2.3 Efficacy of NO against biofilms. Previous research has inarguably shown the effectiveness of NO as an antibacterial agent.[18-23] Most of these studies, however, have evaluated bacteria either in a planktonic state or within hours after adhesion. More than half of infections, however, are caused by bacteria present in a biofilm community, which are notoriously difficult to treat (Section 1.1.4). In light of NO's antimicrobial properties, a final promising avenue of investigation would be characterization of anti-biofilm activity. Some recent studies have begun to evaluate the efficacy of NO on biofilm communities. High levels of NO delivered from diazeniumdiolate-modified silica nanoparticles were effective at killing a range of day-old biofilm-based microbes,[23] while low levels of NO delivered from *S*-nitrosothiols have been implicated in initiating dispersal of *P. aeruginosa* biofilms.[24]

To further investigate the anti-biofilm properties of NO, we propose the combined use of SEM and confocal fluorescence microscopy. The excellent resolution afforded by SEM allows detailed observation of biofilm morphology before and after NO-treatment. As discussed in Section 1.2.1, fluorescent labelling is a particularly versatile method for studying specific qualities of bacteria. For example, fluorescent tags may be used to distinguish between viable and dead bacteria subsequent to treatment. In addition, the simultaneous use of a confocal microscope would allow three-dimensional visualization of fluorescence to elucidate properties of the structured community, such as the depth to which

NO is capable of rendering bactericidal activity. To compliment these techniques, metabolic activity and biofilm dispersal may be monitored by sampling the liquid matrix containing the biofilms. Certain metabolic intermediates (e.g., ATP) may also be fluorescently labelled and quantified, while viable planktonic cells characteristic of dispersal may be detected by plating aliquots onto nutrient agar plates and counting the colonies that grow. Each of these techniques could be used to study the pathogen- and dose-dependent effects of NO on biofilm viability.

5.3 Conclusions

While it is widely accepted that bacterial adhesion is a time-dependent process, surprisingly little is known about how the strength of adhesion changes subsequent to initial attachment, primarily as a methodology suitable for acquiring accurate and high-throughput force data was lacking. To address this gap in the infection model, a quantitative technique was developed and then applied to obtain the first reported measurements of the kinetics of late-stage bacterial adhesion. Besides contributing to the fundamental understanding of how bacterial adhesion changes with time, this technique may be applied to evaluate ultra-low adhesion materials that would aid in resisting colonization as well as probing the strength of bacteria-protein interactions. In terms of investigating the problem of infection, the atomic force microscope proved an invaluable tool not only for measuring the forces of adhesion, but also for visualizing the morphologies of bacteria subsequent to antimicrobial treatment. Based on the observed changes in bacterial shape and surface roughness, one cytotoxic mechanism of NO proposed was membrane stress. The presumed increase in cell wall permeability would potentially allow improved intracellular access to other antibiotics. Upon combination of NO and AgSD, synergistic activity was indeed noted against a wide range of pathogens, including antibiotic-resistant species, highlighting the potential clinical application of NO in combination therapy. Further studies aimed at elucidating the synergistic mechanism would aid in identifying additional promising therapeutic combinations.

5.4 References

(1) Kaufman, M. R.; Taylor, R. K. Identification of bacterial cell-surface virulence determinants with Tn*pho*A. *Meth. Enzymol.* **1994**, *235*, 426-448.

(2) Seltmann, G.; Holst, O. *The Bacterial Cell Wall*; Springer: Berlin, 2002; 280.

(3) Sokurenko, E. V.; Vogel, V.; Thomas, W. E. Catch-bond mechanism of force-enhanced adhesion: Counterintuitive, elusive, but...widespread? *Cell Host & Microbe* **2008**, *4*, 314-323.

(4) Thomas, W. E.; Trintchina, E.; Forero, M.; Vogel, V.; Sokurenko, E. V. Bacterial adhesion to target cells enhanced by shear force. *Cell* **2002**, *109*, 913-923.

(5) Burne, R. A.; Quivey, R. G.-J. Use of transposons to dissect pathogenic strategies of Gram-positive bacteria. *Meth. Enzymol.* **1994**, *235*, 405-426.

(6) Clarke, S. R.; Foster, S. J. Surface adhesins of *Staphylococcus aureus*. *Adv. Microb. Physiol.* **2006**, *51*, 187-224.

(7) Patti, J. M.; Allen, B. L.; McGavin, M. J.; Hook, M. MSCRAMM-mediated adherence of microorganisms to host tissues. *Annu. Rev. Microbiol.* **1994**, *48*, 585-617.

(8) Campoccia, D.; Montanaro, L.; Arciola, C. R. The significance of infection related to orthopedic devices and issues of antibiotic resistance. *Biomaterials* **2005**, *27*, 2331-2339.

(9) Darouiche, R. O. Treatment of infections associated with surgical implants. *New Engl. J. Med.* **2004**, *250*, 1422-1429.

(10) Deupree, S. M.; Schoenfisch, M. H. Quantitative method for determining the lateral strength of bacterial adhesion and application for characterizing adhesion kinetics. *Langmuir* **2008**, *24*, 4700-4707.

(11) Levy, S. B. *The Antibiotic Paradox*; 2nd ed.; Perseus: Cambridge, 2002.

(12) Crawford, M. J.; Goldberg, D. E. Role for the *Salmonella* flavohemoglobin in protection from nitric oxide. *J. Biol. Chem.* **1998**, *273*, 12543-12547.

(13) Fang, F. C. Host/pathogen interactions: Mechanisms of nitric oxide-related antimicrobial activity. *J. Clin. Invest.* **1997**, *99*, 2818-2825.

(14) Hausladen, A.; Gow, A. J.; Stamler, J. S. Nitrosative stress: Metabolic pathway involving the flavohemoglobin. *Proc. Natl. Acad. Sci. USA* **1998**, *95*, 14100-14105.

(15) Nunoshiba, T.; de Rojas-Walker, T.; Wishnok, J. S.; Tannenbaum, S. R.; Demple, B. Activation by nitric oxide of an oxidative-stress response that defends *Escherichia coli* against activated macrophages. *Proc. Natl. Acad. Sci. USA* **1993**, *90*, 9993-9997.

(16) Richardson, A. R.; Libby, S. J.; Fang, F. C. A nitric oxide-inducible lactate dehydrogenase enables *Staphylococcus aureus* to resist innate immunity. *Science* **2009**, *319*, 1672-1676.

(17) Li, X.-Z.; Nikaido, H.; Williams, K. E. Silver-resistant mutants of *Escherichia coli* display active efflux of Ag^+ and are deficient in porins. *J. Bacteriol.* **1997**, *179*, 6127-6132.

(18) Deupree, S. M.; Schoenfisch, M. H. Morphological analysis of the antimicrobial action of nitric oxide on Gram-negative pathogens using atomic force microscopy. *Acta Biomater.* **2009**, *(in press)*.

(19) Hetrick, E. M.; Schoenfisch, M. H. Antibacterial nitric oxide-releasing xerogels: Cell viability and parallel plate flow cell adhesion studies. *Biomaterials* **2007**, *28*, 1948-1956.

(20) Hetrick, E. M.; Shin, J. H.; Stasko, N. A.; Johnson, B. A.; Wespe, D. A. et al. Bactericidal efficacy of nitric oxide-releasing silica nanoparticles. *ACS Nano* **2007**, *2*.

(21) Ghaffari, A.; Miller, C. C.; McMullin, B.; Ghahary, A. Potential application of gaseous nitric oxide as a topical antimicrobial agent. *Nitric Oxide* **2006**, *14*, 21-29.

(22) Miller, C.; McMullin, B.; Ghaffari, A.; Stenzler, A.; Pick, N. et al. Gaseous nitric oxide bactericidal activity retained during intermittent high-dose short duration exposure. *Nitric Oxide* **2009**, *20*, 16-23.

(23) Hetrick, E. M.; Shin, J. H.; Paul, H. S.; Schoenfisch, M. H. Anti-biofilm efficacy of nitric oxide-releasing silica nanoparticles. *Biomaterials* **2009**, *(in press)*.

(24) Barraud, N.; Hassett, D. J.; Hwang, S.-H.; Rice, S. A.; Kjelleberg, S. et al. Involvement of nitric oxide in biofilm dispersal of *Pseudomonas aeruginosa*. *J. Bacteriol.* **2006**, *188*, 7344-7353.

Appendix:

Discussion of assumptions in force measurement

Two assumptions associated with the validity of our technique for force measurement were examined: (1) the vectors of the normal force had comparable lateral components over the range of cantilever compression values, and (2) all bending of the cantilever occurred in a manner that could be modeled, via adaptation of Hooke's Law ($F = k\,d$), to the compression of a spring (i.e., along the long axis of the cantilever).

The force directly measured by the AFM is applied in a direction normal to the bending probe (e.g. F_z when scanning a level, flat surface as in Figure 2.1A). However, when the contact point changes from the tip of the probe to the side of the probe, as when imaging a large feature such as a bacterium, the applied force (F_{app}) felt by the feature is a component of the measured force (Eq. 2.1). The lateral component F_{lat} is the shear force that detaches the cell and is directly proportional to the normal force F_{app} (Eq. 2.2) (Fig. 2.1B), where θ is the angle between F_{app} and F_{lat}.

The actual shape of the cantilever curve as a function of total cantilever compression is difficult to predict. It is thus impossible to accurately determine θ as a function of cantilever compression. By accounting for the geometry of the probe and the cantilever, a model was conceived that would yield an approximate value for θ that varies with the degree of cantilever deflection. The lengths of cantilevers used were 115 μm and 196 μm, and the maximum displacement from equilibrium achieved during any measurement conducted in these

experiments did not exceed 800 nm. As the curvature of the cantilever is slight, it can be approximated at a straight line, forming the opposite side of a right triangle (Fig. 2.1B). The tilt of the cantilever from a horizontal position is given by the angle Φ and is equal to 11° for our MFP 3D cantilever holder at free air deflection. As shown in Figure 2B, a direct relationship between the angle Φ and the angle θ between the normal force vector and the lateral, or shear, component along the x axis can be established under such an approximation for a pyramidal probe of known geometry. The maximum change $\Delta_{max}\theta$ between the value of θ at free air deflection θ_{min} and that at maximum compression θ_{max} is 0.41° for cantilevers at 115 μm length and 0.25° for cantilevers at 186 μm length. The resulting decrease in Φ corresponds directly with the increase in θ. Using the two equations

$$F_{lat,\ free\ air} = k\ d \sin(\theta_{min} + \Phi_{max}) \cos(\theta_{min}) \text{ and}$$

$$F_{lat,\ maximum\ compression} = k\ d \sin(\theta_{max} + \Phi_{min}) \cos(\theta_{max})$$

to determine the variation in vector contribution that could be expected at minimum and maximum compression of the cantilevers, we determined that the maximum potential error introduced to F_{lat} calculations by assuming the angle θ to be constant is 0.2 % and 0.1 % for 115 μm and 186 μm cantilevers, respectively. In all reported F_{lat}, we used a value of 24° for θ, which corresponds to the value at free air deflection.

By adapting Hooke's Law to calculate forces applied by the probe, this study also assumes the cantilever can be modeled by an ideal spring. In this case the laser position will only move along a vertical course on an aligned photodiode in response to lever compression. However, some degree of torsion (i.e., a twisting motion) in the cantilever will naturally occur as a function

of normal scanning of a featured surface. Twist in the cantilever affects the measured deflection by causing the position of the laser on the photodiode to move with both a vertical and lateral component. Hooke's Law converts the measured change in deflection to applied force, and deflection measurements are thus read only as the change in output signal resulting from vertical displacement of the laser position. Torsion in the cantilever may become problematic if the feedback loop attempts to compensate for the lost z-deflection measured if the twisting is either sustained or ill-timed to coincide with piezo adjustment by the feedback loop or if a significant lateral force is applied during natural correction of the torque.

To monitor the level of torsion that occurs during normal scanning, one channel of the AFM was directed to monitor the lateral signal (i.e., the displacement of the laser position to the left or right of the vertical axis to which it is aligned). For typical microfabricated triangular cantilevers such as the ones used in this study, the detector response for lateral signal change is ~20 – 80 times smaller than for normal force signals.[1] However, we found that under our experimental conditions the change in the lateral signal is on the order of nV, at least three orders of magnitude smaller than the changes measured in vertical deflection (mV to V), indicating only minor degrees of torsion in the cantilever.

(1) Ogletree, D. F.; Carpick, R. W.; Salmeron, M. Calibration of frictional forces in atomic force microscopy. *Rev. Sci. Instrum.* **1996**, *67*, 3298-3306.